



2008-03-17

# Mechanisms by Which Apoptotic Membranes Become Susceptible to Secretory Phospholipase A<sub>2</sub>

Rachel Williams Bailey  
*Brigham Young University - Provo*

Follow this and additional works at: <https://scholarsarchive.byu.edu/etd>

 Part of the [Cell and Developmental Biology Commons](#), and the [Physiology Commons](#)

---

## BYU ScholarsArchive Citation

Bailey, Rachel Williams, "Mechanisms by Which Apoptotic Membranes Become Susceptible to Secretory Phospholipase A<sub>2</sub>" (2008).  
*All Theses and Dissertations*. 1343.  
<https://scholarsarchive.byu.edu/etd/1343>

This Thesis is brought to you for free and open access by BYU ScholarsArchive. It has been accepted for inclusion in All Theses and Dissertations by an authorized administrator of BYU ScholarsArchive. For more information, please contact [scholarsarchive@byu.edu](mailto:scholarsarchive@byu.edu), [ellen\\_amatangelo@byu.edu](mailto:ellen_amatangelo@byu.edu).

MECHANISMS BY WHICH APOPTOTIC MEMBRANES BECOME  
SUSCEPTIBLE TO SECRETORY PHOSPHOLIPASE A2

by

Rachel W. Bailey

A thesis submitted to the faculty of

Brigham Young University

In partial fulfillment of the requirements for the degree of

Master of Science

Department of Physiology & Developmental Biology

Brigham Young University

April 2008

BRIGHAM YOUNG UNIVERSITY

GRADUATE COMMITTEE APPROVAL

of a thesis submitted by

Rachel W. Bailey

This thesis has been read by each member of the following graduate committee and by majority vote has been found to be satisfactory.

\_\_\_\_\_  
Date

\_\_\_\_\_  
John D. Bell, Chair

\_\_\_\_\_  
Date

\_\_\_\_\_  
Allan M. Judd

\_\_\_\_\_  
Date

\_\_\_\_\_  
William S. Bradshaw

BRIGHAM YOUNG UNIVERSITY

As the chair of the candidate's graduate committee, I have read the thesis of Rachel W. Bailey in its final form and have found that (1) its format, citations, and bibliographical style are consistent and acceptable and fulfill university and department style requirements; (2) its illustrative materials including figures, tables, and charts are in place; and (3) the final manuscript is satisfactory to the graduate committee and is ready for submission to the university library.

---

Date

---

John D. Bell  
Chair, Graduate Committee

Accepted for the Department

---

James P. Porter  
Department Chair

Accepted for the College

---

Rodney J. Brown  
Dean, College of Life Sciences

## ABSTRACT

### MECHANISMS BY WHICH APOPTOTIC MEMBRANES BECOME SUSCEPTIBLE TO SECRETORY PHOSPHOLIPASE A<sub>2</sub>

Rachel W. Bailey

Department of Physiology & Developmental Biology

Master of Science

During apoptosis, changes occur in T-lymphocyte membranes that render them susceptible to hydrolysis by secretory phospholipase A<sub>2</sub> (sPLA<sub>2</sub>). To study the relevant mechanisms, a simplified model of apoptosis using a calcium ionophore was first applied. Kinetic and flow cytometry experiments provided key observations regarding ionophore treatment: initial hydrolysis rate was elevated, total reaction product was increased four-fold, and adsorption of the enzyme to the membrane surface was unaltered. Analysis of these results suggested that susceptibility during calcium-induced apoptosis is limited by substrate availability rather than enzyme adsorption. Fluorescence experiments identified three membrane alterations that might affect substrate access to the sPLA<sub>2</sub> active site. First, intercalation of merocyanine 540 into the membrane was improved, suggesting increased lipid spacing. Second, laurdan detected

increased solvation of the lower head group region of the membrane. Third, the rate at which fluorescent lipids could be removed from the membrane by albumin was enhanced, implying greater vertical mobility of phospholipids. Thus, it was proposed that the apoptotic membranes become susceptible to sPLA<sub>2</sub> through a reduction in lipid-neighbor interactions which facilitates migration of phospholipids into the enzyme active site.

This proposal was then examined in T-lymphocytes treated with glucocorticoid, a more physiologically relevant apoptotic stimulant, using similar techniques. The following observations corresponded to induction of membrane susceptibility: increased merocyanine 540 intercalation; phosphatidylserine flip-flop, detected by annexin binding; and alterations in laurdan fluorescence properties. These observations implied a relationship among sPLA<sub>2</sub> susceptibility, lipid spacing, and phosphatidylserine exposure. To clarify this relationship, additional assays were also performed using dibutyryl-cAMP to induce apoptosis, a drug reported to induce apoptosis in S49 cells without the typical translocation of phosphatidylserine. Our results indicated that in cells treated with dibutyryl-cAMP, the merocyanine 540 response and its correlation with sPLA<sub>2</sub> susceptibility was similar to that observed with dex-treated samples. This suggests that the underlying mechanisms which promote sPLA<sub>2</sub> hydrolysis lead to alterations that may be facilitated by but do not require phosphatidylserine exposure. Taken together, all of the results suggest that direct regulation of the biophysical microenvironment of the membrane is the mode of control of membrane susceptibility to the hydrolytic activity of sPLA<sub>2</sub>.

## ACKNOWLEDGEMENTS

First, I acknowledge my mentor John Bell and committee members William Bradshaw and Allan Judd. I recognize the contributions of fellow graduate students Erin Olson and Jennifer Keller, as well as a host of undergraduate students: Elizabeth Gibbons, Mara Whitworth, Celestine Yeung, Leslie Robertson, Thaothanh Nguyen, Jacob Bell, Ryan Christensen, Kristen H. Parker, Mai Vu, Taylor Brueseke, Summer King, Anne Heiner, Aubrielle Williamsen, and Chisako McLemore. Most importantly, I thank my husband, Chris Bailey, for all of his support.

Two-photon excitation microscopy images were acquired at the Laboratory for Fluorescence Dynamics at the University of California, Irvine. Flow cytometry experiments were conducted with the assistance of Sandra Burnett and Nels Nielson at the BYU Research Instrumentation Core Facility. Confocal microscopy images were collected with the assistance of Michael Stark and Adam Daniels at BYU in the PDBio Microscopy Lab. This work was funded by NIH Grant GM073997, the BYU Cancer Research Center Graduate Summer Fellowship, and the BYU Graduate Studies Research Fellowship.

## TABLE OF CONTENTS

|                       |    |
|-----------------------|----|
| Introduction          | 1  |
| Materials and Methods | 3  |
| Results, Part I       | 8  |
| Discussion, Part I    | 13 |
| Results, Part II      | 18 |
| Discussion, Part II   | 24 |
| Conclusion            | 29 |
| References            | 30 |
| Figure Legends        | 40 |



## LIST OF TABLES

|  |    |
|--|----|
| 1. Parameter values for Fig. 11  | 46 |
| 2. Categories of dex-treated cells by laurdan GP   | 47 |
| 3. Midpoints with 95% confidence intervals for sigmoid fits in Figs.<br>12, 15, 16, and 19 | 48 |

## LIST OF FIGURES

|  |    |
|--|----|
| 1. Effects of ionomycin treatment on the time course of membrane hydrolysis by sPLA <sub>2</sub>                 | 50 |
| 2. Secretory PLA <sub>2</sub> concentration dependence of the initial rate of hydrolysis                         | 51 |
| 3. Reversibility of adsorption of L-PLA <sub>2</sub> to S49 cells  | 52 |
| 4. Concentration dependence of L-PLA <sub>2</sub> adsorption to S49 cells  | 53 |
| 5. Ability of L-PLA <sub>2</sub> to interfere with cell membrane hydrolysis by sPLA <sub>2</sub>                 | 54 |
| 6. Effect of ionomycin treatment on MC540 fluorescence   | 55 |
| 7. Effect of ionomycin treatment on laurdan GP   | 56 |
| 8. Effect of ionomycin treatment on bis-pyrene and DPH fluorescence  | 57 |
| 9. Effect of ionomycin on the rate of NBD-PC extraction by BSA   | 58 |
| 10. Effect of actin disruption on susceptibility to sPLA <sub>2</sub> hydrolytic activity                        | 59 |
| 11. Analysis of hydrolysis results in terms of Scheme 1  | 60 |
| 12. Onset and progression of dex-stimulated susceptibility to sPLA <sub>2</sub> hydrolysis                       | 61 |
| 13. Effect of dex treatment on the rate of NBD-PC extraction by BSA  | 62 |
| 14. The complex progression of the pattern of laurdan GP over cell surface in response to dex treatment          | 63 |
| 15. Effect of dex treatment on MC540 fluorescence intensity measured by spectroscopy                             | 64 |
| 16. Effect of dex treatment on MC540 fluorescence intensity measured by flow cytometry                           | 65 |
| 17. Representative confocal micrographs of MC540 fluorescence intensity  | 66 |
| 18. Effect of ionomycin treatment on histograms of MC540 fluorescence intensity from confocal micrographs        | 67 |
| 19. Correlation between dex-stimulated changes in MC540 and FITC-annexin fluorescence measured by flow cytometry | 68 |

|  |    |
|--|----|
| 20. Example two-dimensional histogram of MC540 and FITC-annexin intensity measured simultaneously by flow cytometry          | 69 |
| 21. Residual plots from linear regression of simulated data with no offset between MC540 and FITC-annexin binding            | 70 |
| 22. Residual plots from linear regression of simulated data with a 3% positive offset between MC540 and FITC-annexin binding | 71 |
| 23. Residual plots from linear regression of simulated data with a 3% negative offset between MC540 and FITC-annexin binding | 72 |
| 24. Comparison of residual plots from actual and simulated data  | 73 |
| 25. Effect of db-cAMP on sPLA <sub>2</sub> susceptibility, MC540 fluorescence intensity, and FITC-annexin binding            | 74 |

## LIST OF SCHEMES

1. Reaction scheme for interaction between sPLA<sub>2</sub> and cell membranes 49

## INTRODUCTION

Apoptosis is a complex process involving numerous alterations to components of the nucleus, cytoplasm and cell membrane (1, 2). Changes occurring at the cell membrane include exposure of phosphatidylserine (PS), ceramide production, microvesicle shedding, membrane blebbing, loss of membrane potential, alterations to cytoskeletal attachments, and loss of membrane integrity (1-9). One of the earliest membrane events documented thus far is a substantial increase in the action of secretory phospholipase A<sub>2</sub> (sPLA<sub>2</sub>) to hydrolyze plasma membrane lipids (9, 10).

Secretory PLA<sub>2</sub>s are calcium-dependent enzymes which hydrolyze the acyl bond in the *sn*-2 position of phospholipids, producing fatty acid and lysophospholipid. This is the first reaction in the synthesis of several lipid-based hormones. Several isoforms have been identified, each with variations in structure, activity, and localization within the body. For example, human group IIA sPLA<sub>2</sub> is highly expressed in inflammatory tissues where the hydrolytic production of arachidonic acid provides substrate for cyclooxygenase 2 and lipoxygenase enzymes, leading to the production of proinflammatory molecules called eicosanoids (11, 12). Human group V may function in innate immunity (13). Elevated concentrations of human isoforms have been detected in several pathological conditions, including sepsis, inflammation, and various cancers and tumors (14). In these roles, sPLA<sub>2</sub> can act both as a signal molecule and as a hydrolytic enzyme. This study focused on the enzyme function of the protein and how it is regulated by physical conditions in the cell membrane.

Isoforms of sPLA<sub>2</sub> have also been isolated from other sources, including the venoms of honeybees and snakes. This study utilized the monomeric aspartate-49 phospholipase A<sub>2</sub> isoform in the venom of *Agkistrodon piscivorus piscivorus* (App D49). This was used as the source of enzyme in this report for several reasons. First, it has been used extensively in previous mechanistic and structural investigations, including studies with erythrocytes and S49 cells (9, 15-26). Second, it is easily purified in large quantities making it convenient for experiments. Third, it behaves similarly to some of the human isoforms of the enzyme during ionomycin-stimulated apoptosis (18).

Secretory PLA<sub>2</sub> has been used extensively for studying enzymatic activity at the water-membrane interface. A key feature of this enzyme is its ability to distinguish between healthy cells, which resist hydrolysis by sPLA<sub>2</sub>, and damaged, necrotic, or apoptotic cells which are often susceptible. Studies with artificial bilayers have demonstrated that the extent to which phospholipids are hydrolyzed by the enzyme depends on specific physical properties and microstructure of the membrane (17, 24-29). It has been proposed that analogous properties also govern the susceptibility of cell membranes (19-22).

A variety of experimental approaches has led to a general concept in which the action of sPLA<sub>2</sub> on the membrane surface involves at least two pre-catalytic steps (15, 17, 23, 27, 30-32). In the first step, sPLA<sub>2</sub> adsorbs to the membrane surface, and in the second, an individual phospholipid migrates into

the active site of the enzyme (Scheme 1). In previous studies, this two-step hypothesis was examined using human erythrocytes as a simplified model for cell membranes (22). For those investigations, the apoptotic state of the cell was mimicked by treatment with ionomycin, a calcium ionophore. The resulting calcium influx produced changes in membrane structure accompanied by increased susceptibility to hydrolysis by sPLA<sub>2</sub>. Analysis of these observations generated the conclusion that the ability of sPLA<sub>2</sub> to attack cell membranes is determined primarily by the ease of vertical migration of phospholipids into the active site of adsorbed enzyme (*i.e.* step two in Scheme 1).

This foundational work from various membrane models has thus generated a testable hypothesis relating bilayer structure and sPLA<sub>2</sub> activity. The ultimate goal is a complete understanding of the biophysical and molecular principles governing this relationship in physiological and pathological settings such as apoptosis. Accomplishing this goal requires experiments with nucleated cells. Given the complexities associated with both apoptosis and cellular models for biophysical studies, I sought an initial experimental system in which measured effects would be synchronous and therefore maximized. Moreover, links to previous mechanistic studies would be plausible. Accordingly, S49 murine lymphoma cells treated with calcium ionophore (ionomycin) were chosen for the first phase of this study because they meet these criteria. Ionomycin stimulates rapid apoptosis that appears synchronized for the majority of the cell population resulting in large and reproducible changes in measured events. Moreover, as in human erythrocytes, the drug induces susceptibility to sPLA<sub>2</sub> that, in S49 cells, occurs with or before other major apoptotic changes (9, 18). The second phase of this study examined S49 cells treated with glucocorticoid in order to extend results from an artificial pharmacological agent to a more physiological stimulus.

Glucocorticoids are a class of steroid hormones that induce apoptosis in various cell types including T-lymphocytes. Apoptotic induction occurs through binding to the cytosolic glucocorticoid receptor (GR). The ligand-receptor complex translocates to the nucleus where it homodimerizes and binds to glucocorticoid response elements (GRE's) found in promoter or enhancer regions of various genes. It is thought that this interaction with GRE's drives transcription of proteins that activate apoptosis (33). While the role of the glucocorticoid-GR complex is well established, the downstream mechanisms are somewhat controversial and appear to vary between cell types (34); moreover, only a few glucocorticoid-induced genes have been reliably identified, including the pro-apoptotic proteins Bim and PUMA (35-37). Interestingly, glucocorticoid-induced cell death does not appear to proceed directly via either of the classical pathways of apoptosis (*i.e.* the mitochondrial or intrinsic pathway and the extrinsic pathway). Nonetheless, both Bcl-2 family proteins and caspases still seem to play roles in glucocorticoid signal transduction (38). In addition to such transcriptional modifications, other so-called non-genomic effects of glucocorticoid have been observed. These non-genomic effects encompass changes that occur too rapidly to be explained by *de novo* protein synthesis, including calcium mobilization and phospholipase C activation. These effects

may involve a poorly defined plasma membrane GR receptor or other non-specific interactions with cellular membranes or unrelated receptors (33, 38).

Nielson et al. characterized certain apoptotic events in S49 cells treated with the glucocorticoid dexamethasone (dex). This investigation found that incubating samples with dex for greater than 24 h stimulated death in nearly 100% of cells (9). Furthermore, while loss of mitochondrial membrane potential, PS exposure, and DNA fragmentation did not change significantly until approximately 20 h, 50% of the maximum susceptibility to sPLA<sub>2</sub> was reached at about 22 h (9). These results demonstrated that enhanced susceptibility is a relatively early event in the time course of apoptosis.

In order to further elucidate the role of PS exposure in dex-stimulated susceptibility to sPLA<sub>2</sub> hydrolytic activity, a third apoptotic stimulus was included. Dibutyl cyclic AMP (db-cAMP), a lipid soluble form of cAMP, induces apoptosis in the S49 cell line and was included in the characterization of pro-apoptotic agents by Nielson et al. (9). According to that report, cells incubated with db-cAMP became increasingly susceptible to sPLA<sub>2</sub> catalysis, similar to dex-treated samples. However, very minimal PS exposure was observed with db-cAMP treatment, suggesting that the mechanisms relating to susceptibility may be independent of PS content in the outer membrane.

In the first phase of this study, experiments were designed to examine each of the parameters shown in Scheme 1 to assess which is/are involved in distinguishing resistant cells from those treated with ionophore. This assessment was accomplished through measurements and analysis of hydrolysis kinetics, enzyme adsorption, and membrane structure. The results demonstrated that modulation of step two ( $K_E$  in Scheme 1) accounted for the increased susceptibility to sPLA<sub>2</sub>. Furthermore, the results in ionomycin-treated samples identified membrane properties and possible mechanistic links between biophysical parameters of membrane structure and vulnerability to sPLA<sub>2</sub> catalysis.

Accordingly, the second phase of this study consisted of assays in which those identified properties were examined in the more physiological setting of glucocorticoid-induced apoptosis. Part two of this study also included experiments with a third apoptotic stimulant, db-cAMP (described above), in order to further investigate the relationship among lipid spacing, PS flip flop, and sPLA<sub>2</sub> hydrolytic activity. Observations in dex-induced apoptotic membranes found strong correlations between specific membrane properties (identified in the ionophore-treated samples) and the onset and progression of sPLA<sub>2</sub> susceptibility.

## **MATERIALS AND METHODS**

### **Reagents**

The monomeric aspartate-49 phospholipase A<sub>2</sub> from the venom of *A. p. piscivorus* was isolated according to the procedure by Maraganore et al. (39).

Ionomycin was purchased from Calbiochem (La Jolla, CA), cytochalasin D was purchased from BIOMOL (Plymouth Meeting, PA), and all were dissolved in dimethylsulfoxide (DMSO). Dibutyl cyclic AMP (db-cAMP) was purchased from BIOMOL and dissolved in deionized distilled water. The probes Oregon Green 488, 2-(6-(7-nitrobenz-2-oxa-1,3-diazol-4-yl)amino)hexanoyl-1-hexadecanoyl-*sn*-glycero-3 phosphocholine (NBD-PC), laurdan, acrylodan-labeled fatty acid-binding protein (ADIFAB), 1,3-Bis-(1-pyrene)propane (bis-pyrene), diphenylhexatriene (DPH), merocyanine 540 (MC540), fluorescein isothiocyanate-conjugated annexin V (FITC-annexin), and propidium iodide (PI) were acquired from Invitrogen (Carlsbad, CA). Bovine serum albumin (BSA) was purchased from Sigma (St. Louis, MO). Probes were dissolved in various solvents as follows: ADIFAB in 50 mM KCl and 3 mM NaN<sub>3</sub>, bis-pyrene and DPH in N,N-dimethylformamide, NBD-PC in ethanol, and all others in DMSO. Other reagents were obtained from standard suppliers.

### Cell culture and experimental protocol

S49 mouse lymphoma cells were grown at 37 °C in humidified air containing 10% CO<sub>2</sub> and prepared for experiments as described (16). Cell viability averaged 89 ± 6% (standard deviation). For spectral and kinetic experiments, an aliquot of cells (usually between 0.4–3.0 × 10<sup>6</sup> cells/ml in MBSS) was then transferred to a quartz fluorometer sample cell and allowed 5 min to equilibrate in the spectrofluorometer (Fluoromax 3, Horiba Jobin-Yvon, Edison, NJ or PC-1, ISS, Champaign, IL). Spectral bandpass varied between 4 and 16 nm depending on the intensity of the probe and instrument sensitivity. Data acquisition over time at multiple wavelengths (ADIFAB, laurdan, and bis-pyrene) was accomplished by rapid sluing of fluorometer mirrors under control of instrument software. Temperature and sample homogeneity were maintained as described previously for spectroscopy experiments (20). Flow cytometry samples were incubated in shaking bath until just prior to data collection. For microscopy experiments, sample temperature was maintained by a heated stage. Most experiments and incubations were performed at 37 °C; some images of laurdan GP in dex-treated samples were collected at room temperature. Classification of cells (into categories described in Results, Part II) from these images did not vary significantly based on temperature. For enzyme adsorption experiments, cells were resuspended in MBSS with 20 mM BaCl<sub>2</sub> in order to inhibit sPLA<sub>2</sub> hydrolytic activity without preventing adsorption (32, 40, 41).

In each procedure where ionomycin was added to cell samples (300 nM final), the experiment was repeated with an equivalent volume of DMSO (0.25% v/v final) added to the cuvette to control for the effects of the solvent. A control for direct effects of ionomycin was also included in assessments of membrane physical properties (see below). For glucocorticoid experiments, cells in culture medium were incubated with dex (100 nM) for 0-48 h; again, each experiment was repeated with an equivalent volume of control solvent (DMSO, 0.02% v/v) added to the culture medium to control for effects of the solvent. For db-cAMP



experiments, cells in culture medium were incubated with db-cAMP (100  $\mu$ M) or an equivalent volume of deionized distilled water for 18 or 30 h.

### Membrane hydrolysis

Release of free fatty acids from cell membranes was assayed in real time with the fatty acid binding protein ADIFAB (excitation, 390 nm; emission, 432 nm and 505 nm). After initiating data acquisition for 100 s, ADIFAB (65 nM final) and ionomycin were added. At 700 s, sPLA<sub>2</sub> (0.7 – 70 nM final) was added and the time course continued for an additional 800 s. Raw data were quantified by calculating the generalized polarization (GP) and fitting to an arbitrary function by nonlinear regression (20). In some cases, hydrolysis were assayed by measurement of the rate of PI (37  $\mu$ M final) uptake by cells due to the action of sPLA<sub>2</sub> as described (16). Previous experiments have demonstrated that assays with ADIFAB and PI give identical results under conditions at which cells are susceptible to the enzyme's catalytic activity (16). Thus, the PI assay was used to assess hydrolysis kinetics only in experiments in which all samples were treated with ionomycin.

Time courses of PI fluorescence were also used to assess the proportion of the cell population susceptible to hydrolysis by sPLA<sub>2</sub> (35 nM) in samples treated with dex or db-cAMP (and their equivalent controls). After data acquisition was initiated, PI, sPLA<sub>2</sub>, and ionomycin were added (with sufficient time between each respective addition for equilibration of the fluorescence signal). Data points between the time of PI addition and ionomycin addition were fit to an arbitrary function by nonlinear regression that allowed quantification of distinct populations of cells in each sample: dead cells susceptible to the enzyme ("dead," *i.e.* those that take up PI prior to enzyme addition) and live cells susceptible to the enzyme ("alive & susceptible," *i.e.* those that take up PI upon enzyme addition). Since apoptotic cells with complete DNA fragmentation become invisible to this assay, the maximum fluorescence signal after ionomycin addition in the control sample was used as a measure of total cells for both the control and the corresponding paired treatment samples. The population of cells with complete DNA fragmentation ("DNA fragmented") was calculated from the difference in expected (*i.e.* the level reached by the control sample, standardized for cell number as described below) and observed maximal signal after ionomycin addition. "Total percent susceptible" was calculated by summing the percentages of the population in the "alive & susceptible", "dead", and "DNA fragmented" categories. To account for variations in cell number, data were normalized to cell count (by light microscopy and hemocytometer) and light scatter values separately. In most experiments both estimates of cell number were available, and the two values were averaged to improve precision. In some cases, only the light scatter data was collected and used.

## Fluorescence spectroscopy of probes of membrane structure

In addition to the “vehicle control” (DMSO) for ionomycin assays, a control experiment was designed to verify that calcium entry into the cell, rather than artifacts resulting from direct effects of ionomycin, was responsible for the observed changes in membrane structure. This control involved incubation of the sample for at least 200 s with the calcium chelator ethylenediaminetetraacetic acid (EDTA; 18 mM final; the pH of the EDTA stock was adjusted to 7.6 at 37 °C to avoid altering sample pH) prior to addition of ionomycin. In every case, the results from this “EDTA control” were indistinguishable from those obtained with the vehicle control. Hence, data from both types of controls are pooled in the presentation of results in Figs. 6-9.

Emission spectra of MC540 (170 nM final) were acquired (excitation, 540 nm; emission, 550–700 nm). Spectra were obtained before the addition of the probe, after equilibration (5 min), and 10 min following addition of ionomycin or control reagent(s). Spectra were analyzed by subtracting the initial spectrum as background and integrating the intensity from 565–615 nm. Effects of ionomycin or control(s) were quantified by calculating the difference in integrated intensity before and after treatment. That difference was divided by the integrated intensity before treatment to account for variations in cell number and lamp intensity. Changes in the wavelength of peak intensity were identified from derivatives of the spectra. In samples treated with dex, db-cAMP, or their equivalent controls, results were quantified from the integrated intensities of spectra as the percent max response (*e.g.*  $I_{\text{dex}} - I_{\text{ionomycin}} / I_{\text{ionomycin}}$ ).

Laurdan and bis-pyrene fluorescence emission was acquired at dual wavelengths in real time. After initiating data acquisition, laurdan (50 nM final; excitation, 350 nm; emission 435 and 500 nm) or bis-pyrene (2.2 μM final; excitation, 344 nm; emission 376 and 480 nm) was added at 100 s. Ionomycin or control reagent(s) was/were included after initial equilibration of cells with the probe (laurdan, 10 min; bis-pyrene, 30 min). The laurdan generalized polarization (GP) and bis-pyrene excimer (480 nm)-to-monomer (376 nm) ratio were calculated from the data as described (20, 42). Background intensity at each wavelength was subtracted from the data prior to calculations.

Data for steady state anisotropy (DPH; excitation, 350 nm; emission, 452 nm) were acquired using Glan-Thompson polarizers in the vertical and horizontal positions. Data were obtained before the addition of the probe to measure background cell fluorescence, after 20 min equilibration with DPH (240 nM final), and 10 min following addition of ionomycin or control reagent(s). Anisotropy was calculated as described (43).

## Phospholipid extraction

The fluorescent phospholipid analog, NBD-PC, was suspended in MBSS immediately prior to experiments as described by Jensen et al. (22). Cell samples were incubated with ionomycin, dex, or control reagent(s) (as in

previous section) for 5 min. NBD-PC (930 nM final) was then introduced and allowed to incorporate into cell membranes (about 30 min). Following this incubation, cells were washed to remove excess probe. Data acquisition (excitation, 485 nm; emission, 535 nm) was then initiated, and BSA (0.7% final) was added for NBD-PC extraction. Apparent extraction rate constants were obtained by fitting the fluorescence intensity data after BSA addition to a double exponential decay function by nonlinear regression.

### **Cytoskeletal disruption**

Cells were incubated with cytochalasin D, an actin inhibitor (10  $\mu$ M final), or control solvent (DMSO, 1% v/v), and sPLA<sub>2</sub> susceptibility was measured with and without ionomycin addition via the PI assay described in Results, Part II (below).

### **Flow cytometry**

Flow cytometry data were collected from 1 ml aliquots of cells in MBSS per sample using a BD FACSCanto flow cytometer (BD Biosciences, San Jose, CA) with an argon laser (Oregon Green and FITC: excitation 488 nm, longpass 502 nm, bandpass filter 515-545 nm; MC540: excitation 488 nm, longpass 556 nm, bandpass filter 564-606 nm).

Adsorption of sPLA<sub>2</sub> to the cell surface of ionomycin-treated samples was assayed by flow cytometry with Oregon Green 488-labeled sPLA<sub>2</sub> (L-PLA<sub>2</sub>). Enzyme labeling was accomplished according to instructions provided with the kit (Invitrogen, Carlsbad, CA). Aliquots of cells (suspended in MBSS containing 20 mM BaCl<sub>2</sub>) were treated with ionomycin or DMSO for 10 min. For isotherm experiments, varying amounts of L-PLA<sub>2</sub> were then added (0.01 – 3  $\mu$ M final), and samples were incubated for an additional 10 min prior to data acquisition. For competition experiments, samples were mixed with various concentrations of sPLA<sub>2</sub> (0.05–1  $\mu$ M final) for 5 min before adding L-PLA<sub>2</sub> (50 nM final), and the incubation was continued an additional 5 min. Samples were then immediately processed in the flow cytometer.

Flow cytometry measurements of MC540 and FITC-annexin fluorescence were also made for samples treated with dex or dbcAMP. In each experiment, samples were treated with dex, DMSO, or ionomycin prior to addition of one or both probes. FITC-annexin labeling was done according to a modified manufacturer protocol (Invitrogen, Carlsbad, CA) in which MBSS was used in place of the reaction buffer provided with the probe. Samples in which MC540 was added (170 nM) were incubated in the dark in a shaking waterbath for 15 min. Samples were then immediately processed in the flow cytometer.

### **Two-photon excitation scanning and confocal microscopy**

Scanning two-photon excitation microscopy images were obtained using an Axiovert 35 inverted microscope (Zeiss, Thornwood, NY) at the Laboratory for

Fluorescence Dynamics (University of California, Irvine) as described previously (20, 44). Laser emission was 940 nm for NBD-PC and 790 nm for Oregon Green 488. For laurdan (250 nM), dual images were collected simultaneously using a beam-splitter and interference filters (Ealing 490 and Ealing 440) with laser emission of 790 nm, and the laurdan concentration was increased to 250 nM to improve image distinction compared to background. For laurdan images of dextrated samples, images of 20 randomly selected fields were collected from each sample.

Confocal microscopy images of MC540 fluorescence were obtained using a FluoView FV300 (Olympus, Center Valley, PA) with a green helium-neon excitation laser (excitation 543 nm). Histograms of intensity per pixel were obtained for confocal images. Histograms from the same experiment (*i.e.* from images collected on the same day, not necessarily the same image) were then combined into one normalized distribution of pixels such that each y value represented the percentage of pixels in all of the combined images at each x value. Image thresholds, contrast, and magnification were internally consistent for all experiments displayed in Fig. 17 and included in the analysis exemplified in Fig. 18, respectively.

## Data analysis & simulations

Data plotting, statistical tests, and linear and nonlinear regression analyses were performed with Prism GraphPad software. Simulations of flow cytometry data were carried out using Microsoft Excel.

## RESULTS, PART I: IONOPHORE-INDUCED APOPTOSIS

### Hydrolysis kinetics

Addition of sPLA<sub>2</sub> to S49 cells previously exposed (10 min) to a control vehicle (DMSO) caused a slight increase in ADIFAB GP followed by a gradual decline, nearly restoring the value to its original level (Fig. 1 curve a). This unusual hydrolysis time course has been shown to represent transient initial hydrolysis followed by re-acylation of the lipids and reincorporation into the membrane (18). In contrast, prior exposure of cells to ionomycin resulted in a large increase in ADIFAB GP that quickly reached a stable plateau (Fig. 1 curve b).

In order to further characterize hydrolysis kinetics, the experiment of Fig. 1 was repeated at various enzyme concentrations. Data were analyzed by nonlinear regression (examples are shown in Fig. 1). From these phenomenological fits, two parameters were determined: the initial rate of hydrolysis and maximum hydrolysis product generated. As displayed in Fig. 2, treatment of cells with ionomycin increased both initial and total hydrolysis at all enzyme concentrations. The maximum hydrolysis rate was  $0.018 \pm 0.004$  GP units  $s^{-1}$  for DMSO-treated samples and  $0.093 \pm 0.011$  GP units  $s^{-1}$  for the ionomycin group. The enzyme concentration at which the hydrolysis rate was one-half the maximum was  $13.5 \pm 7.8$  nM and  $9.4 \pm 3.2$  nM for the two groups,

respectively. Two-way analysis of variance indicated that both the effects of enzyme concentration and ionomycin treatment on the initial hydrolysis rate were highly significant ( $p < 0.0001$ ). A significant interaction ( $p < 0.0001$ ) between the two variables was also observed suggesting that the magnitude of the effect of ionomycin depended on enzyme concentration. The ability of ionomycin treatment to increase total hydrolysis product was also significant ( $p < 0.0001$ ).

### Enzyme adsorption

Initial attempts to quantify adsorption of sPLA<sub>2</sub> to the cell surface involved a conventional centrifugation assay with fluorescently-labeled enzyme (L-PLA<sub>2</sub>) as done previously with erythrocytes (22). However, control experiments suggested that the observed association of enzyme with the cells was not reversible. Analysis of microscopy images indicated that this irreversible interaction reflected endocytosis of the labeled enzyme, a phenomenon previously described for nucleated cells (45-47).

Flow cytometry experiments were designed to distinguish endocytosis of labeled enzyme from reversible adsorption to the cell surface. Cells were treated with ionomycin or DMSO for 5 min. All samples were then mixed with L-PLA<sub>2</sub>, and half of the samples were washed to remove free enzyme. Fig. 3 displays histograms of L-PLA<sub>2</sub> fluorescence intensity per cell in each of these four groups. Most of the data from DMSO-treated samples appeared to originate from a single population of cells (Panel A). The intensity of this group was reduced ten-fold (*i.e.* one log unit along the abscissa) by washing (Panel C), suggesting that this peak represented reversible adsorption of L-PLA<sub>2</sub> to the cell exterior. In unwashed ionomycin-treated samples (Panel B), at least two distinct populations were identified in the histogram of fluorescence intensity. Cells with low fluorescence intensity (Panel B, left arrow) accounted for a majority of the sample yet they only contributed about 20% of the total fluorescence signal. The fluorescence of this population was also reduced ten-fold by washing, similar to the DMSO-treated cells (Panel D, left arrow). In contrast, the high intensity staining was less affected by washing (Panels B and D, right arrow), suggesting that this staining represented internalization of the enzyme (45-47). This irreversibility corroborated observations from 2-photon microscopy (not shown; see previous paragraph). Given that reversible surface adsorption is the relevant phenomenon for interpreting the hydrolysis kinetics, we focused our analysis on the low intensity population.

Fig. 4 displays the amount of reversible surface adsorption of various concentrations of L-PLA<sub>2</sub>. The average apparent equilibrium constant for adsorption of L-PLA<sub>2</sub> to DMSO-treated cells was  $2.5 \times 10^6 \text{ M}^{-1}$ . There was no detectable effect of ionomycin treatment on either the apparent equilibrium constant ( $1.7 \times 10^6 \text{ M}^{-1}$ ,  $p = 0.39$ ) or the maximum number of adsorption sites per cell ( $p = 0.20$ ).

In order to relate these adsorption results to native sPLA<sub>2</sub>, competition experiments were performed. Unlabeled sPLA<sub>2</sub> competed for about 30 to 40% of

the L-PLA<sub>2</sub> adsorption sites at all concentrations within the range tested (0.05–1 μM sPLA<sub>2</sub> with 50 nM L-PLA<sub>2</sub>). This result suggested that more than half of these adsorption sites might not be relevant to hydrolysis by sPLA<sub>2</sub>. The observation that competition was already maximal when the same concentrations of sPLA<sub>2</sub> and L-PLA<sub>2</sub> were used (50 nM) indicated that the enzyme adsorbs more tightly when it is not labeled. This inference is consistent with the relatively high potency of the unlabeled enzyme shown in Fig. 2.

To better estimate the apparent adsorption constant for unlabeled sPLA<sub>2</sub> ( $K_{app}$ ), we took advantage of control observations (not shown) demonstrating that L-PLA<sub>2</sub> is a weak enzyme (possessing  $\leq 1/10$  the activity of sPLA<sub>2</sub>). Accordingly, we repeated the competition experiments using a hydrolysis assay at constant sPLA<sub>2</sub> concentration (70 nM final,  $E_T$  in Eq. 1) in the presence of various amounts of L-PLA<sub>2</sub> (0.05 – 20 μM final,  $L_T$  in Eq. 1). The initial hydrolysis rate data ( $dP/dt$ ) were fit to the following equation with  $\alpha$  as an arbitrary proportionality constant:

$$\frac{dP}{dt} = \frac{\alpha K_{app} E_T}{1 + K_{app} E_T + K_L L_T} \quad (1)$$

We assumed that  $K_L$ , the adsorption constant for L-PLA<sub>2</sub>, was the same at sites of hydrolysis as that estimated for the entire cell in Fig. 4. Results shown in Fig. 5 provide convincing evidence for competition. Analysis of the data by nonlinear regression estimated that  $K_{app}$  equals  $2.7 \times 10^7 \text{ M}^{-1}$ .

## Physical changes in the cell membrane

Previous experiments with erythrocytes revealed several physical changes in the cell membrane that appeared to explain the basis for increased susceptibility to the action of sPLA<sub>2</sub>. These included increases in the spacing among bilayer lipids, the average level of lipid order, and the rate at which fluorescent phospholipids could be extracted from the cell membrane (22). Similar experiments have been included here to test the relevance of those findings to nucleated cells.

### *Phospholipid spacing*

Changes in phospholipid spacing were assessed with MC540, a probe that intercalates between the phospholipid heads in the outer leaflet of cell membranes (48-50). Treatment of cells with ionomycin resulted in a significant increase in MC540 total fluorescence (Fig. 6A) and a red-shift in peak wavelength from about 583 to 586 nm (Panel B) consistent with increased binding of the probe (51). As shown in Panels C and D, these effects were reproducible. Control experiments in which cells were treated with ionomycin in the presence of a calcium chelator (EDTA) demonstrated that these effects were due to calcium influx rather than representing artifacts caused directly by the presence of ionomycin in the membrane. Since EDTA controls were

indistinguishable from DMSO-treated samples, data from both types of controls were pooled in the presentation of results for MC540 and all other probes of membrane physical properties (see legends to Figs. 6-9). These spectral changes in MC540 fluorescence suggested that treatment with ionomycin increased the spacing among membrane phospholipids.

### *Membrane order*

Three fluorescent probes were used to examine the relationship between susceptibility and membrane order. Laurdan intercalates at the level of the glycerol backbones (52). The shape of laurdan's emission spectrum is highly sensitive to the solvent relaxation effect and is quantified as GP (see Materials and Methods). GP varies between -1.0 and 1.0 and has been interpreted to reflect the degree to which lipid molecules are ordered within the membrane (a value of 1.0 denotes a highly ordered membrane in which no solvent relaxation occurs, Ref. 42, 43). Bis-pyrene has traditionally been used to evaluate the level of "fluidity" in the membrane, implying the ability of molecules to diffuse laterally along the bilayer plane (53). More recent experiments exploring the phosphatidylcholine/cholesterol phase diagram indicated that the probe is more sensitive to phospholipid acyl chain order (54). Presumably, bis-pyrene resides deep in the membrane based on the partitioning of the parent compound, pyrene (55). Diphenylhexatriene also locates deep in the membrane (56). The anisotropy of DPH is sensitive to both fluidity (which alters the rotational diffusion rate of the probe) and environmental constraints imposed by the level of chain order (54, 57).

Laurdan GP before and after treatment with ionomycin and subsequent controls are illustrated in Fig. 7. In Panel A, laurdan GP over time is displayed. Ionomycin (added at *arrow*) caused GP values to decrease until reaching a minimum 10 min after treatment. This effect was significant (Panel B). Images collected by two-photon microscopy verified that the changes reported in Fig. 7B were confined to the plasma membrane (Figs. 7C–F). In contrast, no differences in apparent lipid order were identified with either bis-pyrene excimer-to-monomer ratio or DPH steady state anisotropy (Fig. 8).

### *Phospholipid extractability*

Changes in the propensity of phospholipids to migrate vertically in the bilayer were estimated by extraction experiments utilizing NBD-PC, a fluorescent phospholipid analog that inserts into lipid bilayers (22, 58). We used the protein BSA as a lipid acceptor in these experiments. This protocol allowed us to estimate the rate of extraction. As shown in Fig. 9A, time courses of NBD-PC fluorescence following BSA addition were fit to a two-phase exponential decay (with  $t=0$  corresponding to the time of BSA addition), with a rapid initial drop in intensity followed by a gradual decline. An overall rate constant was derived from the regressions and compared for multiple samples (Fig. 9B). Ionophore

treatment generated a reproducible two-fold increase in the rate of NBD-PC extraction.

Initial and final fluorescence intensities often differed between DMSO- and ionomycin-treated samples (generally greater in the ionophore group, not shown). For this reason, the data in Fig. 9A are normalized. We used flow cytometry and two-photon microscopy to address the possibility that intensity differences reflected artifacts (due to the extent of extraction and/or labeling) that might interfere with our analysis. Flow cytometry experiments demonstrated that the amount of fluorophore removed by BSA was comparable between control and treatment groups (89% and 85% respectively, not shown). Two-photon microscopy images revealed that it was common for cells to display labeling of internal compartments in addition to the plasma membrane (more prominent in ionomycin-treated cells; example shown in Figs. 9C–E). Upon BSA addition (between Panels C and D), fluorescence intensity decreased quickly from the perimeter of the cells and more gradually from the interior (Panel D: 2 min after addition, Panel E: 4 min after addition). These experiments convinced us that at least the initial rapid decay of fluorescence intensity, dominant in the analysis shown in Figs. 9A and B, could reasonably be interpreted to represent lipid extraction from the cell membrane.

### **Cytoskeletal disruption**

The drug cytochalasin D was employed to elucidate the role of the actin cytoskeletal network in determining susceptibility to sPLA<sub>2</sub> catalysis. Cytochalasin D is a cell-permeable drug that binds to the barbed end of actin filaments, inhibits both the association and dissociation of subunits, and thus disrupts actin filaments and inhibits actin polymerization (59-61). Cells were incubated for 15-60 min with cytochalasin D or control solvent, and sPLA<sub>2</sub> hydrolytic activity was assessed via the PI assay (see Materials and Methods). Cytochalasin D exposure did not affect the proportion of the population susceptible to the enzyme (Fig. 10,  $p = 0.34$ ). Analysis of the effect of cytochalasin D treatment on the kinetics of PI fluorescence changes upon ionophore addition showed mixed results. While the maximum rate of PI uptake in the presence of sPLA<sub>2</sub> and ionomycin was greater in cytochalasin D treated-samples (data not shown,  $p = 0.02$ ), the half-time of ionomycin response was unchanged by the actin inhibitor (Fig. 10,  $p = 0.55$ ). Interestingly, long incubations with cytochalasin D (*i.e.* long enough for the drug to induce apoptosis, Ref. 62) did not show increased proportion of cells susceptible to sPLA<sub>2</sub> (data not shown). Furthermore, assays of MC540 fluorescence spectroscopy confirmed that cytochalasin D treatment did not increase MC540 fluorescence intensity (data not shown,  $p = 0.48$ ,  $n = 6$ , 3 treatment and 3 control). These results suggested that inhibition of f-actin by cytochalasin D did not significantly affect lipid spacing or the interaction between the membrane surface and sPLA<sub>2</sub>, even in the presence of ionomycin.



## DISCUSSION, PART I: IONOPHORE-INDUCED APOPTOSIS

The goal of this portion of the study was to identify how changes in the cell membrane induced by calcium ionophore treatment might increase the rate of phospholipid hydrolysis by extracellular sPLA<sub>2</sub>. To this end, the model shown in Scheme 1 was used to analyze the results of the kinetic experiments displayed in Fig. 2. The initial rate of lipid catalysis ( $dP/dt$ ) is given by

$$\frac{dP}{dt} = \frac{\beta K_A E_T K_E S_T}{1 + K_A E_T (1 + K_E S_T)} \quad (2)$$

where  $\beta$  is proportional to  $k_{cat}$  and the total number of adsorption sites for the enzyme ( $E_T$ ) (22). It is assumed that  $\beta$  does not change with experimental treatment because alterations to membrane structure would presumably affect reaction steps preceding the catalytic event (see Ref. 22 and discussion below). For simplicity,  $\beta$  is assigned a value of 1.0 GP units s<sup>-1</sup>.  $S_T$  represents the mole fraction of membrane phospholipids available to the enzyme. In previous analyses, it has not been considered separately from  $K_E$  since the two parameters are completely linked in the model (see Eq. 2 and Ref. 22). However, the data of Fig. 2B demonstrate that  $S_T$  is subject to change upon experimental treatment and provide information to quantify the magnitude of that change.  $S_T$  is therefore included specifically as a parameter in Eq. 2 and expressed in relative units (*i.e.* it is assigned a value of 1.0 under control conditions).

As shown in Fig. 11A, the control data from Fig. 2A were well fit by Eq. 2. The value of  $K_A$  ( $6.7 \times 10^7 \text{ M}^{-1}$ ) matched favorably the value estimated from competition with L-PLA<sub>2</sub> ( $2.7 \times 10^7 \text{ M}^{-1}$  in Fig. 5). The effect of ionomycin on the initial hydrolysis rate was evaluated by considering  $S_T$ ,  $K_A$ , and  $K_E$  individually in the fit in order to identify the minimum criteria required by the results (parameter values summarized in Table 1). The data of Fig. 2B indicated that  $S_T$  increased by a factor of about 4.4 with ionophore treatment. Accordingly, Eq. 2 was recalculated maintaining all parameter values from the fit of the control data with the exception of  $S_T$ . The 4.4-fold increase, however, was insufficient to account for the ionomycin data (Fig. 11B). In fact, a reasonable fit was obtained only with a much larger (8.1-fold) increase in  $S_T$ , one that cannot be justified based on the data of Fig. 2B (Fig. 11C). Since  $K_E$  and  $S_T$  are linked in Eq. 2, the dilemma can obviously be resolved by increasing  $K_E$  by a factor of 1.8 in addition to a fixed 4.4-fold increase in  $S_T$  (Fig. 11D). Alternatively, allowing  $K_A$  to vary instead of  $K_E$  was inadequate to accommodate the data (Fig. 11E). The best fit, of course, was obtained when both  $K_A$  and  $K_E$  were allowed to float in combination with the prescribed increase in  $S_T$  (Fig. 11F). This ideal fit corresponded to a 2-fold increase in  $K_E$  (in strong agreement with that of Panel D) coupled with a *reduction* in  $K_A$  by about 16% (corroborating the result in Panel E). Thus, I concluded from this analysis that increased susceptibility following ionomycin treatment has little or nothing to do with the strength of adsorption ( $K_A$ ) and can be explained entirely by increases in the accessibility of lipids to the enzyme active site ( $K_E$  and  $S_T$ ).

It is important to note that the differences between control and treatment curves in Fig. 2A could easily be explained by adjustments to  $k_{cat}$ . Variations in  $k_{cat}$  could be due to either cofactor availability or enzyme conformational change. Since the same medium was used in all data sets, availability of the cofactor calcium was not an issue. Moreover, if changes in membrane microstructure stabilized the transition to an activated enzyme conformation, that stabilization would be reflected by enhanced adsorption of sPLA<sub>2</sub> to the membrane surface. While multiple conformations of sPLA<sub>2</sub> have indeed been observed and may be linked to adsorption and/or substrate binding (63), I have no evidence that adsorption of the enzyme is altered by ionomycin. Therefore, it is unlikely that conformational transitions are affected by ionophore treatment, and the use of a constant value for  $k_{cat}$  (*i.e.* the parameter “ $\beta$ ” in Table 1 and Eq. 2) is appropriate.

It may seem surprising that the affinity of the enzyme to adsorb to the membrane surface ( $K_A$ ) was not altered by ionomycin treatment (Fig. 4). It is well established that calcium influx promotes exposure of anionic PS on the outer surface of the cell membrane (64, 65). In previous studies with ionophore-treated S49 cells, this lipid flip-flop occurred as early as could be detected and corresponded temporally with increased susceptibility to sPLA<sub>2</sub> activity (9). Moreover, the presence of anionic lipids greatly promotes sPLA<sub>2</sub> adsorption in artificial bilayers and some cell types (17, 66-68). Since much of the adsorption of L-PLA<sub>2</sub> observed in Fig. 4 appeared unrelated to membrane hydrolysis (for example, binding to heparin sulfate, Ref. 69), it could be argued that the methods employed to assess  $K_A$  were incapable of discerning relevant changes. For this reason, we applied the kinetic analysis detailed in Fig. 11, which substantiated the idea that differential membrane susceptibility is not determined by variation in enzyme adsorption. Furthermore, experiments in human erythrocytes with an inhibitor of PS translocation supported the conclusion that exposure of anionic lipids was not a requirement for enhanced hydrolysis upon ionomycin treatment (9, 19). This view is supported by studies which indicate that apoptotic stimuli other than ionomycin induced sPLA<sub>2</sub> susceptibility prior to PS exposure in S49 cells (9). Overall, these findings suggest that transbilayer movement of specific phospholipids does not necessarily provide a preferred substrate for the enzyme, nor is flip-flop the primary determinant of membrane vulnerability to sPLA<sub>2</sub>. Nonetheless, loss of membrane asymmetry could possibly alter other properties of the phospholipid bilayer which then render the membrane sensitive to sPLA<sub>2</sub> activity. For example, exposure of PS could contribute to the increased lipid spacing I observed (70).

A caveat to the conclusion that increased membrane susceptibility to sPLA<sub>2</sub> does not result from enhanced enzyme adsorption and/or flip-flop of PS is the fact that the experiments reported here were conducted with enzyme purified from snake venom. Several isoforms of sPLA<sub>2</sub> have been identified which differ in their intrinsic catalytic activity ( $k_{cat}$ ), their affinity for membrane surfaces, and their dependence on the presence of anionic lipids (71). Thus, the degree to which PS exposure and potential differences in  $K_A$  contribute to the level of membrane hydrolysis under different experimental or physiological conditions may well depend on the isoform in question. Nevertheless, previous experiments

with human groups IIa and V sPLA<sub>2</sub> species displayed behavior toward S49 cells that was qualitatively identical to that observed with the snake venom enzyme (18). Therefore, although quantitative differences exist among various sPLA<sub>2</sub> types, the concept that substrate availability contributes, at least in part, to the level of membrane susceptibility probably applies to all of them.

Structural evidence suggests that sPLA<sub>2</sub> acts at the membrane surface with its active site displaced physically from the position normally occupied by bilayer phospholipids (31). If this is true, substrate availability ( $S_T$ ) represents the number of lipids capable of making a vertical movement from their normal position, which, according to the results (Fig. 2B), increases during a sustained calcium influx. Moreover, the larger value of  $K_E$  required to fit the data indicated that this vertical transition also occurred more easily.

I focused my analysis primarily on the initial rate of hydrolysis to avoid concerns about latent hydrolysis of internal bilayers such as the perinuclear membrane (46, 47). Of course, measurement of total hydrolysis would include any internal hydrolysis product generated during the 10 min time frame of the experiment (see Fig. 2B), especially with ionomycin treatment which promoted internalization of L-PLA<sub>2</sub> (see Fig. 3B). Therefore, it may be unreasonable to include the full measured value of  $S_T$  in the analysis with Eq. 2. The observation that the majority of total hydrolysis to be accomplished is complete within about 50 s (Fig. 1) mitigates this concern since this time scale is shorter than that reported for internalization (46, 47). Based on the linkage of  $K_E$  and  $S_T$  in Eq. 2, overestimation of  $S_T$  corresponds to underestimation of  $K_E$ ; thus, changes in  $K_E$  may be greater than was assumed in the analysis detailed in Fig. 11 and Table 1. Regardless of the relative contributions of those two parameters to the effect of ionomycin on the initial rate, the argument that the membrane properties have changed to facilitate availability of substrate (either kinetically,  $K_E$ , or physically,  $S_T$ ) to the active site of the enzyme is still valid. Obviously, the mechanistic basis for increased  $S_T$  in the presence of ionomycin requires additional investigation.

What could account for the increase in substrate access to the enzyme? The fluorescence of three of the five membrane probes we examined changed reproducibly due to ionophore. For example, MC540 bound more easily to the membrane, and laurdan emission was red-shifted consistent with increased penetration of water molecules into the bilayer. These two observations suggest that the membrane surface had become more accommodating to intercalation of contaminating molecules from the aqueous phase. This result, together with an enhanced rate of NBD-PC extraction from the outer leaflet of the cell membrane, implied that the strength of interaction among neighboring phospholipids was diminished by calcium influx. With the loss of favorable interactions coupled with increased hydration of the bilayer, the hydrophobic active site of the enzyme would presumably become a more attractive alternative to the membrane thus enhancing the probability of hydrolysis.

Another possible explanation for the laurdan fluorescence relates to phospholipid chain dynamics. Many studies have suggested that changes in solvent access to laurdan correlate with the level of phospholipid chain order (42,

43, 72-74). The experiments conducted with bis-pyrene and DPH allowed me to examine whether such was the case here since both probes are sensitive to the order of their environment (54). Interestingly, neither probe detected any change associated with ionomycin treatment. Therefore, the average level of phospholipid chain order in the membrane appeared to remain stable during calcium influx, and my interpretation of laurdan fluorescence relating to hydration changes at the membrane surface appears more plausible.

Initially, it may seem counterintuitive to propose that disruptive alterations occurred that were detected readily at the membrane surface without removing constraints on probe motion deep in the bilayer. One possibility is that ionophore treatment generated local regions of high curvature stress in the membrane causing an increase in head group spacing simultaneous with crowding of the chains. Since phospholipid micelles are excellent substrates for sPLA<sub>2</sub> (75), such local curvature could explain the various observations in this report. I also note that changes in lipid spacing can occur without accompanying alterations in lipid order and/or lipid fluidity within liquid-ordered phases in both erythrocytes and artificial membranes (54).

This result (alterations at the surface with no change in chain order) contrasts observations from erythrocytes in which treatment with ionomycin actually increased the average lipid order of the membrane (19-21). Two distinctions between erythrocytes and lymphocytes are helpful in understanding this difference. First, susceptibility to hydrolysis upon ionophore treatment is about six times greater in lymphocytes than in erythrocytes (comparison of data in Fig. 2 to Ref. 19). Logically, one would expect that membrane changes relevant to hydrolysis would also be more prominent in S49 cells. Changes observed in laurdan GP and MC540 fluorescence intensity were enhanced by factors of about 10 (in the opposite direction) and 70, respectively, fulfilling this criterion (comparison of data in this report with raw data used in Ref. 21, 22). Second, microscopic images of erythrocytes revealed that ionomycin-induced alterations in lipid order were confined to specific membrane domains (19, 21). In general, membrane domains in nucleated cells are much smaller than those of erythrocytes (76), making it unlikely that similar observations of increased order in discrete domains would be possible in lymphocytes, especially against the background of a more pronounced membrane hydration described above. Nevertheless, it is important to note that the data described for erythrocytes led to the same conclusion as that inferred here: that increased susceptibility to enzyme hydrolysis is precipitated by a reduction in the strength of lipid-neighbor interactions.

A major remaining question is the means by which ionophore treatment produces membrane changes responsible for elevated sPLA<sub>2</sub> activity. Resolution of this matter will require genetic and biochemical approaches beyond the scope of this study. Nevertheless, possible candidates may be identified from existing reports. The fact that cells rapidly become susceptible to sPLA<sub>2</sub> (*i.e.* within 10 min) during ionomycin-induced apoptosis helps evaluate the possibilities and exclude those events that arise too late (9). One obvious

candidate for linking known apoptotic events with membrane sensitivity to sPLA<sub>2</sub> is the exposure of PS. As discussed above, this event appears unable to explain the increase in membrane hydrolysis, at least for the snake venom enzyme. Membrane blebbing and loss of integrity can also be eliminated as major contributing factors because these events occur much later than the onset of susceptibility (9). The images in Figs. 7 and 9 corroborate the observation with respect to blebbing. The sustained loss of membrane potential associated with ionophore and hormone-induced apoptosis in lymphocytes also appears to occur on a time scale well beyond that relevant to the phospholipase (3, 5).

Ceramide accumulation, through *de novo* synthesis and cleavage of sphingomyelin, is well established as a participant in apoptotic signaling pathways (2). Furthermore, it has been suggested that sphingomyelin inhibits sPLA<sub>2</sub>, and that its removal could therefore promote increased activity of the enzyme (77, 78). The details of ceramide's role in apoptosis vary among cell types (2) and have not yet been characterized in S49 cells. Nonetheless, in prior experiments, treatment of S49 cells with sphingomyelinase did not enhance sPLA<sub>2</sub> activity (18).

In addition to blebbing, apoptotic cells sometimes shed smaller pieces of the plasma membrane known as microvesicles. Such is the case with ionomycin-stimulated S49 cells (18). This microvesiculation appears to be facilitated by both PS exposure and cytoskeletal cleavage, and the vesicles released are susceptible to the enzyme (19, 77, 79-82). These observations raise the question of whether the increase in membrane susceptibility reflects direct hydrolysis of the plasma membrane or instead degradation of released microvesicles. This issue has been addressed extensively in studies of human erythrocytes and S49 cells. In both cases, the conclusion was reached that while microvesicles are attacked by the enzyme, they represent a minor fraction of the total hydrolysis with the remainder representing membranes associated with the cells (18, 19).

Cytoskeletal alterations are more likely candidates for apoptotic events that might alter the membrane's response to sPLA<sub>2</sub> (6-8). Given the sensitivity of various membrane properties to cytoskeletal structure during apoptosis (6), it is reasonable to speculate that the same may be true for the response to sPLA<sub>2</sub>. For example, membrane tension could be highly important in determining the access of lipids to the enzyme active site (30) and certainly would be affected by the arrangement and number of cytoskeletal attachments. Likewise, cytoskeletal elements may regulate the lateral distribution of membrane lipids. Disruption of domain structure upon cytoskeletal rearrangement could free additional substrate for catalysis that previously was inaccessible to the enzyme (thus, the increase in S<sub>7</sub>). Furthermore, cytoskeletal disruption itself can induce apoptosis in thymocytes (62). However, as shown in Fig. 10, short incubations with cytochalasin D did not induce sPLA<sub>2</sub> susceptibility. This suggested that disruption of the actin network alone in S49 cells was not sufficient to render membranes vulnerable to sPLA<sub>2</sub> catalysis. Moreover, cytochalasin D treatment did not accelerate the action of ionomycin. This result implied that, even if actin

disruption is a part of the mechanism whereby ionophore induces susceptibility to the enzyme, it is not the rate limiting step. This does not, however, rule out possible involvement of actin filaments or other cytoskeletal elements in the conversion of cells from resistant to susceptible during the progression of apoptosis. The role of cytoskeletal attachments and dynamics in membrane integrity and resistance to sPLA<sub>2</sub> requires further investigation.

In summary, the results from Part I strongly suggested that membrane hydrolysis by snake venom sPLA<sub>2</sub> is promoted by increased lipid spacing, water penetration into the bilayer, and diminished inter-lipid interactions during ionophore-stimulated apoptosis. These changes appear to enhance hydrolysis by facilitating phospholipid entry into the enzyme's active site rather than by increasing enzyme adsorption to the membrane surface. These observations raised several questions. How do the results for the snake venom enzyme apply to the various human isoforms of sPLA<sub>2</sub>? Are the results relevant to other, more physiological, inducers of apoptosis? What is the temporal relationship among these membrane physical changes, susceptibility to sPLA<sub>2</sub>, and known membrane events during apoptosis, such as the exposure of PS? The first question is beyond the scope of this thesis, but the other two were addressed by studying glucocorticoid- and cAMP-provoked apoptosis.

## **RESULTS, PART II: GLUCOCORTICOID & DIBUTYRYL CYCLIC AMP-INDUCED APOPTOSIS**

### **Time course of sPLA<sub>2</sub> susceptibility**

In order to quantify susceptibility on a percentage basis, a control was developed to identify the maximum level of susceptibility for each sample. Susceptibility was measured using a time course of PI fluorescence in cells pre-treated with dex or DMSO (see Materials and Methods, exemplified in Fig. 12A). Propidium iodide was added at *arrow 1*, and sPLA<sub>2</sub> was added after equilibration with the probe (*arrow 2*). Once the fluorescence signal stabilized after enzyme addition, ionomycin was added (*arrow 3*). The purpose of adding ionomycin was to render any resistant cells remaining in the population susceptible, providing a measure of maximal PI fluorescence intensity that corresponded to 100% of cells staining with the dye. The ability of ionomycin to induce maximal susceptibility was confirmed by repeating the assay with detergent added after ionomycin (data not shown). Percentages of the cell population susceptible or resistant to the enzyme were calculated from each PI time course (see Materials and Methods for details). Fig. 12B illustrates the progression of total susceptibility as a function of percent of cells dead (measured by trypan blue uptake) fit to a sigmoid function by nonlinear regression (midpoint = 45.42% dead ± 3.12%; see Table 3). The sigmoidal relationship between susceptibility and apoptotic cell death reported here agrees with previous observations (9).

Measurement of cell death by trypan blue uptake is more useful for calibrating progress through apoptosis than length of incubation with dex due to intersample variability with respect to the kinetics of the apoptotic response. This

is likely due to asynchronous cell cycling, cell density, and other factors. Therefore, “percent dead” is used in place of “time of incubation” in the display of data throughout the results in Part II. Corresponding measurements of PI fluorescence were obtained for each of the samples included in Figs. 13-16, 18, 25 in order to directly compare physical changes in the membrane and susceptibility to sPLA<sub>2</sub> during glucocorticoid- and dbcAMP-stimulated apoptosis.

## **Physical changes in the cell membrane**

### *Phospholipid extractability*

To determine whether alterations in phospholipid-neighbor interactions were present and contributing to the onset of susceptibility, extraction experiments with NBD-labeled lipids were repeated in dex-treated samples (see Results, Part I for explanation of protocol). The results suggested a trend between dex-induced cell death and NBD-PC extraction rate constant, consistent with observations in ionophore-treated samples (Fig. 13). However, the apparent trend was not significant based on linear regression ( $p = 0.19$ ,  $r^2 = 0.26$ ,  $n = 8$ ). This difficulty in measuring reproducible changes in extraction rate was not surprising since the effect was already small under optimal experimental conditions (*i.e.* during synchronous apoptosis initiated by ionomycin, Fig. 9). Hence, one would anticipate that the effect would be smaller and therefore harder to detect in the heterogeneous mixture intrinsic to dex treatment.

### *Water penetration*

DPH and bis-pyrene experiments did not detect any changes in the membrane interior during ionomycin-induced apoptosis (Fig. 8). Accordingly, laurdan was the only probe of membrane interior that was used to assess the membrane during dex-induced cell death. Initial attempts to monitor laurdan GP by spectroscopy detected no changes in dex-treated samples (data not shown). There are several possible explanations for this observation: there may be no changes during dex-stimulated apoptosis, changes could be very subtle, cells at different points along the apoptotic continuum probably coexist in the same sample, and/or changes in laurdan GP may sequentially change in more than one direction from the initial level.

To explore these possibilities, the spatial distribution of laurdan GP values in dex-treated cell membranes was visualized by two-photon excitation microscopy. This approach allowed laurdan GP to be calculated for individual cells and not averaged for entire samples as in the cuvette. Twenty images were collected for each experiment in order to obtain a representative sample. During the collection and analysis of these images, one major observation was made. Cells could be classified into three distinct categories based on the pattern of GP values across the surface of the cell: “ring,” “mixed,” and “red”. The divisions among categories were evident both through GP values (of the whole cell and the interior) and visual sorting. The numerical distinctions for each category are

summarized in Table 2. Examples of the three categories are displayed in Figs. 14A-D. The cell populations were initially composed mostly of “ring” cells with few “mixed” or “red”. As apoptosis progressed to about 40% dead, there was a rise in “mixed” cells concurrent with a reduction in the proportion of “ring”. Finally, once the population reached 75% dead, “mixed” and “ring” cells both decreased, and “red” became the dominant pattern (displayed in Panel E). This progression suggested that cells start in the “ring” configuration, progress through the “mixed” intermediate, and end in the “red” configuration. The timing of the appearance of “mixed” cells corresponded to the appearance of the “alive & susceptible” population, as illustrated in Panel F.

### *Phospholipid spacing*

Spectroscopic measurements of MC540 fluorescence were obtained to determine whether changes in lipid spacing corresponded with the timing of susceptibility in dex-stimulated apoptosis. Similar to the PI assay (described above), spectra were obtained on each control/treatment sample before and 10 min after ionomycin addition in order to compare dex-induced spectral changes to the maximal response. Fig. 15 displays the results of these experiments. Panel A shows a representative set of spectra from a control sample (black dashed curve), a corresponding sample treated with dex for 24 h (black solid curve), and the dex sample after additional incubation with ionomycin for 10 min (red curve). These results were quantified as the percent of maximal response (described in Materials and Methods) and scaled to the complete range of values for the data set ( $\Delta/\Delta_{\max}$ ). As shown in Panel B, the change in MC540 intensity corresponded to the onset of sPLA<sub>2</sub> activity. This correlation was confirmed by linear regression between  $\Delta/\Delta_{\max}$  and total percent susceptible ( $p < 0.0001$ ,  $r^2 = 0.57$ ,  $n = 68$ ; 35 treatment samples and 33 control samples). Furthermore, the midpoint of the sigmoid fit of  $\Delta/\Delta_{\max}$  was 46.98% dead  $\pm$  6.53%. Since this range overlaps the 95% confidence interval for the total percent susceptible midpoint value, these two processes are statistically indistinguishable (see Table 3).

MC540 fluorescence was also quantified for individual cells using flow cytometry. Examples of histograms of the flow cytometry data are shown in Fig. 19A. These histograms were analyzed by two different methods. First, the mean fluorescence intensity (denoted by the abscissa) was normalized to the maximum mean and graphed as a function of percent dead. Second, a normalized ratio was obtained for each histogram. This ratio was calculated by counting the number of cells in the “response” peak (high intensity fluorescence, region 2 in Panel A) and dividing by the number of cells in the “background” peak (low intensity fluorescence centered around zero, region 1 in Panel A). Unlike the mean, the histogram ratio is independent of fluorescence intensity; it depends only upon the proportion of cells that have migrated from the background to the response peak. Therefore, these two analysis methods (histogram mean and cell ratio) capture different aspects of MC540 fluorescence in the cell population. As demonstrated in Fig. 16A, the mean of the histogram varied sigmoidally with respect to percent of cells dead. More importantly, the midpoint of this fit



(44.41% dead  $\pm$  5.45%) was statistically indistinguishable from those of both MC540  $\Delta/\Delta_{\max}$  (Fig. 15) and total percent of cells susceptible to sPLA<sub>2</sub> (see Table 3). This observation suggested that spectroscopic  $\Delta/\Delta_{\max}$  and mean intensity from the flow cytometry assessments corresponded to each other and reflected the same membrane properties. On the other hand, the second analysis method of flow cytometry data, the histogram cell ratio, did not correspond to these other two measures of MC540 fluorescence. While its relationship to percent dead also appeared to be sigmoidal (Figs. 16B, 19C), the midpoint was delayed to 64.19% dead  $\pm$  5.39%, a statistically robust offset of approximately 20% on the abscissa compared to the other two measures of MC540 response (see Table 3). This intriguing result implies that the two analyses of the flow cytometry data are revealing separate aspects of the membrane properties detected by MC540 during dex-stimulated apoptosis. The nonlinear regression fits for the histogram mean, the cell ratio, and the  $\Delta/\Delta_{\max}$  are overlaid together with the total percent dead in Fig. 16C to visually display these relationships. The midpoints and confidence intervals from these sigmoid fits are also summarized in Table 3.

Images of MC540 fluorescence were also obtained by confocal microscopy. The purpose of these experiments was two-fold: to verify that MC540 was reporting changes in the plasma membrane and not internal compartments and to assess changes in the proportion of high-intensity pixels in the labeled cell membrane in response to apoptotic stimuli. With respect to the first objective, MC540 fluorescence appeared to be well confined to the membrane in control samples. There was some internal staining of cells with the probe at longer incubations with dex (*e.g.* 48 h), although these caused little concern since the focus was on events during the first half of the apoptosis time course. Staining of intracellular membranes also increased during long incubations with ionomycin (*i.e.* greater than 15 min). However, internal staining at only 10 min after ionomycin did not appear to be responsible for spectroscopic results. Furthermore, it was difficult to distinguish internal labeling from changes in the volume and shape of cells and apoptotic bodies in samples which are approaching the endpoint of apoptosis. Example images are displayed in Fig. 17.

The proportion of high intensity pixels was first assessed in ionomycin-treated samples. Normalized pixel values were obtained from histograms of confocal images as described (see Materials and Methods) and plotted as a function of intensity. As shown in Fig. 18, the proportion of low intensity pixels decreased after 5-10 min incubation with ionophore (seen in the reduction in the peak indicated by *arrow 1* in the red data points compared to the gray data points). By default, the decrease in the low intensity peak indicated that those pixels had redistributed to higher intensities (since the area under each curve equals 100%). To statistically assess this redistribution, two analyses were performed. First, histograms of pixel distributions from individual experiments were fit by nonlinear regression to an arbitrary function with fitting parameters that correspond to the maximum y value (*i.e.* the low intensity peak, indicated by *arrow 1*) and the pixel percentage at an intensity value of 2000 (considered the lower boundary of the “higher intensity” region, indicated by *arrow 2*). The ratio

of these two parameters (*i.e.* (ordinate value at *arrow 1*) / (ordinate value at *arrow 2*)) was calculated for each of the samples exemplified in Fig. 18, before and after ionomycin ratios were compared by unpaired Student's t-test ( $p = 0.029$ ,  $n = 6$ ). In the second analysis, the histograms of pixels before and after ionomycin were gated into four bins based on the intensity (*i.e.* 0-1000, 1001-2000, 2001-3000, and 3001-4100). The pixel percentages before and after ionomycin were then compared in each of those four regions by one-way analysis of variance, which found a significant difference in the percentage of pixels in each bin ( $p < 0.0001$ ) and, more meaningfully, a significant interaction between ionomycin treatment and percentage of pixels in each bin ( $p = 0.0071$ ,  $n = 6$ , no matching). This corroborated the first analysis in finding a significant redistribution of pixels from lower to higher intensity levels in apoptotic membranes. This second analysis was repeated in cells treated with dex or DMSO. However, dex samples did not show a redistribution of pixels towards higher intensity values compared to control cells. This may be due to the lack of before-after measurement of the same cell sample as well as to the asynchronous onset of apoptosis in response to dex.

### *PS exposure*

Transbilayer movement of PS to the outer leaflet was evaluated by flow cytometry. Cells treated with dex or DMSO were mixed with FITC-annexin, a fluorescently labeled protein which binds to exposed PS (83). Histograms of FITC-annexin fluorescence were analyzed by the same two methods as the MC540 histograms (described above), and example histograms are displayed in Fig. 19B. An interesting phenomenon was observed in the histograms of FITC-annexin over time of dex incubation. At time points of about 24 h (corresponding to roughly 50% of cells dead), the response peak obtained a maximal intensity (*i.e.* the abscissa value of region 3 in Panel B). However, at longer time points, the maximal intensity receded toward the background peak (*i.e.* region 2 in Panel B). After further inspection, it appeared that this progression and regression was simply due to limited probe as the number of PS binding sites continued to increase. Since probe became limiting, the mean intensity of the histograms is likely not an accurate measure of phospholipid asymmetry during apoptosis, especially towards the end of the apoptosis time course in cell samples. Therefore, only the histogram ratio of FITC-annexin fluorescence intensity was included in the presentation of data and comparisons.

## **Relationship between PS exposure and MC540 fluorescence**

### *Dex treatment*

The relationship between PS exposure and MC540 fluorescence in response to dex treatment was examined with various analyses. First, the histogram ratios of MC540 and FITC-annexin fluorescence (from flow cytometry data, described above) were found to correlate very strongly, quantified by linear regression (data

not shown;  $p < 0.0001$ ,  $r^2 = 0.93$ ,  $n = 31$  treatment samples and 30 controls). The sample size reflected 61 matched pairs in which both probes were added either simultaneously to the same tube or to separate tubes from the same cell culture and incubated parallel to one another. The comparability between the sigmoid fits of the histogram ratios of FITC-annexin and MC540 fluorescence is illustrated by virtually identical midpoints (see Fig. 19C and the last two lines of Table 3). Furthermore, the histogram ratios of MC540 and FITC-annexin displayed relationships that both lagged behind the curve of total percent of cells susceptible to sPLA<sub>2</sub>, as shown in Fig. 19C.

An additional analysis was performed for those samples in which the fluorescence of both probes was assessed simultaneously in cells labeled with MC540 and FITC-annexin. Two-dimensional histograms of the fluorescence from both probes in each cell were plotted and analyzed by linear regression. An example plot with the accompanying linear regression is displayed in Fig. 20A. I found a distinct, nonsymmetrical pattern in the residuals from these linear regressions, exemplified in Panel B. This pattern involved a right-skewed peak above the x-axis and a gradual decreasing slope in the shape of the values below the x-axis.

In order to interpret this pattern in terms of a temporal displacement between MC540 and FITC-annexin fluorescence, simple data simulations were performed in Excel. These simulations generated data for 10,000 cells over the course of apoptosis (simulated by a sigmoid function, verified by data in Figs. 12, 15, 16, and 19) and were analyzed by linear regression to create residual plots. Simulated residual plots were produced for three different situations: one in which the sigmoid midpoint parameter was shared for both probes (*i.e.* no temporal offset, Fig. 21), a second in which the midpoint for MC540 binding narrowly preceded that of FITC-annexin (*i.e.* a positive offset, Fig. 22), and a third in which the midpoint of FITC-annexin binding narrowly preceded that of MC540 (*i.e.* negative offset, Fig. 23). Each of these figures show plots of simulations at 0, 5, 10, and 15% dead (Panels A, B, C, and D, respectively). The simulated data allowed me to distinguish two aspects of the residual shape: the change in shape due simply to the progression into apoptosis (seen in the transition from a residual symmetric about the x axis in Fig. 21A to a tilted but still symmetrical shape in Fig. 21D) and the irregularity due to temporal offset between the binding of the two probes. The simulated data revealed that positive versus negative offset produced two different patterns of residuals. In the positive offset condition (Fig. 22), the residual pattern showed a prominent right-skewed peak above the x-axis. The pattern in the negative offset condition appeared, predictably, to be the mirror image of the positive offset, with the line of symmetry running from the origin to the upper right corner of the graph (*e.g.* compare Fig. 22D to Fig. 23D). In comparing simulated to actual data, it became clear that the residual patterns in actual data more closely resembled the simulated data with a positive offset (exemplified in Fig. 24, which displays Fig. 20B and Fig. 22B side by side for easier comparison). This suggested that MC540 binding precedes PS exposure by a narrow but consistent window in dext-treated cells.

### *Dibutyryl-cAMP treatment*

Assays of PI fluorescence, MC540 spectroscopy, and MC540 and FITC-annexin flow cytometry were repeated in cell samples treated with db-cAMP to further assess the dependence of MC540 fluorescence changes upon PS exposure. As shown in Fig. 25A, the MC540  $\Delta/\Delta_{\max}$  from spectroscopic analysis increased with db-cAMP treatment. The parabolic shape of this response with respect to percent dead qualitatively matched the onset of sPLA<sub>2</sub> susceptibility (as shown in the overlaid curves in Panel B) and the normalized mean from MC540 flow cytometry histograms (Panel C). The MC540 histogram ratio was not a match with the  $\Delta/\Delta_{\max}$ , (black curve in Panel D) similar to the results from the dex assays. Furthermore, the histogram ratio reached only about 0.4 at its highest point. On the other hand, PS exposure measured by the histogram ratio was very low compared to dex-treated samples, as displayed in Panel C (compare the green curve for the db-cAMP samples with the red curve for the dex-samples). These results are complicated but suggest that lipid spacing increases with db-cAMP treatment, that it relates temporally to susceptibility, and that it does not require concomitant PS flip-flop.

## **DISCUSSION, PART II: GLUCOCORTICOID & DIBUTYRYL CAMP-INDUCED APOPTOSIS**

The results from three probes of membrane structure, laurdan, MC540, and FITC-annexin, identified several intriguing correlations between the activity of the enzyme sPLA<sub>2</sub> and the physical state of the membrane. First, micrographs of laurdan GP revealed two distinct populations that emerge as a result of glucocorticoid stimulation: one with decreased lipid order (*i.e.* “mixed” in Fig. 14) and one with increased lipid order (*i.e.* “red” in Fig. 14) with respect to the healthy/untreated state (*i.e.* “ring” in Fig. 14). The fact that the “mixed” population appeared and disappeared over the course of apoptosis suggested that it represents an intermediate state between “ring” and “red”. Even more suggestive of an intermediate state is the fact that the fraction of “mixed” cells in the population corresponded with the “alive & susceptible” group, a group that by definition is transitory between “alive & resistant” and “dead”. All together, these observations strongly suggested that the mechanisms which lead from the “ring” to the “mixed” configuration of lipid order also lead to the transition between resistance and susceptibility in live cells. This inference is supported by similar observations in samples incubated with ionomycin for long time periods (4-5 h). Laurdan GP declined immediately following ionomycin addition, and the transition from “ring” to “mixed” was observed (*e.g.* the change from Fig. 7E to Fig. 7F); after 4 h of incubation, the GP value increased above pre-treatment levels (data not shown). While the mechanisms leading to these fluctuations in laurdan GP require further investigation, clearly the properties which it is reporting are of great importance in the determination of resistance versus susceptibility to the snake venom isoform of sPLA<sub>2</sub>. Moreover, laurdan GP is directly sensitive to penetration of the bilayer by water molecules. Experimental and theoretical data have shown that relative hydrolytic efficiencies of App D49 sPLA<sub>2</sub> of various

synthetic phospholipids depend upon the access of water molecules to the active site afforded by the configuration of the substrate-enzyme complex (84, 85), which corroborates the correlation between increased water penetration and onset of sPLA<sub>2</sub> activity observed in both ionomycin- and dex-treated samples.

The analysis of assays of MC540 fluorescence also found correlations with enzyme activity. Three parameters related to MC540 fluorescence were assessed: changes in the proportion of higher-intensity pixels over the cell surface (from microscopy experiments), total intensity changes ( $\Delta/\Delta_{\max}$  from spectroscopy and the mean intensity from flow cytometry histograms) and changes in the cell population with respect to MC540 fluorescence (ratios from flow cytometry histograms).

The proportion of higher-intensity pixels was evaluated to determine whether increased MC540 fluorescence observed via spectroscopy and flow cytometry was due to increased probe binding or increased quantum yield of probe molecules already bound. This evaluation was accomplished through analysis of histograms of confocal images. The logic used to address this question was as follows. If the rise in total MC540 fluorescence intensity (from spectroscopy) and intensity per cell (from flow cytometry) in response to dex or ionomycin treatment were due solely to increased probe binding, then the shape of the distribution of pixel intensity would not change. If, on the other hand, higher overall intensity involved increased quantum yield of bound probes, the distribution would change so that high-intensity pixels would replace those of lower intensity. Analysis of the histograms revealed an increase in the proportion of pixels in the highest intensity range concomitant with a reduction in the proportion of pixels at lower intensity values in cells treated with ionomycin (see Fig. 18). These observations suggest that increased MC540 fluorescence intensity is due at least in part to increased quantum yield of probes already bound to the membrane, which is indicative of a change in the environment the probe encounters in the membrane (*i.e.* from more solid to more fluid, Ref. 86). Furthermore, visual inspection of the images suggested an increase in the heterogeneity of pixel distribution across the membrane surface in response to apoptotic stimulant.

A caveat to this proposed explanation is that the image resolution is not great enough for individual probes to be resolved or to ensure that individual pixels do not represent multiple probes. Therefore, an alternative explanation of this observation could be that, in apoptotic membranes, the MC540 molecules tend to aggregate together or bind preferentially to discrete sites which are very close together, thus leading to brighter pixels in specific regions of the cell surface. Distinction between these two possibilities would require further experimentation, possibly using the number and brightness analysis developed by Digman et al. (87).

Sigmoid fits of MC540  $\Delta/\Delta_{\max}$  and mean intensity from histograms of MC540 flow cytometry data were almost identical to the fit of the progression of total percent of population susceptible to sPLA<sub>2</sub>, suggesting that both of these measures of MC540 behavior are detecting the same properties and that those

properties are highly relevant to sPLA<sub>2</sub> hydrolytic activity. Furthermore, analysis of confocal microscopy data point to a heterogeneous distribution of higher-intensity pixels, suggesting that lipid spacing is not uniform throughout the plasma membrane. This is corroborated by results with laurdan in erythrocytes and suggests a correlation between the proliferation of boundaries between lipid regions of differing physical properties (88). Moreover, it has been proposed previously that sPLA<sub>2</sub> may be most active at such boundaries (19, 88). Heterogeneity of lipid spacing implies that alterations in the packing of lipids in the outer leaflet are spatiotemporally regulated during the process of apoptosis. However, the cell population changes in MC540 intensity seemed to lag behind the total intensity changes. Fig. 16 illustrates this separation. Apparently, there are two separate phases of membrane alterations to which MC540 is sensitive: an initial increase in intensity in a smaller population of cells followed by shift in the remaining population.

One possible explanation for reduced lipid packing in apoptotic cells is the translocation of PS to the outer leaflet. In fact, MC540 binding has been used as an assay of PS exposure in various published reports (89, 90); moreover, previous studies have found high temporal correlation between these two parameters in different cell types (51, 91). In order to clarify this relationship in dex-treated S49 cells, I included flow cytometry assays in which cells were stained with both MC540 and FITC-annexin. The results displayed in Fig. 19 showed a strong correlation between the ratios of MC540 and FITC-annexin ( $r^2 = 0.93$ ). However, the curves for measures of MC540 total intensity (shown in Fig. 16) clearly show relationships that correspond to total percent susceptible and which *precede* the changes detected by the histogram ratios of either probe. This suggested that the initial phase of MC540 response is independent of PS exposure while the second phase could be linked to loss of membrane asymmetry. That the initial phase of MC540 response is independent was corroborated by analysis of samples labeled with both probes (Fig. 20). MC540 intensity increased slightly before FITC-annexin binding increases in individual cells treated with dex for 2-8 h (confirmed by data simulations, see Figs. 20-24). Furthermore, these analyses also emphasize the initial phase of MC540 response corresponded strongly with sPLA<sub>2</sub> activity, while the second phase and PS exposure appeared to occur too late to be causative of the initial onset of membrane susceptibility in S49 cells.

The temporal separation between the first phase of MC540 response and the second phase of MC540 response (that corresponds to PS exposure) implies that the so-called second phase of MC540 response is more likely a result than a cause of PS exposure, and the first and second phases of MC540 response may not be related to one another. Said differently, if phase two is a continuation of phase one, then the correlation between PS and MC540 phase two is probably *casual*. If the relationship between PS and phase two is *causal*, then the two phases represent independent events since phase one precedes PS exposure.

In order to further clarify this complicated relationship among lipid spacing, PS flip flop, and sPLA<sub>2</sub> activity, flow cytometry and spectroscopy assays of

MC540 and FITC-annexin were repeated in cells treated with db-cAMP. Dibutyl cAMP was selected because previous studies reported that it induces apoptosis in the absence of the characteristic PS exposure (9). Our results confirmed that, indeed, PS translocation is greatly attenuated with db-cAMP compared to dex treatment (compare green curve for db-cAMP to red curve for dex in Fig. 25D). Spectroscopy data showed that MC540  $\Delta/\Delta_{\max}$  reached levels close to that found in dex-treated samples (compare Fig. 25A to Fig. 15B). As in the dex data set, the ratios of MC540 and FITC from the flow cytometry histograms were again very similar, while the histogram mean was a good qualitative match with both the  $\Delta/\Delta_{\max}$  and the total percent susceptible (although the correlations were not as strong as in the dex data set, possibly due to smaller sample size). These experiments provide corroborating evidence suggesting that PS exposure is not a requirement for the change in total MC540 intensity.

The qualification to this logic is that it assumes a proportional relationship between MC540 and PS exposure. The results exemplified in Fig. 20 suggest that MC540 fluorescence intensity precedes FITC-annexin binding in individual cells. However, such an observation does not rule out the possibility that a small amount of PS exposure initiates MC540 binding and/or sPLA<sub>2</sub> activity. Since PS exposure does not appear to be an all-or-none event (based on the steepness of the sigmoid curve in Fig. 19C, red curve), it is impossible to exclude this possibility. Results from cells treated with db-cAMP found a small amount of PS exposure in a reasonable amount of cells; therefore, it is still plausible that low levels of PS exposure facilitate relaxed lipid packing and the ensuing onset of sPLA<sub>2</sub> susceptibility. More detailed studies in which PS exposure is inhibited will be required to definitely establish whether even minimal levels of PS translocation are required for and/or permit altered lipid spacing.

It is important to compare these observations to the existing body of knowledge regarding thymocyte apoptosis. As mentioned above, the alteration in lipid spacing detected by MC540 simultaneous with PS exposure in apoptotic membranes has been previously reported (89, 90). These reports relied on less precise measures of MC540 fluorescence, both in terms of quantitative accuracy and temporal resolution in terms of apoptotic progression in individual samples. Moreover, I was led to re-examine the flow cytometry results reported here because of the discrepancy between the spectroscopic analysis and the histogram ratio data; the combination of spectroscopy, microscopy, and flow cytometry was essential in recognizing that multiple processes appear to be contributing distinguishably to detectable changes in MC540 fluorescence behavior. This report thus represents a novel finding with respect to two phases of MC540 response and the temporal delay between MC540 initial response and the bulk of PS exposure during dex-stimulated apoptosis. However, it is essential to note that the observations described herein may be wholly dependent upon the apoptotic stimulant, as the order of specific apoptotic events has been found to be variable dependent upon the treatment applied (described further below), and caution must be employed in interpreting these results as contradictory to earlier findings.

How do these reported changes in laurdan, MC540, FITC-annexin, and sPLA<sub>2</sub> activity correspond to the timing of other apoptotic hallmarks? Nielson et al. found loss of mitochondrial membrane potential to be a late apoptotic event in dex-treated S49 cells, preceded by sPLA<sub>2</sub> susceptibility, early DNA fragmentation, and PS exposure (9), suggesting that alterations leading to sPLA<sub>2</sub> susceptibility are independent of both mitochondrial signaling and the downstream caspase activation. Since the changes I observed with MC540 and laurdan GP correlated with sPLA<sub>2</sub> susceptibility onset, it is likely that the mechanisms that lead to membrane alterations are likewise independent of mitochondrial signaling. Such independence is supported by experiments with an inhibitor of caspase 3 (an effector caspase), which reported that MC540 and FITC-annexin labeling were both independent of caspase activation in murine splenocytes (92). Preliminary experiments in the Bell lab have also found that a general caspase inhibitor does not attenuate the apoptotic response in ionophore-treated S49 cells (not shown). Moreover, detection of membrane unpacking by MC540 has also been reported to precede DNA cleavage in B cells, T cells, and thymocytes treated with cycloheximide (70).

On the other hand, some studies have shown disruption of mitochondrial integrity to be essential to glucocorticoid-induced cell death (93-96). Still others have found that the so-called non-genomic effects of glucocorticoid signal transduction include translocation of the activated glucocorticoid receptor directly to the mitochondria (97). These disparate findings highlight the ongoing controversy regarding the mechanisms of glucocorticoid-induced apoptosis, the timing of apoptotic events in response to glucocorticoids, and the role of mitochondrial proteins and their supposed downstream targets, caspases (38). Moreover, these discrepancies also reflect the growing understanding that the sequence and interrelation of apoptotic events is dependent upon both cell type and method of apoptotic induction. For example, in murine lymphoid cells, order of apoptotic events and dependence upon caspase activation were reported to be specific to the cell type and apoptotic stimulant (92). In S49.1 cells stimulated with gamma ray irradiation, MC540 and FITC-annexin binding occurred simultaneously, followed shortly by appearance of hypodiploid nuclei, then loss of membrane integrity, and finally fragmentation of DNA. Other studies have also found that PS exposure and DNA fragmentation (which is generally the result of caspase activation of endonucleases, (98, 99) are independent of one another in Jurkat T cells and HL-60 monocytic cells (100). The observations presented here do not appear to be relevant to signals transduced via mitochondrial pathways involving caspase activation. Experiments with caspase inhibitors are currently underway in the Bell lab to confirm whether the changes in membrane biophysical properties induced by both ionophore and dex are dependent upon caspase activity (mentioned above).

This raises the obvious question, then, of what the mechanistic links could be between dex signaling and membrane changes which render the membrane susceptible if not mitochondrial signal transduction. Other possible candidates include cytoskeletal alterations, changes in raft clustering or distribution, and variations in lipid and protein content of the membrane. While none of these



candidates was assessed directly in this portion of the study, existing reports allow plausible inferences to be made. As described in Part I, the cytoskeleton appears to play an important role in certain forms of apoptosis. For example, it is essential to fas-mediated apoptosis (61). Cytoskeletal rearrangement or disruption could certainly affect membrane rigidity and could also be linked to raft redistribution. The heterogeneity of MC540 fluorescence intensity detected by confocal microscopy suggests uneven distribution of lipid properties that is often associated with rafts. The relationship between MC540 binding and raft dynamics is unclear since cholesterol depletion does increase the interaction of MC540 with the membrane surface in erythrocytes (51). The role of cholesterol in the membrane properties assessed here requires further investigation and is difficult to undertake in nucleated cells since cholesterol depletion assays almost surely have confounding effects on cell homeostasis. Furthermore, although snake venom sPLA<sub>2</sub> activity has not been shown to correspond to availability of a preferred lipid substrate (31), change in content of lipids and proteins in membrane could facilitate the altered lipid spacing and hydration reported here, thus leading to increased access of lipid monomers and the nucleophilic reactant (water) to the enzyme's active site. Therefore, while such possibilities require further examination, these new observations provide intriguing evidence that increased sPLA<sub>2</sub> susceptibility corresponds temporally to specific biophysical alterations, including increased lipid spacing and altered membrane hydration.

## **CONCLUSION**

The long-term goal of this line of research is an understanding of the relationship between cell membrane structure and the differential activity of sPLA<sub>2</sub> in physiological settings. To that end, this report applies the model of sPLA<sub>2</sub> action developed by multiple researchers (see Scheme 1) to nucleated cells to test hypotheses derived from erythrocyte studies. Erythrocytes were employed in those prior studies because they offer a simplified, quasi-cellular model devoid of certain experimental complications such as probes binding to intracellular membranes. Fortunately, these complications were addressed here using flow cytometry, confocal microscopy, and two-photon microscopy to assist in the interpretation of the data. The move to lymphocytes was a meaningful step towards a biologically relevant system in which susceptibility to sPLA<sub>2</sub> occurs during physiological processes including apoptosis. Moreover, the inclusion of glucocorticoid-stimulated cell cultures, a system which mimics an endogenous process of apoptosis induction, represents the culmination of much foundational work in artificial and simplified biological membranes. Most importantly, this investigation demonstrated means by which biophysical techniques and information regarding membrane-protein interactions can be applied to studies of nucleated cells.

## REFERENCES

- 1 Arnold, R., D. Brenner, M. Becker, C. R. Frey, and P. H. Krammer. 2006. How T lymphocytes switch between life and death. *Eur. J. Immunol.* 36:1654-1658.
- 2 Taha, T. A., T. D. Mullen, and L. M. Obeid. 2006. A house divided: ceramide, sphingosine, and sphingosine-1-phosphate in programmed cell death. *Biochim. Biophys. Acta* 1758:2027-2036.
- 3 Bortner, C. D., M. Gomez-Angelats, and J. A. Cidlowski. 2001. Plasma membrane depolarization without repolarization is an early molecular event in anti-Fas-induced apoptosis. *J. Biol. Chem.* 276:4304-4314.
- 4 Mann, C. L., C. D. Bortner, C. M. Jewell, and J. A. Cidlowski. 2001. Glucocorticoid-induced plasma membrane depolarization during thymocyte apoptosis: association with cell shrinkage and degradation of the Na(+)/K(+)-adenosine triphosphatase. *Endocrinology* 142:5059-5068.
- 5 Mann, C. L. and J. A. Cidlowski. 2001. Glucocorticoids regulate plasma membrane potential during rat thymocyte apoptosis in vivo and in vitro. *Endocrinology* 142:421-429.
- 6 Martin, S. J., D. M. Finucane, G. P. Amarante-Mendes, G. A. O'Brien, and D. R. Green. 1996. Phosphatidylserine externalization during CD95-induced apoptosis of cells and cytoplasts requires ICE/CED-3 protease activity. *J. Biol. Chem.* 271:28753-28756.
- 7 LeDuc, P. P. and R. R. Bellin. 2006. Nanoscale intracellular organization and functional architecture mediating cellular behavior. *Ann. Biomed. Eng* 34:102-113.
- 8 Coleman, M. L. and M. F. Olson. 2002. Rho GTPase signalling pathways in the morphological changes associated with apoptosis. *Cell Death. Differ.* 9:493-504.
- 9 Nielson, K. H., C. A. Olsen, D. V. Allred, K. L. O'Neill, G. F. Burton, and J. D. Bell. 2000. Susceptibility of S49 lymphoma cell membranes to hydrolysis by secretory phospholipase A(2) during early phase of apoptosis. *Biochim. Biophys. Acta* 1484:163-174.
- 10 Atsumi, G., M. Murakami, M. Tajima, S. Shimbara, N. Hara, and I. Kudo. 1997. The perturbed membrane of cells undergoing apoptosis is susceptible to type II secretory phospholipase A2 to liberate arachidonic acid. *Biochim. Biophys. Acta* 1349:43-54.

- 11 Murakami, M., R. S. Koduri, A. Enomoto, S. Shimbara, M. Seki, K. Yoshihara, A. Singer, E. Valentin, F. Ghomashchi, G. Lambeau, M. H. Gelb, and I. Kudo. 2001. Distinct arachidonate-releasing functions of mammalian secreted phospholipase A2s in human embryonic kidney 293 and rat mastocytoma RBL-2H3 cells through heparan sulfate shuttling and external plasma membrane mechanisms. *J. Biol. Chem.* 276:10083-10096.
- 12 Bayburt, T., B. Z. Yu, H. K. Lin, J. Browning, M. K. Jain, and M. H. Gelb. 1993. Human nonpancreatic secreted phospholipase A2: interfacial parameters, substrate specificities, and competitive inhibitors. *Biochemistry* 32:573-582.
- 13 Kikawada, E., J. V. Bonventre, and J. P. Arm. 2007. Group V secretory PLA2 regulates TLR2-dependent eicosanoid generation in mouse mast cells through amplification of ERK and cPLA2{alpha} activation. *Blood*
- 14 Vadas, P., J. Browning, J. Edelson, and W. Pruzanski. 1993. Extracellular phospholipase A2 expression and inflammation: the relationship with associated disease states. *J. Lipid Mediat.* 8:1-30.
- 15 Sheffield, M. J., B. L. Baker, D. Li, N. L. Owen, M. L. Baker, and J. D. Bell. 1995. Enhancement of Agkistrodon piscivorus piscivorus venom phospholipase A2 activity toward phosphatidylcholine vesicles by lysolecithin and palmitic acid: studies with fluorescent probes of membrane structure. *Biochemistry* 34:7796-7806.
- 16 Wilson, H. A., W. Huang, J. B. Waldrip, A. M. Judd, L. P. Vernon, and J. D. Bell. 1997. Mechanisms by which thionin induces susceptibility of S49 cell membranes to extracellular phospholipase A2. *Biochim. Biophys. Acta* 1349:142-156.
- 17 Henshaw, J. B., C. A. Olsen, A. R. Farnbach, K. H. Nielson, and J. D. Bell. 1998. Definition of the specific roles of lysolecithin and palmitic acid in altering the susceptibility of dipalmitoylphosphatidylcholine bilayers to phospholipase A2. *Biochemistry* 37:10709-10721.
- 18 Wilson, H. A., J. B. Waldrip, K. H. Nielson, A. M. Judd, S. K. Han, W. Cho, P. J. Sims, and J. D. Bell. 1999. Mechanisms by which elevated intracellular calcium induces S49 cell membranes to become susceptible to the action of secretory phospholipase A2. *J. Biol. Chem.* 274:11494-11504.
- 19 Smith, S. K., A. R. Farnbach, F. M. Harris, A. C. Hawes, L. R. Jackson, A. M. Judd, R. S. Vest, S. Sanchez, and J. D. Bell. 2001. Mechanisms by which intracellular calcium induces susceptibility to secretory

- phospholipase A2 in human erythrocytes. *J. Biol. Chem.* 276:22732-22741.
- 20 Harris, F. M., S. K. Smith, and J. D. Bell. 2001. Physical properties of erythrocyte ghosts that determine susceptibility to secretory phospholipase A2. *J. Biol. Chem.* 276:22722-22731.
  - 21 Best, K., A. Ohran, A. Hawes, T. L. Hazlett, E. Gratton, A. M. Judd, and J. D. Bell. 2002. Relationship between Erythrocyte Membrane Phase Properties and Susceptibility to Secretory Phospholipase A2. *Biochemistry* 41:13982-13988.
  - 22 Jensen, L. B., N. K. Burgess, D. D. Gonda, E. Spencer, H. A. Wilson-Ashworth, E. Driscoll, M. P. Vu, J. L. Fairbourn, A. M. Judd, and J. D. Bell. 2005. Mechanisms governing the level of susceptibility of erythrocyte membranes to secretory phospholipase A2. *Biophys. J.* 88:2692-2705.
  - 23 Burack, W. R. and R. L. Biltonen. 1994. Lipid bilayer heterogeneities and modulation of phospholipase A2 activity. *Chem. Phys. Lipids* 73:209-222.
  - 24 Burack, W. R., A. R. Dibble, M. M. Allietta, and R. L. Biltonen. 1997. Changes in vesicle morphology induced by lateral phase separation modulate phospholipase A2 activity. *Biochemistry* 36:10551-10557.
  - 25 Tatulian, S. A. 2001. Toward understanding interfacial activation of secretory phospholipase A2 (PLA2): membrane surface properties and membrane-induced structural changes in the enzyme contribute synergistically to PLA2 activation. *Biophys. J.* 80:789-800.
  - 26 Honger, T., K. Jorgensen, D. Stokes, R. L. Biltonen, and O. G. Mouritsen. 1997. Phospholipase A2 activity and physical properties of lipid-bilayer substrates. *Methods Enzymol.* 286:168-190.
  - 27 Gelb, M. H., M. K. Jain, A. M. Hanel, and O. G. Berg. 1995. Interfacial enzymology of glycerolipid hydrolases: lessons from secreted phospholipases A2. *Annu. Rev. Biochem.* 64:653-688.
  - 28 Berg, O. G., J. Rogers, B. Z. Yu, J. Yao, L. S. Romsted, and M. K. Jain. 1997. Thermodynamic and kinetic basis of interfacial activation: resolution of binding and allosteric effects on pancreatic phospholipase A2 at zwitterionic interfaces. *Biochemistry* 36:14512-14530.
  - 29 Yu, B. Z., M. J. Poi, U. A. Ramagopal, R. Jain, S. Ramakumar, O. G. Berg, M. D. Tsai, K. Sekar, and M. K. Jain. 2000. Structural basis of the

anionic interface preference and  $k_{cat}$  activation of pancreatic phospholipase A2. *Biochemistry* 39:12312-12323.

- 30 Verger, R., M. C. Mieras, and G. H. de Haas. 1973. Action of phospholipase A at interfaces. *J. Biol. Chem.* 248:4023-4034.
- 31 Scott, D. L., S. P. White, Z. Otwinowski, W. Yuan, M. H. Gelb, and P. B. Sigler. 1990. Interfacial catalysis: the mechanism of phospholipase A2. *Science* 250:1541-1546.
- 32 Yu, B. Z., O. G. Berg, and M. K. Jain. 1993. The divalent cation is obligatory for the binding of ligands to the catalytic site of secreted phospholipase A2. *Biochemistry* 32:6485-6492.
- 33 Tuckermann, J. P., A. Kleiman, K. G. McPherson, and H. M. Reichardt. 2005. Molecular mechanisms of glucocorticoids in the control of inflammation and lymphocyte apoptosis. *Crit Rev. Clin. Lab Sci.* 42:71-104.
- 34 Wang, D., N. Muller, K. G. McPherson, and H. M. Reichardt. 2006. Glucocorticoids engage different signal transduction pathways to induce apoptosis in thymocytes and mature T cells. *J. Immunol.* 176:1695-1702.
- 35 Wang, Z., M. H. Malone, H. He, K. S. McColl, and C. W. Distelhorst. 2003. Microarray analysis uncovers the induction of the proapoptotic BH3-only protein Bim in multiple models of glucocorticoid-induced apoptosis. *J. Biol. Chem.* 278:23861-23867.
- 36 Abrams, M. T., N. M. Robertson, K. Yoon, and E. Wickstrom. 2004. Inhibition of glucocorticoid-induced apoptosis by targeting the major splice variants of BIM mRNA with small interfering RNA and short hairpin RNA. *J. Biol. Chem.* 279:55809-55817.
- 37 Han, J., C. Flemington, A. B. Houghton, Z. Gu, G. P. Zambetti, R. J. Lutz, L. Zhu, and T. Chittenden. 2001. Expression of *bbc3*, a pro-apoptotic BH3-only gene, is regulated by diverse cell death and survival signals. *Proc. Natl. Acad. Sci. U. S. A* 98:11318-11323.
- 38 Herold, M. J., K. G. McPherson, and H. M. Reichardt. 2006. Glucocorticoids in T cell apoptosis and function. *Cell Mol. Life Sci.* 63:60-72.
- 39 Maraganore, J. M., G. Merutka, W. Cho, W. Welches, F. J. Kezdy, and R. L. Heinrikson. 1984. A new class of phospholipases A2 with lysine in place of aspartate 49. Functional consequences for calcium and substrate binding. *J. Biol. Chem.* 259:13839-13843.

- 40 Dam-Mieras, M. C., A. J. Slotboom, W. A. Pieterse, and G. H. de Haas. 1975. The interaction of phospholipase A2 with micellar interfaces. The role of the N-terminal region. *Biochemistry* 14:5387-5394.
- 41 Yu, B. Z., J. Rogers, G. R. Nicol, K. H. Theopold, K. Seshadri, S. Vishweshwara, and M. K. Jain. 1998. Catalytic significance of the specificity of divalent cations as  $KS^*$  and  $kcat^*$  cofactors for secreted phospholipase A2. *Biochemistry* 37:12576-12587.
- 42 Parasassi, T., G. De Stasio, G. Ravagnan, R. M. Rusch, and E. Gratton. 1991. Quantitation of lipid phases in phospholipid vesicles by the generalized polarization of Laurdan fluorescence. *Biophys. J.* 60:179-189.
- 43 Harris, F. M., K. B. Best, and J. D. Bell. 2002. Use of laurdan fluorescence intensity and polarization to distinguish between changes in membrane fluidity and phospholipid order. *Biochim. Biophys. Acta* 1565:123-128.
- 44 Yu, W., P. T. So, T. French, and E. Gratton. 1996. Fluorescence generalized polarization of cell membranes: a two-photon scanning microscopy approach. *Biophys. J.* 70:626-636.
- 45 Murakami, M., T. Kambe, S. Shimbara, S. Yamamoto, H. Kuwata, and I. Kudo. 1999. Functional association of type IIA secretory phospholipase A(2) with the glycosylphosphatidylinositol-anchored heparan sulfate proteoglycan in the cyclooxygenase-2-mediated delayed prostanoid-biosynthetic pathway. *J. Biol. Chem.* 274:29927-29936.
- 46 Cho, W. 2000. Structure, function, and regulation of group V phospholipase A(2). *Biochim. Biophys. Acta* 1488:48-58.
- 47 Kim, Y. J., K. P. Kim, H. J. Rhee, S. Das, J. D. Rafter, Y. S. Oh, and W. Cho. 2002. Internalized group V secretory phospholipase A2 acts on the perinuclear membranes. *J. Biol. Chem.* 277:9358-9365.
- 48 Lelkes, P. I., D. Bach, and I. R. Miller. 1980. Perturbations of membrane structure by optical probes: II. Differential scanning calorimetry of dipalmitoyllecithin and its analogs interacting with Merocyanine 540. *J. Membr. Biol.* 54:141-148.
- 49 Lelkes, P. I. and I. R. Miller. 1980. Perturbations of membrane structure by optical probes: I. Location and structural sensitivity of merocyanine 540 bound to phospholipid membranes. *J. Membr. Biol.* 52:1-15.

- 50 Onganer, Y. and E. L. Quitevis. 1994. Dynamics of merocyanine 540 in model biomembranes: photoisomerization studies in small unilamellar vesicles. *Biochim. Biophys. Acta* 1192:27-34.
- 51 Lagerberg, J. W., K. J. Kallen, C. W. Haest, J. VanSteveninck, and T. M. Dubbelman. 1995. Factors affecting the amount and the mode of merocyanine 540 binding to the membrane of human erythrocytes. A comparison with the binding to leukemia cells. *Biochim. Biophys. Acta* 1235:428-436.
- 52 Chong, P. L. and P. T. Wong. 1993. Interactions of Laurdan with phosphatidylcholine liposomes: a high pressure FTIR study. *Biochim. Biophys. Acta* 1149:260-266.
- 53 Melnick, R. L., H. C. Haspel, M. Goldenberg, L. M. Greenbaum, and S. Weinstein. 1981. Use of fluorescent probes that form intramolecular excimers to monitor structural changes in model and biological membranes. *Biophys. J.* 34:499-515.
- 54 Wilson-Ashworth, H. A., Q. Bahm, J. Erickson, A. Shinkle, M. P. Vu, D. Woodbury, and J. D. Bell. 2006. Differential Detection of Phospholipid Fluidity, Order, and Spacing by Fluorescence Spectroscopy of Bis-pyrene, Prodan, Nystatin, and Merocyanine 540. *Biophys. J.* 91:4091-4101.
- 55 Vanderkooi, J. M. and J. B. Callis. 1974. Pyrene. A probe of lateral diffusion in the hydrophobic region of membranes. *Biochemistry* 13:4000-4006.
- 56 Kaiser, R. D. and E. London. 1998. Location of diphenylhexatriene (DPH) and its derivatives within membranes: comparison of different fluorescence quenching analyses of membrane depth. *Biochemistry* 37:8180-8190.
- 57 Wang, S., J. M. Beechem, E. Gratton, and M. Glaser. 1991. Orientational distribution of 1,6-diphenyl-1,3,5-hexatriene in phospholipid vesicles as determined by global analysis of frequency domain fluorimetry data. *Biochemistry* 30:5565-5572.
- 58 Williamson, P., A. Kulick, A. Zachowski, R. A. Schlegel, and P. F. Devaux. 1992. Ca<sup>2+</sup> induces transbilayer redistribution of all major phospholipids in human erythrocytes. *Biochemistry* 31:6355-6360.
- 59 Casella, J. F., M. D. Flanagan, and S. Lin. 1981. Cytochalasin D inhibits actin polymerization and induces depolymerization of actin filaments formed during platelet shape change. *Nature* 293:302-305.

- 60 Verrey, F., P. Groscurth, and U. Bolliger. 1995. Cytoskeletal disruption in A6 kidney cells: impact on endo/exocytosis and NaCl transport regulation by antidiuretic hormone. *J. Membr. Biol.* 145:193-204.
- 61 Jasinska, A., Z. Strakova, M. Szmidt, and A. T. Fazleabas. 2006. Human chorionic gonadotropin and decidualization in vitro inhibits cytochalasin-D-induced apoptosis in cultured endometrial stromal fibroblasts. *Endocrinology* 147:4112-4121.
- 62 Suria, H., L. A. Chau, E. Negrou, D. J. Kelvin, and J. Madrenas. 1999. Cytoskeletal disruption induces T cell apoptosis by a caspase-3 mediated mechanism. *Life Sci.* 65:2697-2707.
- 63 Tatulian, S. A., R. L. Biltonen, and L. K. Tamm. 1997. Structural changes in a secretory phospholipase A2 induced by membrane binding: a clue to interfacial activation? *J. Mol. Biol.* 268:809-815.
- 64 Zhou, Q., J. Zhao, J. G. Stout, R. A. Luhm, T. Wiedmer, and P. J. Sims. 1997. Molecular cloning of human plasma membrane phospholipid scramblase. A protein mediating transbilayer movement of plasma membrane phospholipids. *J. Biol. Chem.* 272:18240-18244.
- 65 Bevers, E. M., P. Comfurius, and R. F. Zwaal. 1983. Changes in membrane phospholipid distribution during platelet activation. *Biochim. Biophys. Acta* 736:57-66.
- 66 Jain, M. K., B. Z. Yu, and A. Kozubek. 1989. Binding of phospholipase A2 to zwitterionic bilayers is promoted by lateral segregation of anionic amphiphiles. *Biochim. Biophys. Acta* 980:23-32.
- 67 Burack, W. R., Q. Yuan, and R. L. Biltonen. 1993. Role of lateral phase separation in the modulation of phospholipase A2 activity. *Biochemistry* 32:583-589.
- 68 Murakami, M., T. Kambe, S. Shimbara, K. Higashino, K. Hanasaki, H. Arita, M. Horiguchi, M. Arita, H. Arai, K. Inoue, and I. Kudo. 1999. Different functional aspects of the group II subfamily (Types IIA and V) and type X secretory phospholipase A(2)s in regulating arachidonic acid release and prostaglandin generation. Implications of cyclooxygenase-2 induction and phospholipid scramblase-mediated cellular membrane perturbation. *J. Biol. Chem.* 274:31435-31444.
- 69 Koduri, R. S., S. F. Baker, Y. Snitko, S. K. Han, W. Cho, D. C. Wilton, and M. H. Gelb. 1998. Action of human group Ila secreted phospholipase A2 on cell membranes. Vesicle but not heparinoid binding determines rate of fatty acid release by exogenously added enzyme. *J. Biol. Chem.* 273:32142-32153.



- 70 Ashman, R. F., D. Peckham, S. Alhasan, and L. L. Stunz. 1995. Membrane unpacking and the rapid disposal of apoptotic cells. *Immunol. Lett.* 48:159-166.
- 71 Singer, A. G., F. Ghomashchi, C. Le Calvez, J. Bollinger, S. Bezzine, M. Rouault, M. Sadilek, M. Lazdunski, G. Lambeau, and M. H. Gelb. 2002. Interfacial kinetic and binding properties of the complete set of human and mouse groups I, II, V, X, and XII secreted phospholipases A2. *J. Biol. Chem.* 277:48535-48549.
- 72 Parasassi, T., G. Ravagnan, R. M. Rusch, and E. Gratton. 1993. Modulation and dynamics of phase properties in phospholipid mixtures detected by Laurdan fluorescence. *Photochem. Photobiol.* 57:403-410.
- 73 Parasassi, T., M. Di Stefano, M. Loiero, G. Ravagnan, and E. Gratton. 1994. Influence of cholesterol on phospholipid bilayers phase domains as detected by Laurdan fluorescence. *Biophys. J.* 66:120-132.
- 74 Parasassi, T., A. M. Giusti, M. Raimondi, and E. Gratton. 1995. Abrupt modifications of phospholipid bilayer properties at critical cholesterol concentrations. *Biophys. J.* 68:1895-1902.
- 75 Verheij, H. M., A. J. Slotboom, and G. H. de Haas. 1981. Structure and function of phospholipase A2. *Rev. Physiol Biochem. Pharmacol.* 91:91-203.
- 76 Parasassi, T., E. Gratton, W. M. Yu, P. Wilson, and M. Levi. 1997. Two-photon fluorescence microscopy of laurdan generalized polarization domains in model and natural membranes. *Biophys. J.* 72:2413-2429.
- 77 Fourcade, O., M. F. Simon, C. Viode, N. Rugani, F. Leballe, A. Ragab, B. Fournie, L. Sarda, and H. Chap. 1995. Secretory phospholipase A2 generates the novel lipid mediator lysophosphatidic acid in membrane microvesicles shed from activated cells. *Cell* 80:919-927.
- 78 Koumanov, K., C. Wolf, and G. Bereziat. 1997. Modulation of human type II secretory phospholipase A2 by sphingomyelin and annexin VI. *Biochem. J.* 326 ( Pt 1):227-233.
- 79 Chang, C. P., J. Zhao, T. Wiedmer, and P. J. Sims. 1993. Contribution of platelet microparticle formation and granule secretion to the transmembrane migration of phosphatidylserine. *J. Biol. Chem.* 268:7171-7178.
- 80 Comfurius, P., J. M. Senden, R. H. Tilly, A. J. Schroit, E. M. Bevers, and R. F. Zwaal. 1990. Loss of membrane phospholipid asymmetry in platelets and red cells may be associated with calcium-induced

shedding of plasma membrane and inhibition of aminophospholipid translocase. *Biochim. Biophys. Acta* 1026:153-160.

- 81 Basse, F., P. Gaffet, and A. Bienvenue. 1994. Correlation between inhibition of cytoskeleton proteolysis and anti- vesiculation effect of calpeptin during A23187-induced activation of human platelets: are vesicles shed by filopod fragmentation? *Biochim. Biophys. Acta* 1190:217-224.
- 82 Vest, R., R. Wallis, L. B. Jensen, A. C. Haws, J. Callister, B. Brimhall, A. M. Judd, and J. D. Bell. 2006. Use of steady-state laurdan fluorescence to detect changes in liquid ordered phases in human erythrocyte membranes. *J. Membr. Biol.* 211:15-25.
- 83 van Engeland, M., H. J. Kuijpers, F. C. Ramaekers, C. P. Reutelingsperger, and B. Schutte. 1997. Plasma membrane alterations and cytoskeletal changes in apoptosis. *Exp. Cell Res.* 235:421-430.
- 84 Peters, G. H., M. S. Moller, K. Jorgensen, P. Ronnholm, M. Mikkelsen, and T. L. Andresen. 2007. Secretory phospholipase A2 hydrolysis of phospholipid analogues is dependent on water accessibility to the active site. *J. Am. Chem. Soc.* 129:5451-5461.
- 85 Linderoth, L., T. L. Andresen, K. Jorgensen, R. Madsen, and G. H. Peters. 2008. Molecular basis of phospholipase A2 activity toward phospholipids with sn-1 substitutions. *Biophys. J.* 94:14-26.
- 86 Stillwell, W., S. R. Wassall, A. C. Dumauual, W. D. Ehringer, C. W. Browning, and L. J. Janski. 1993. Use of merocyanine (MC540) in quantifying lipid domains and packing in phospholipid vesicles and tumor cells. *Biochim. Biophys. Acta* 1146:136-144.
- 87 Digman, M. A., R. Dalal, A. F. Horwitz, and E. Gratton. 2008. Mapping the number of molecules and brightness in the laser scanning microscope. *Biophys. J.* 94:2320-2332.
- 88 Best, K. B., A. J. Ohran, A. C. Hawes, T. L. Hazlett, E. Gratton, A. M. Judd, and J. D. Bell. 2002. Relationship between erythrocyte membrane phase properties and susceptibility to secretory phospholipase A2. *Biochemistry* 41:13982-13988.
- 89 Fadok, V. A., D. R. Voelker, P. A. Campbell, J. J. Cohen, D. L. Bratton, and P. M. Henson. 1992. Exposure of phosphatidylserine on the surface of apoptotic lymphocytes triggers specific recognition and removal by macrophages. *J. Immunol.* 148:2207-2216.

- 90 Callahan, M. K., P. Williamson, and R. A. Schlegel. 2000. Surface expression of phosphatidylserine on macrophages is required for phagocytosis of apoptotic thymocytes. *Cell Death. Differ.* 7:645-653.
- 91 Laakko, T., L. King, and P. Fraker. 2002. Versatility of merocyanine 540 for the flow cytometric detection of apoptosis in human and murine cells. *J. Immunol. Methods* 261:129-139.
- 92 Hess, K. L., J. D. Johnson, and J. M. Cook-Mills. 2001. Different orders for acquisition of apoptotic characteristics by leukocytes. *J. Leukoc. Biol.* 70:405-412.
- 93 Memon, S. A., M. B. Moreno, D. Petrak, and C. M. Zacharchuk. 1995. Bcl-2 blocks glucocorticoid- but not Fas- or activation-induced apoptosis in a T cell hybridoma. *J. Immunol.* 155:4644-4652.
- 94 Huang, S. T. and J. A. Cidlowski. 2002. Phosphorylation status modulates Bcl-2 function during glucocorticoid-induced apoptosis in T lymphocytes. *FASEB J.* 16:825-832.
- 95 Mann, C. L., F. M. Hughes, Jr., and J. A. Cidlowski. 2000. Delineation of the signaling pathways involved in glucocorticoid-induced and spontaneous apoptosis of rat thymocytes. *Endocrinology* 141:528-538.
- 96 Susin, S. A., H. K. Lorenzo, N. Zamzami, I. Marzo, B. E. Snow, G. M. Brothers, J. Mangion, E. Jacotot, P. Costantini, M. Loeffler, N. Larochette, D. R. Goodlett, R. Aebersold, D. P. Siderovski, J. M. Penninger, and G. Kroemer. 1999. Molecular characterization of mitochondrial apoptosis-inducing factor. *Nature* 397:441-446.
- 97 Sionov, R. V., S. Kfir, E. Zafir, O. Cohen, Y. Zilberman, and E. Yefenof. 2006. Glucocorticoid-induced apoptosis revisited: a novel role for glucocorticoid receptor translocation to the mitochondria. *Cell Cycle* 5:1017-1026.
- 98 Loeffler, M. and G. Kroemer. 2000. The mitochondrion in cell death control: certainties and incognita. *Exp. Cell Res.* 256:19-26.
- 99 Nagata, S. 2000. Apoptotic DNA fragmentation. *Exp. Cell Res.* 256:12-18.
- 100 Bratton, D. L., V. A. Fadok, D. A. Richter, J. M. Kailey, L. A. Guthrie, and P. M. Henson. 1997. Appearance of phosphatidylserine on apoptotic cells requires calcium- mediated nonspecific flip-flop and is enhanced by loss of the aminophospholipid translocase. *J. Biol. Chem.* 272:26159-26165.

## FIGURE LEGENDS

**SCHEME 1** Reaction scheme for interaction between sPLA<sub>2</sub> and cell membranes.  $E$ , free sPLA<sub>2</sub>;  $E_B$ , sPLA<sub>2</sub> adsorbed to membrane surface sites ( $M_S$ );  $S$ , available substrate (membrane phospholipid);  $E_B^S$ , adsorbed enzyme with substrate bound to the active site;  $K_A$ , equilibrium constant for enzyme adsorption to the membrane;  $K_E$ , equilibrium constant for substrate migration into the enzyme active site;  $k_{cat}$ , turnover number for substrate hydrolysis;  $P$ , product (fatty acid).

**FIGURE 1** Effects of ionomycin treatment on the time course of membrane hydrolysis by sPLA<sub>2</sub>. S49 cells were incubated with ADIFAB and treated for at least 600 s with DMSO (curve a) or ionomycin (curve b) as explained in Materials and Methods. At the time indicated by the *arrows*, sPLA<sub>2</sub> (70 nM final) was added. Data points represent the raw data (expressed in GP units), and curves represent nonlinear regression fits of the data using an arbitrary function consisting of the sum of two exponential functions. The amount of hydrolysis observed in curve a constitutes approximately 2–5% of the plasma membrane phospholipid (18).

**FIGURE 2** Secretory PLA<sub>2</sub> concentration dependence of the initial rate of hydrolysis. Panel A: the experiments of Fig. 1 were repeated at the indicated concentrations of sPLA<sub>2</sub> for cells treated with DMSO (squares) or ionomycin (triangles). The initial rate was defined as the amount of product generated during 5 s from the time of enzyme addition. This number was calculated from nonlinear regression fits of the data as shown in Fig. 1. Data were analyzed by two-way analysis of variance to assess the contribution of sPLA<sub>2</sub> concentration (37% of variation,  $p < 0.0001$ ), ionomycin treatment (13% of variation,  $p < 0.0001$ ), and the interaction between the two (20% of variation,  $p < 0.0001$ ). Data points represent the raw data (expressed in GP units), and curves represent nonlinear regression fits of the data using an arbitrary function. Panel B: the total amount of product after 600 s (or at the maximum for time courses shaped like that of curve a in Fig. 1) for enzyme concentrations  $\geq 18$  nM. The data were significant based on two-tailed unpaired Student's *t* test ( $p < 0.0001$ ,  $n = 1-4$  at each datum).

**FIGURE 3** Reversibility of adsorption of L-PLA<sub>2</sub> to S49 cells. Data represent histograms for Oregon Green fluorescence intensity obtained by flow cytometry as explained in Materials and Methods. Panels A and B: Cells were treated with DMSO (A) or ionomycin (B) for 5 min followed by 5 min incubation with 1  $\mu$ M L-PLA<sub>2</sub>. Samples were then transferred immediately to the flow cytometer. Panels C and D: The experiments of Panels A (C) and B (D) were repeated as stated except that cells were separated from the supernatant by centrifugation and washed in fresh MBSS with 20 mM BaCl<sub>2</sub> prior to flow cytometry. In Panels B and D, the left arrow indicates the low intensity, reversible staining of cells with L-PLA<sub>2</sub>, and the right arrow indicates the high intensity staining that was not removed by washing (explained in Results).

FIGURE 4 Concentration dependence of L-PLA<sub>2</sub> adsorption to S49 cells. Panel A: The experiments of Figs. 3A and B were repeated at the indicated concentrations of L-PLA<sub>2</sub>. The amount of adsorbed L-PLA<sub>2</sub> was estimated from the fluorescence intensity represented by the mode of the low-intensity peak in the flow cytometry histograms (e.g. as indicated by the left arrow in Fig. 3B). Data (squares: DMSO; triangles: ionomycin) were fit by nonlinear regression to a standard Langmuir binding isotherm function. Panel B: values for an apparent adsorption constant ( $K_L$ ) and the maximum adsorption at saturation ( $A_{max}$ ) were obtained from fits such as those shown in Panel A for four independent experiments. The data for DMSO and ionomycin-treated samples were compared by two-tailed paired Student's t test. Adsorption constant:  $p = 0.39$ ; maximum adsorption:  $p = 0.20$ . Data are expressed as mean  $\pm$  SE.

FIGURE 5 Ability of L-PLA<sub>2</sub> to interfere with cell membrane hydrolysis by sPLA<sub>2</sub>. Cells were treated 400 s with ionomycin and then subjected to hydrolysis by 70 nM sPLA<sub>2</sub>. Hydrolysis was assayed using propidium iodide (see Materials and Methods). The relative hydrolysis rate was calculated as the inverse of the half-time for uptake of propidium iodide by the cells (16). The experiment was repeated in the presence of the indicated concentrations of L-PLA<sub>2</sub>. The data were fit by nonlinear regression to Eq. 1 as described in Results.

FIGURE 6 Effects of ionomycin treatment on MC540 fluorescence. Panel A: Representative emission spectra showing the intensity of MC540 bound to S49 cells before (solid curve, labeling details explained in Materials and Methods) and 10 min after ionomycin addition (dashed curve). Panel B: Spectra displayed in panel A were normalized to their respective maximum intensities. The change in MC540 fluorescence intensity (Panel C, quantified as described in Materials and Methods) and shift in wavelength of emission maximum (Panel D) were compared for controls (vehicle and EDTA controls; see Materials and Methods) and ionomycin-treated samples by two-tailed unpaired Student's t test. Data are expressed as mean  $\pm$  SE. Panel C:  $p < 0.0001$ ; Panel D:  $p = 0.005$ ;  $n = 6$  (Controls) or  $n = 3$  (Ionomycin).

FIGURE 7 Effect of ionomycin on laurdan GP. Panel A: Cells labeled with laurdan were treated without (curve a, vehicle control) or with ionomycin (curve b) at the arrows. 30 points prior to arrow were averaged for each experiment and pooled in the "Before Treatment" group ( $n = 12$ ) in Panel B. "Controls" ( $n = 6$ ) and "Ionomycin" ( $n = 6$ ) groups represent the average of 30 points after stabilization of the fluorescence signal. Data are expressed as mean  $\pm$  SE and analyzed by one-way analysis of variance with Bonferroni's Multiple Comparison Post Test ( $p < 0.0001$  overall; Before Treatment compared to Controls:  $p > 0.05$ ; Before Treatment compared to Ionomycin:  $p < 0.001$ ; Controls compared to Ionomycin:  $p < 0.001$ ). Panels C–F: Two-photon images of S49 cells were collected before and after incubation with ionomycin in the absence or presence of EDTA (as a control). In each image, the left half displays a broad range of GP values from  $-0.1$  (white) to  $0.62$  (dark gray), and the right half displays the same image with a basement threshold of  $0.1$  so that only pixels corresponding to high

GP values are shown. Panel C: EDTA, Panel D: EDTA + ionomycin, Panel E: normal calcium, panel F: normal calcium + ionomycin.

FIGURE 8 Effect of ionomycin on bis-pyrene and DPH fluorescence. Panel A: Time course of bis-pyrene excimer-to-monomer ratio; ionomycin was added at the *arrow*. Panel B: Cells were labeled with DPH as explained in Materials and Methods, and anisotropy measurements obtained before ( $n=10$ , all samples pooled) and after treatment with control reagent(s) ( $n=6$ ) or ionomycin ( $n=4$ ). Data are expressed as mean  $\pm$  SE and were not significant based on one-way analysis of variance ( $p = 0.61$ ).

FIGURE 9 Effect of ionomycin on the rate of NBD-PC extraction by BSA. Panel A: time course of NBD-PC fluorescence in samples treated with ionomycin (gray) or control reagent(s) (black) with  $t=0$  corresponding to the time of BSA addition. Data points are normalized to the maximum and minimum fluorescence intensity, and curves are two-phase exponential decay fits. Panel B: The rate constant obtained from these fits for controls ( $n=7$ ) and ionomycin-treated ( $n=5$ ) samples were compared by two-tailed unpaired Student's  $t$  test. Data are expressed as mean  $\pm$  SE ( $p = 0.003$ ). Panels C–E: Two photon images of an S49 cell labeled with NBD-PC and treated with ionomycin before (C), 2 min after (D), and 4 min after (E) addition of BSA.

FIGURE 10 Effect of actin disruption on susceptibility to sPLA<sub>2</sub> hydrolytic activity. Cells were treated with cytochalasin D as explained in Materials and Methods, and values presented were obtained from analysis of PI time courses as described (see Materials and Methods and Results, Part II, "Time course of sPLA<sub>2</sub> susceptibility"). White Columns (graphed on left axis): "% Alive & Susceptible" values were calculated in samples treated with cytochalasin D or DMSO (Control). Columns analyzed by two-tailed paired Student's  $t$  test ( $p = 0.34$ ,  $n = 9$ ). Gray columns (graphed on right axis): half time values were calculated as 50% of the time to reach maximal fluorescence from baseline fluorescence upon addition of ionomycin in the presence of sPLA<sub>2</sub>. Columns analyzed by two-tailed paired Student's  $t$  test ( $p = 0.55$ ,  $n = 9$ ).

FIGURE 11 Analysis of hydrolysis results in terms of Scheme 1. Initial sPLA<sub>2</sub> hydrolysis rates from Fig. 2A were fit by nonlinear regression to Eq. 2 multiple times with various combinations of constraints. Panel A: baseline parameter values were obtained by fitting the control (DMSO) data from Fig. 2A; parameter values are listed in the first row of Table 1. Some parameters were allowed to float in fits of the ionomycin data (Panels B–F) as detailed below.  $S_T$  was fixed at 1.0 GP units in Panel A and at 4.66 GP units with the ionomycin data (except in Panel C) as explained in the text. The remaining parameters were kept fixed at the values obtained in Panel A (details in rows 2–6 of Table 1). The parameters allowed to float during the fits for each panel were: Panel B: none, Panel C:  $S_T$ , Panel D:  $K_E$ , Panel E:  $K_A$ , Panel F:  $K_E$  and  $K_A$ .

FIGURE 12 Onset and progression of dex-stimulated susceptibility to sPLA<sub>2</sub> hydrolysis. Panel A: Representative time course of propidium iodide fluorescence. Cells were incubated with dex for 24 h. Propidium iodide added at

arrow 1, sPLA<sub>2</sub> added at arrow 2, and ionomycin added at arrow 3. Three cell populations were quantified from these time courses: cells that were already dead and thus susceptible (increase from a to b, due to immediate uptake of PI); cells that were alive and susceptible (increase from b to c, due to additional uptake upon sPLA<sub>2</sub> hydrolysis); and cells that were alive and resistant to sPLA<sub>2</sub> activity (increase from c to d, due to ionomycin treatment). In each case the changes in fluorescence in these intervals was compared to the total fluorescence increase (increase from a to d) after ionomycin addition. See Materials and Methods for further explanation. Panel B: Total percentage of cell population susceptible to hydrolysis by sPLA<sub>2</sub> as a function of percent dead in each sample, measured by trypan blue uptake. Data points were fit to a variable slope sigmoid function with bottom and top fixed at 0 and 100. See Table 3 for relevant fit parameters.

FIGURE 13 Effect of dex treatment on the rate of NBD-PC extraction by BSA. Extraction experiments were carried out in cell samples treated with dex or DMSO as described in Fig. 9 and exemplified in Fig. 9A. Rate constants obtained from fitting time courses to 1-phase exponential decay function by nonlinear regression, with  $t=0$  at BSA addition. Normalized change in rate constant was calculated for each matched treatment-control pair by:  $(k_{\text{dex}} - k_{\text{DMSO}})/k_{\text{DMSO}}$ . These values were plotted as a function of percent dead in dex sample.

FIGURE 14 The complex progression of the pattern of laurdan GP over cell surface in response to dex treatment. Cells were incubated with DMSO for 24 h (Panel A) or with dex for 6 h (Panel B), 24 h (Panel C), or 48 h (Panel D) were labeled with laurdan, and images of laurdan GP were obtained by two-photon excitation microscopy. Cells were classified into three categories: “ring” (e.g. cell 1), “mixed” (e.g. cell 2), or “red” (e.g. cell 3). Panel E: Fraction of population in each category (“red” in red, “ring” in black, and “mixed” in blue) as a function of percent dead. 20 random images were obtained from each of the 25 cell samples included. “Red” and “ring” data points were fit to a variable slope sigmoid function (red and black curves, respectively). Midpoints from sigmoid fits with 95% confidence intervals: 57.64% dead  $\pm$  13.77% (red); 56.43% dead  $\pm$  16.19% (ring). Panel F: Data points for the “mixed” fraction from Panel E (blue, plotted on left y axis) with the percent of cells alive and susceptible to the enzyme (from assays of PI fluorescence described in Materials and Methods and the legend to Fig. 12; gray, plotted on right y axis). Corresponding curves represent Gaussian fits of the data points.

FIGURE 15 Effect of dex treatment on MC540 fluorescence intensity measured by spectroscopy. Panel A: Normalized emission spectra of MC540 bound to cells after 24 h treatment with control solvent (dashed black), 24 h treatment with dex (solid black), and after incubation with ionomycin (red). Ionomycin treatment induces a maximal response in terms of increased MC540 fluorescence emission; therefore, spectra were collected for each sample before and after ionomycin treatment in order to compare each sample to its respective maximum possible response. Panel B: Percent  $\Delta/\Delta_{\text{max}}$  MC540 response is plotted as a

function of percent dead. The y axis was quantified as described in Materials and Methods. Data were fit to a variable slope sigmoid function (black curve) with bottom and top fixed at 0 and 100. See Table 3 for relevant fit parameters. Blue dashed curve is an overlay of the fit from Fig. 12B to compare MC540 fluorescence changes to total percentage of cell population susceptible to hydrolysis by sPLA<sub>2</sub>.

FIGURE 16 Effect of dex treatment on MC540 fluorescence intensity measured by flow cytometry. Mean intensities (Panel A) and normalized ratios (Panel B) of flow cytometry histograms of MC540 fluorescence intensity (from histograms exemplified in Fig. 18A) versus percent dead. Data were fit to a variable slope sigmoid function (black and red curve, respectively) with bottom and top fixed at 0 and 100 (Panel A) or 0 and 1.0 (Panel B). Panel C provides an overlay of the fits from Panels A and B along with the fit from Fig. 12B (blue dashed curve) to compare MC540 fluorescence changes to total percentage of cell population susceptible to hydrolysis by sPLA<sub>2</sub>. See Table 3 for relevant fit parameters.

FIGURE 17 Representative confocal micrographs of MC540 fluorescence intensity. Cells incubated 12 h with dex then labeled with MC540 and imaged before (Panel A) and 10 min after (Panel B) addition of ionomycin. Equivalent controls with 12 DMSO before (Panel C) and after (Panel D) ionomycin.

FIGURE 18 Effect of ionomycin treatment on histograms of MC540 fluorescence intensity from confocal micrographs. Representative histograms from one experiment are displayed. Y axis represents percentage of pixels at each intensity value, calculated as described (see Materials and Methods). Histograms were calculated for images taken before (red squares) and 5-10 min after ionomycin addition (gray triangles). Each histogram includes pixels from multiple images captured before and after addition of ionophore. Data were fit by nonlinear regression to an arbitrary function (overlaid black curves). Arrows approximately indicate x values used to calculate ratios for statistical comparison as detailed in Results, Part II.

FIGURE 19 Correlation between dex-stimulated changes in MC540 and FITC-annexin fluorescence measured by flow cytometry. Panels A and B: Representative histograms of MC540 (Panel A) or FITC-annexin fluorescence (Panel B) in control samples (24 h DMSO, grey curves), 24 h dex samples (solid curves; black, MC540; red, FITC-annexin), and 48 h dex samples (dashed curves; black, MC540; red, FITC-annexin). Regions indicated by brackets and numbers represent the response peak (region 2 in Panel A, regions 2 and 3 in Panel B) and the background peak (region 1 in both panels) used to calculate the cell ratio described in Results, Part II. Panel C: Normalized ratios of histograms for MC540 (black) and FITC-annexin (red) as a function of percent dead. Ratios were quantified as described in Results, Part II, "Phospholipid spacing". Data were fit to a variable slope sigmoid function with bottom and top fixed at 0 and 1. See Table 3 for relevant fit parameters. Blue dashed curve is an overlay of the fit from Fig. 12B to compare ratios to total percentage of cell population susceptible to hydrolysis by sPLA<sub>2</sub>.



FIGURE 20 Example two-dimensional histogram of MC540 and FITC-annexin intensity measured simultaneously by flow cytometry. Panel A: MC540 fluorescence intensity as a function of FITC-annexin intensity per cell from an 8 h dex-treated sample labeled with both probes. Line represents linear regression. Panel B: Residual plot of the linear regression from Panel A.

FIGURE 21 Residual plots from linear regression of simulated data with no offset between MC540 and FITC-annexin binding. Simulations were run at different points along the apoptotic sigmoid progression: 0% dead (Panel A, *i.e.* control), 5% dead (Panel B), 10% dead (Panel C), and 15% dead (Panel D).

FIGURE 22 Residual plots from linear regression of simulated data with a 3% positive offset between MC540 and FITC-annexin binding. 3% positive offset refers to the midpoint of the sigmoid function being set at 17% for MC540 and 20% for FITC-annexin. Simulations were run at different points along the apoptotic sigmoid progression: 0% dead (Panel A, *i.e.* control), 5% dead (Panel B), 10% dead (Panel C), and 15% dead (Panel D).

FIGURE 23 Residual plots from linear regression of simulated data with a 3% negative offset between MC540 and FITC-annexin binding. 3% negative offset refers to the midpoint of the sigmoid function being set at 23% for MC540 and 20% for FITC-annexin. Simulations were run at different points along the apoptotic sigmoid progression: 0% dead (Panel A, *i.e.* control), 5% dead (Panel B), 10% dead (Panel C), and 15% dead (Panel D).

FIGURE 24 Comparison of residual plots from actual and simulated data. Panel A: Same as Fig. 20A. Panel B: Same as Fig. 22B.

FIGURE 25 Effect of db-cAMP on sPLA<sub>2</sub> susceptibility, MC540 fluorescence intensity, and FITC-annexin binding. Panel A: Percent  $\Delta/\Delta_{\max}$  MC540 response is plotted as a function of percent dead. For explanation of how this was calculated, see the legend to Fig. 15 and Materials and Methods. Data points were fit to an arbitrary function (one-site binding hyperbola,  $K_d = 6.04\% \pm 5.90\%$ ). Panel B: Total percent susceptible is plotted on the left y axis. Data points were fit to an arbitrary function (one-site binding hyperbola, blue curve,  $K_d = 16.8\% \pm 32.59\%$ ). Black curve is an overlay of the curve from Panel A (graphed on the right y axis). Panel C: Normalized means of MC540 histograms from flow cytometry data as a function of percent dead. Panel D: Normalized ratios of flow cytometry histograms for both MC540 (black) and FITC-annexin (green) were fit to a variable slope sigmoid function with bottom fixed at 0. Red curve is an overlay of the curve from Fig. 18C (except that the top was not fixed at 1.0), illustrating the level of PS exposure in dex-treated samples as a comparison.

**TABLE 1** Parameter values for Fig. 11

| Fig. 10 Panel | Parameters                             |                              |             |                           |
|---------------|--|------------------------------|-------------|---------------------------|
|               | $\beta$<br>(GP units s <sup>-1</sup> ) | $K_A$<br>(nM <sup>-1</sup> ) | $K_E$       | $S_T$<br>(relative units) |
| A             | 1.0                                    | 0.067                        | 0.10        | 1.0                       |
| B             | 1.0                                    | 0.067                        | 0.10        | 4.43                      |
| C             | 1.0                                    | 0.067                        | 0.10        | <u>8.12</u>               |
| D             | 1.0                                    | 0.067                        | <u>0.18</u> | 4.43                      |
| E             | 1.0                                    | <u>0.273</u>                 | 0.10        | 4.43                      |
| F             | 1.0                                    | <u>0.056</u>                 | <u>0.20</u> | 4.43                      |

Parameter values were obtained by nonlinear regression using Eq. 2 as explained in the legend to Fig. 11. Values allowed to float in the regression are underscored.

**TABLE 2** Categories of dex-treated cells by laurdan GP

| Category | Whole cell GP range | Interior GP range | Exterior GP range |
|----------|---------------------|-------------------|-------------------|
| Ring     | 0.08-0.18           | 0.02-0.10         | 0.10-0.25         |
| Mixed    | 0.18-0.30           | 0.18-0.30         | 0.18-0.30         |
| Red      | >0.35               | >0.35             | >0.35             |

Pixels isolated to calculate interior GP represented approximately 70% of whole cell pixels in each case. Ranges are approximate; categorization was confirmed by visual analysis. Analysis performed using SimFCS software provided by the Laboratory for Fluorescence Dynamics (University of California, Irvine). Exterior GP calculated by:  $(\text{whole cell GP} \times \text{whole cell pixels} - \text{interior GP} \times \text{interior pixels}) / \text{exterior pixels}$ .

**TABLE 3** Midpoints with 95% confidence intervals for sigmoid fits in Figs. 12, 15, 16, and 18

| Measurement                  | Parameters           |                     |                     |
|------------------------------|----------------------|---------------------|---------------------|
|                              | Midpoint<br>(% dead) | C.I. lower<br>limit | C.I. upper<br>limit |
| Total % susceptible          | 45.42                | 42.30               | 48.54               |
| MC540 $\Delta/\Delta_{\max}$ | 46.98                | 40.45               | 53.51               |
| MC540 histogram mean         | 44.41                | 38.97               | 49.86               |
| MC540 histogram ratio        | 64.19                | 58.80               | 69.58               |
| FITC-annexin histogram ratio | 60.41                | 55.61               | 65.21               |

Parameter values were obtained by nonlinear regression as explained in the legends to Figs. 12, 15, 16, and 18.

**SCHEME 1**

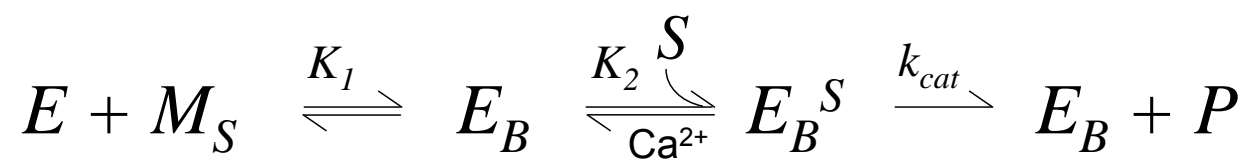


FIGURE 1

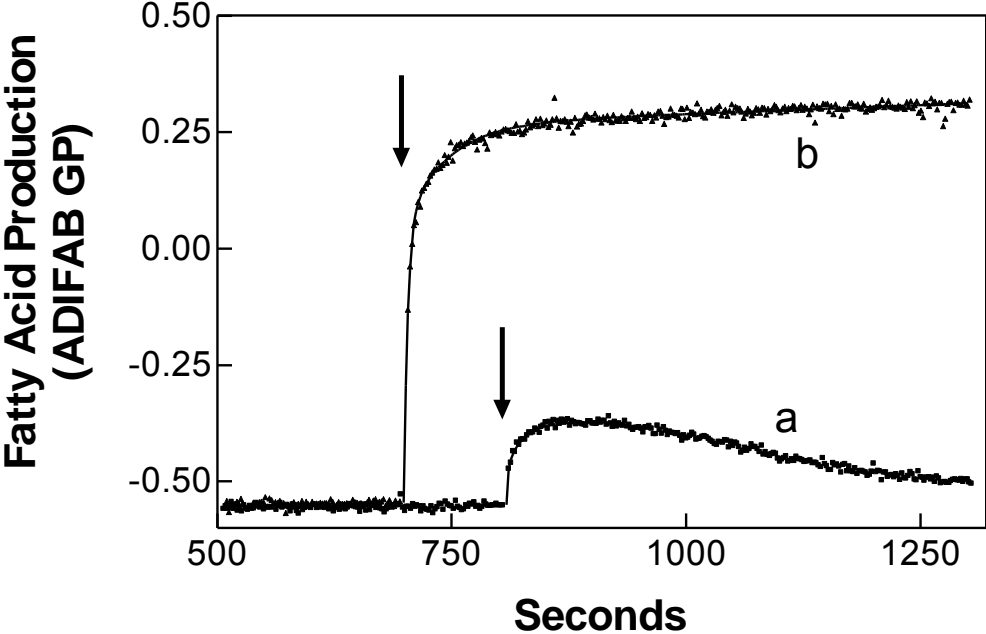


FIGURE 2

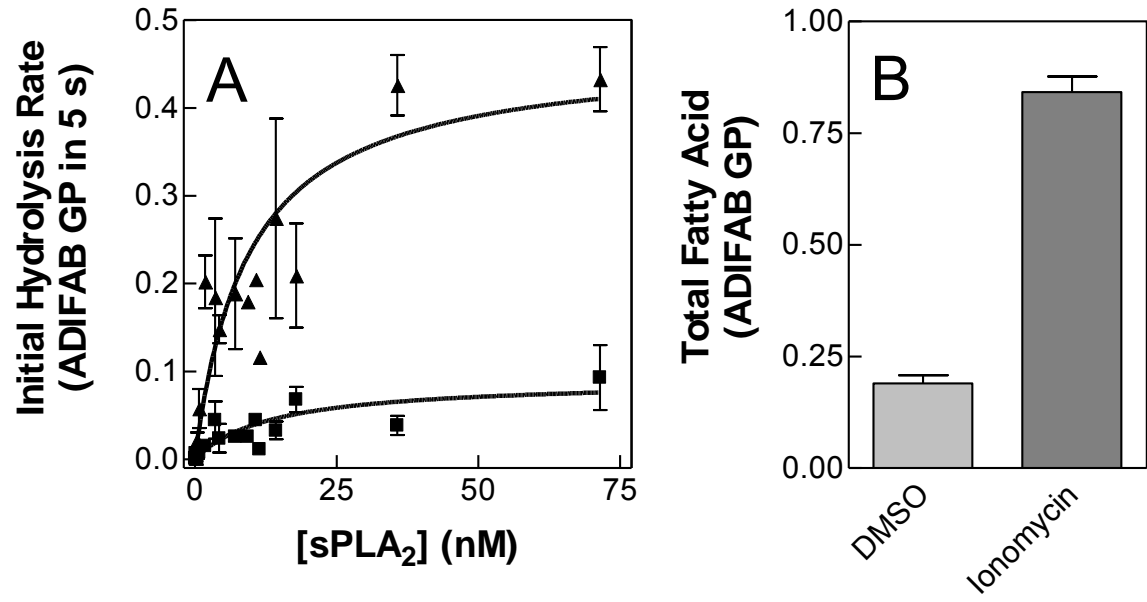


FIGURE 3

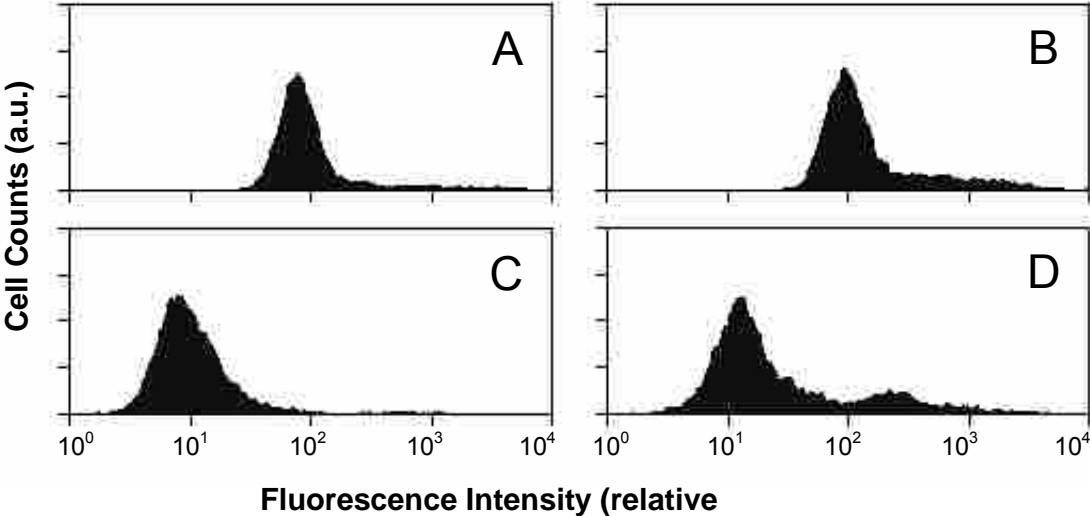




FIGURE 4

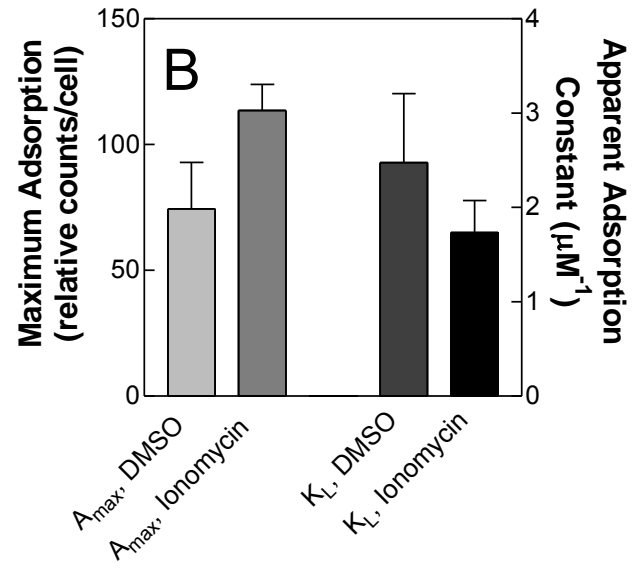
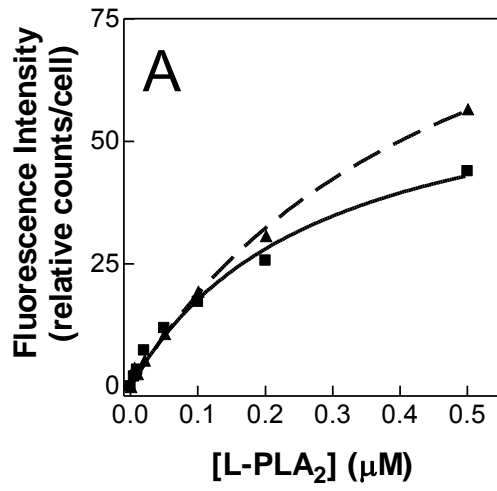


FIGURE 5

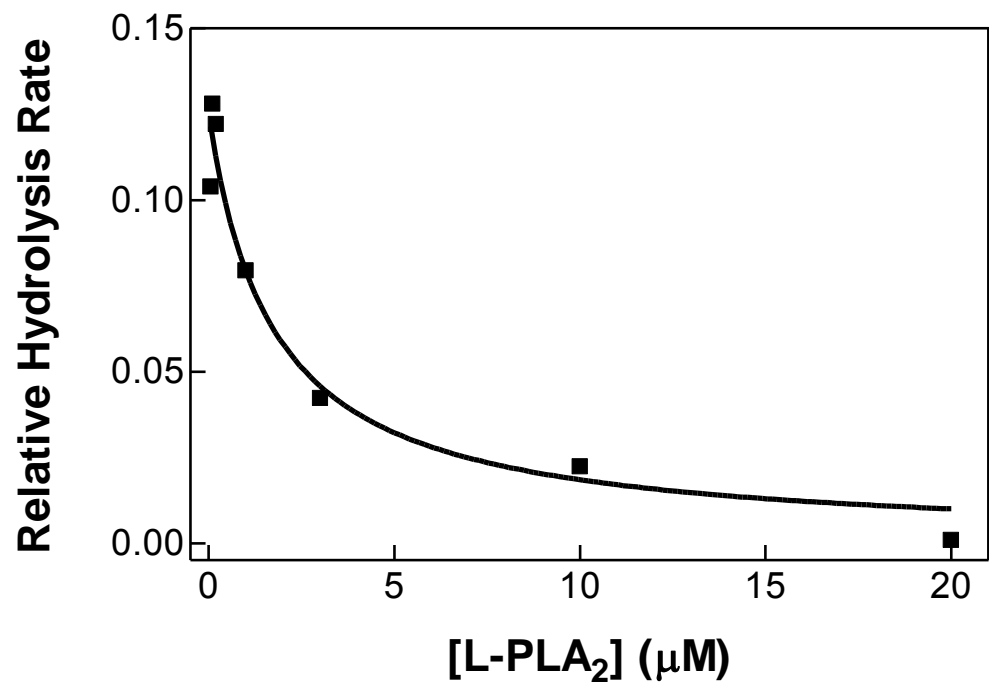


FIGURE 6

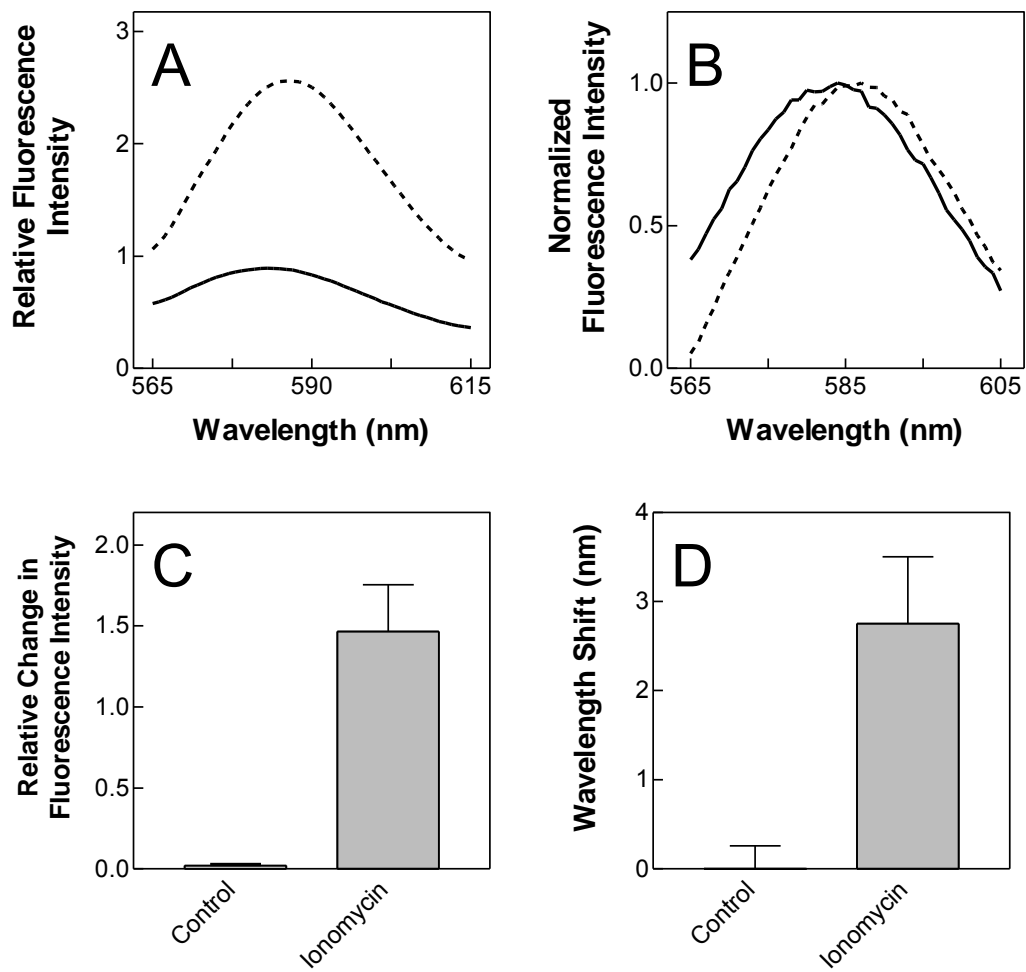
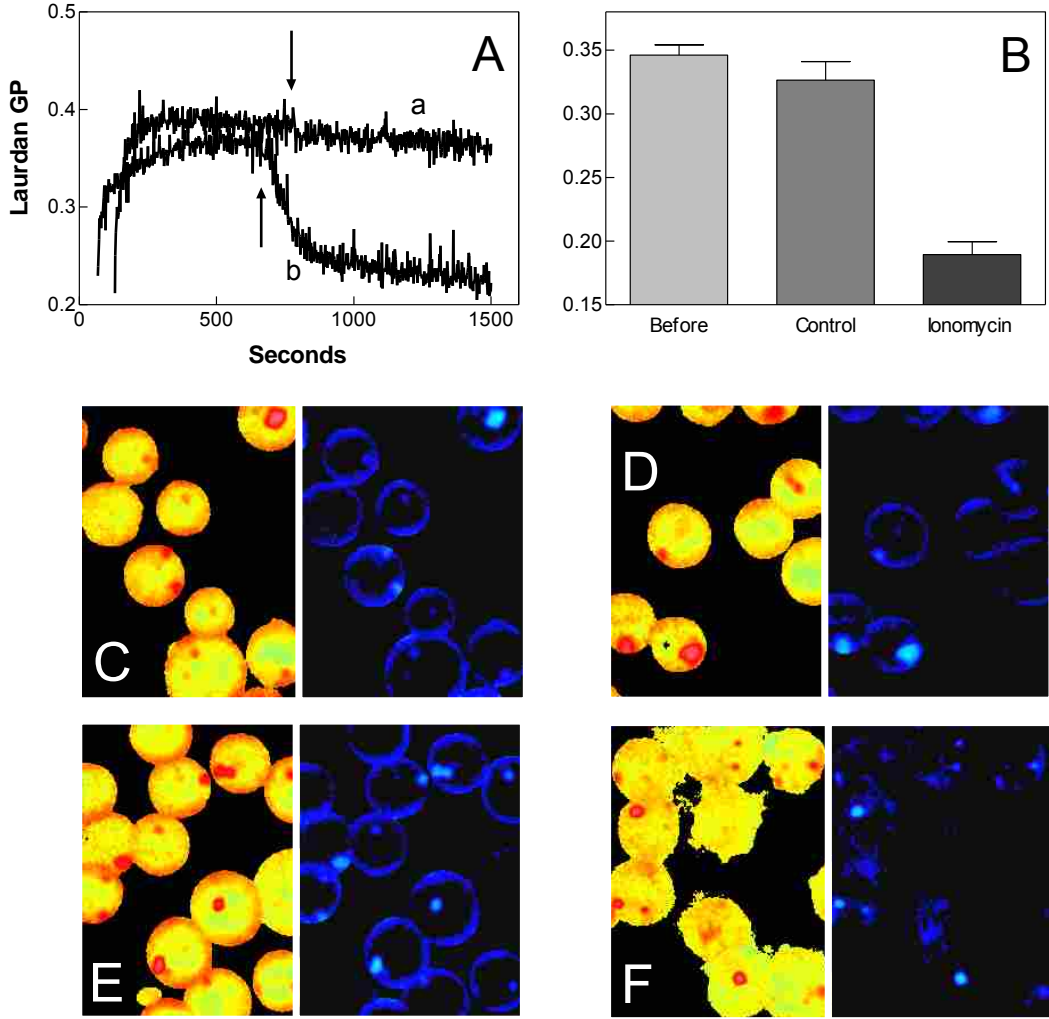


FIGURE 7



**FIGURE 8**

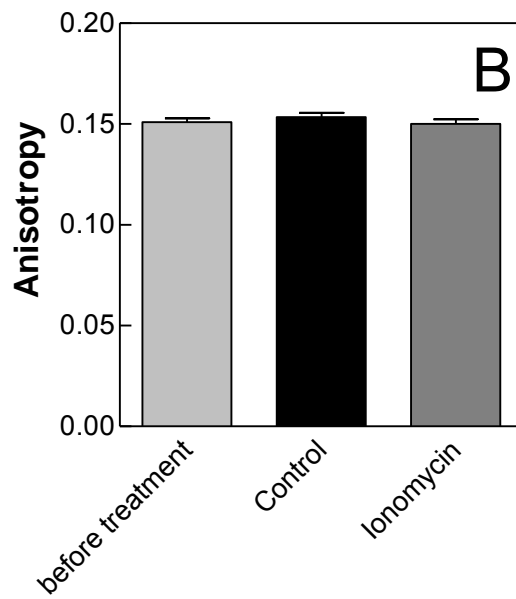
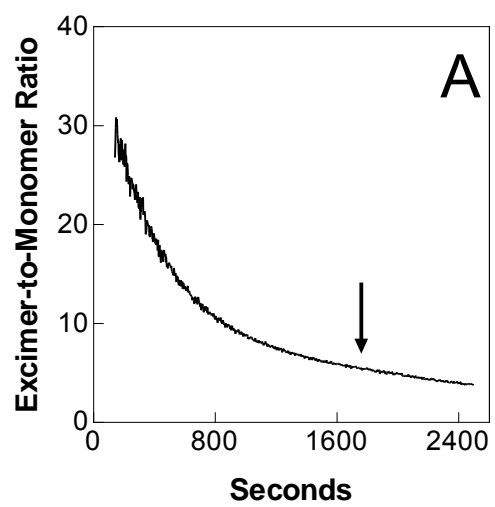


FIGURE 9

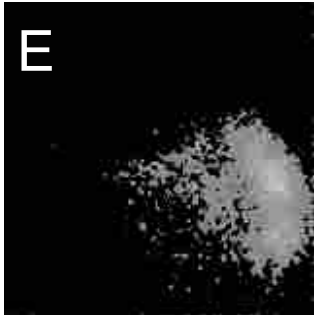
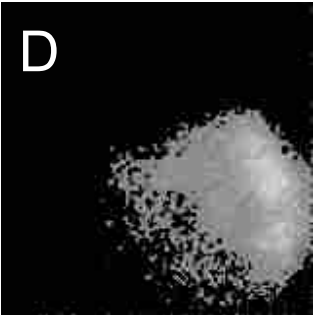
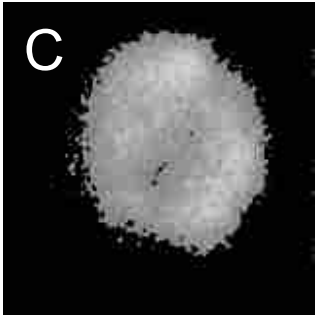
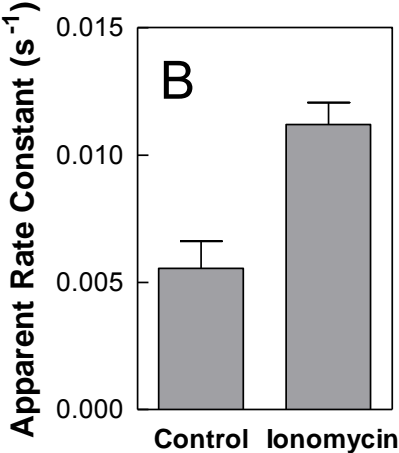
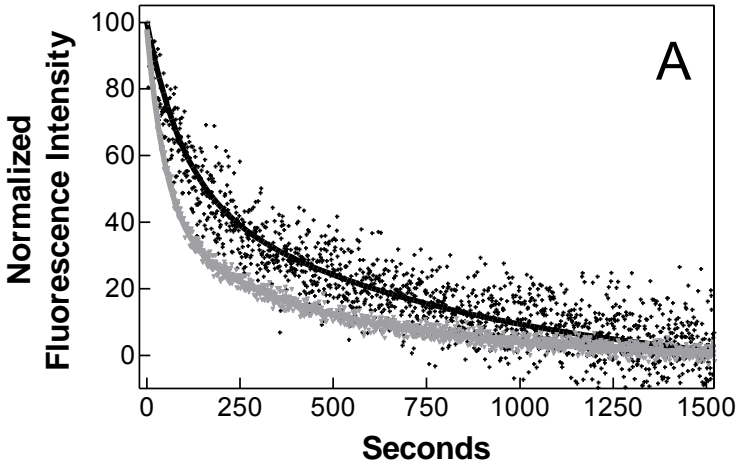


FIGURE 10

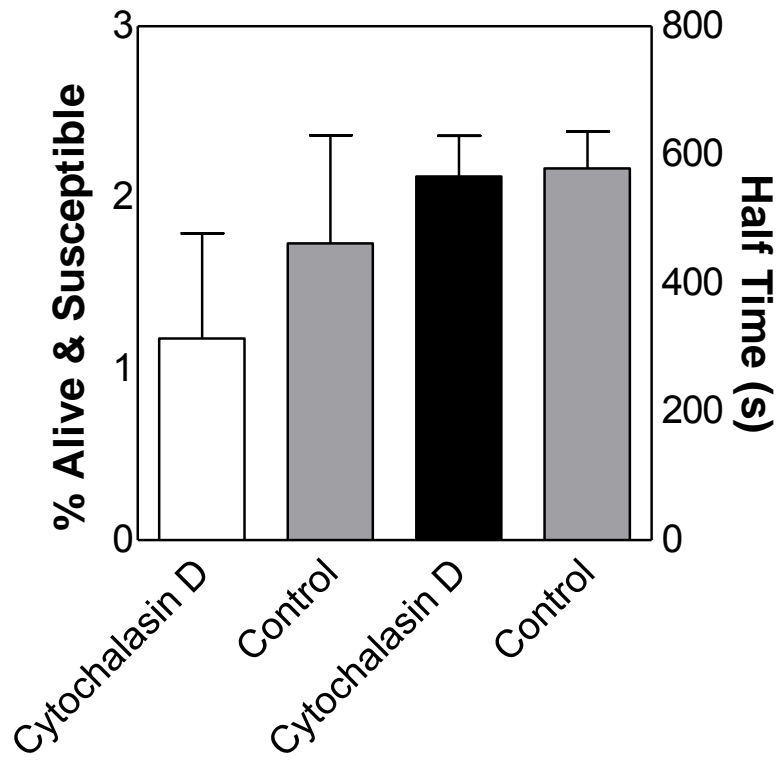


FIGURE 11

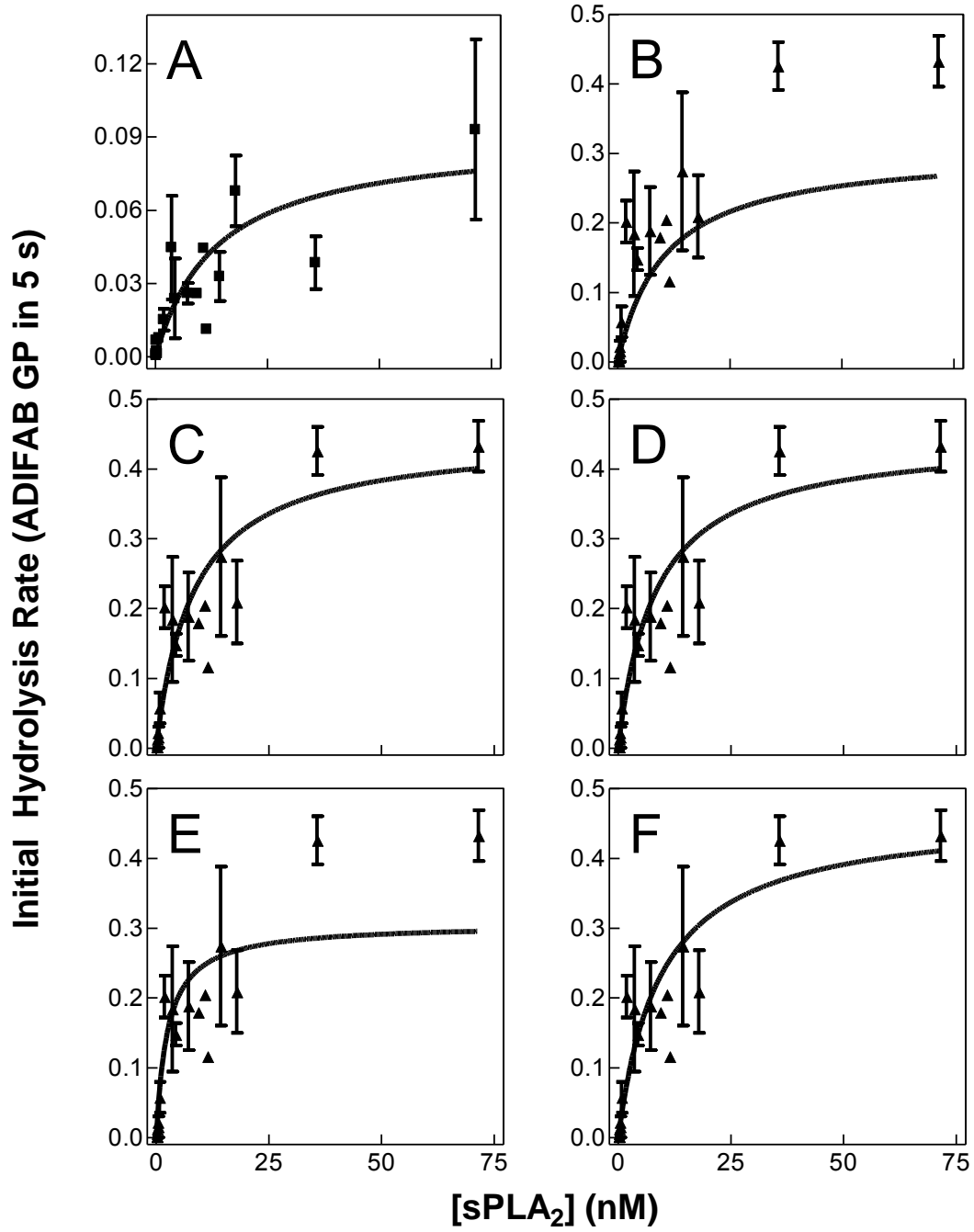




FIGURE 12

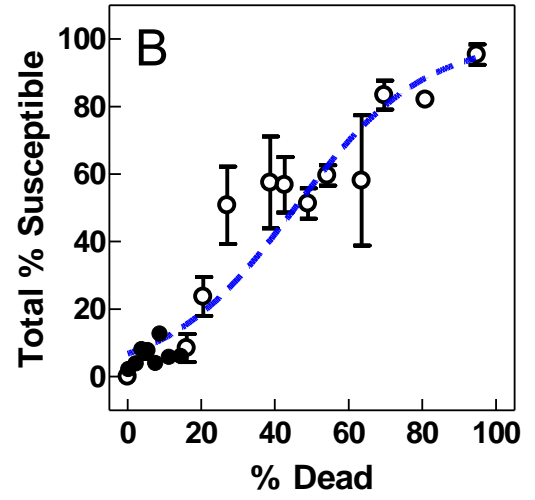
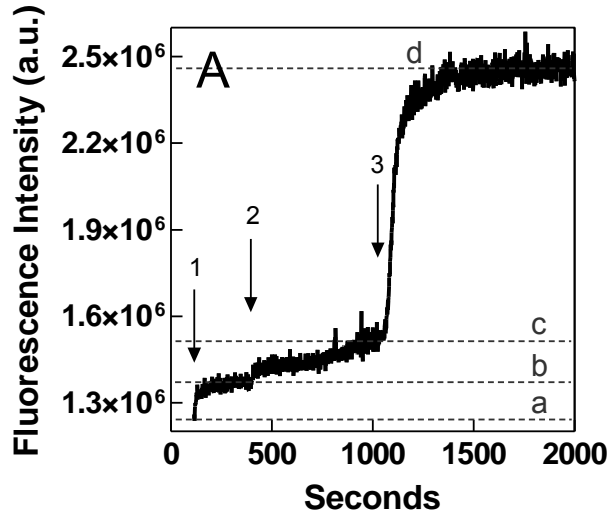


FIGURE 13

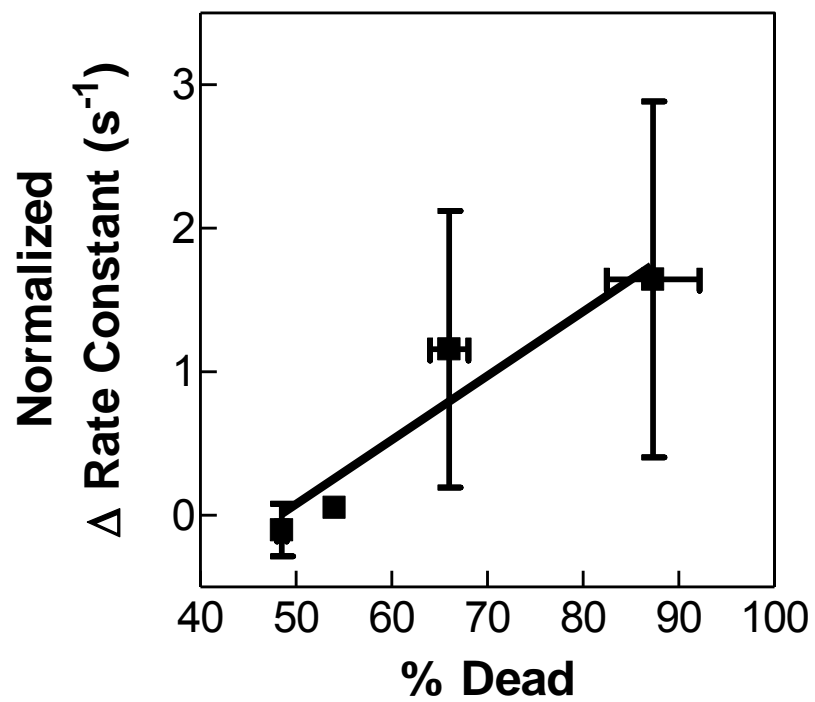


FIGURE 14

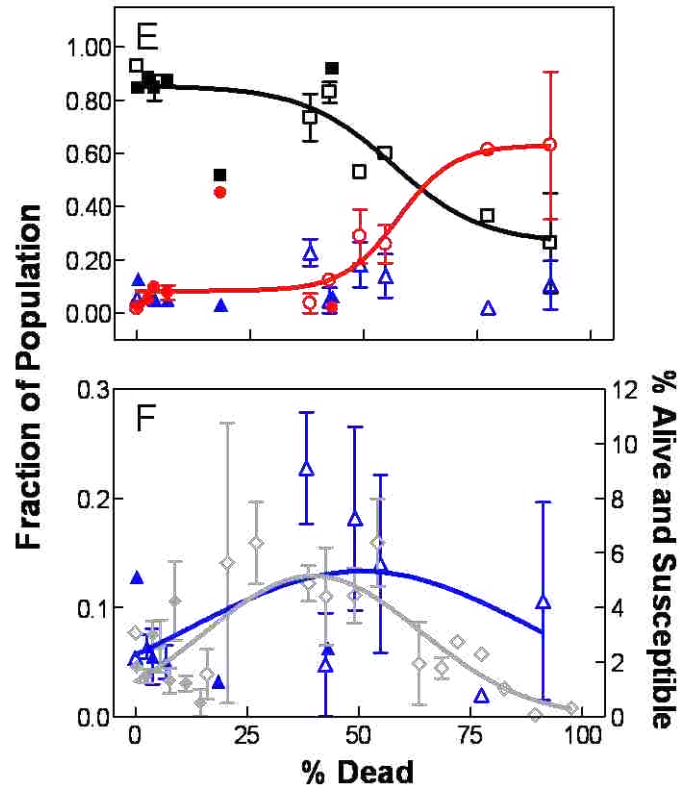
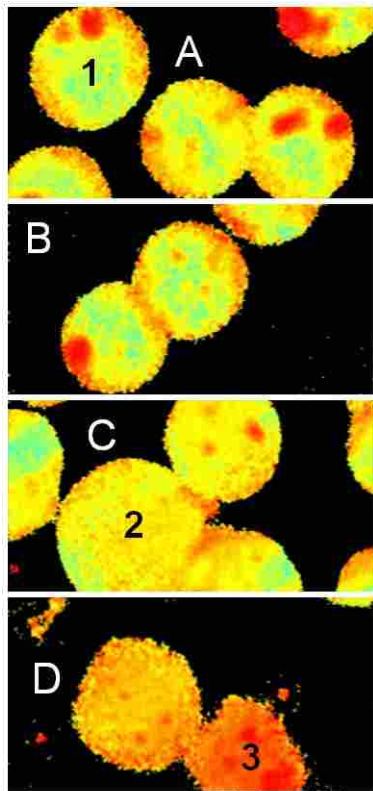


FIGURE 15

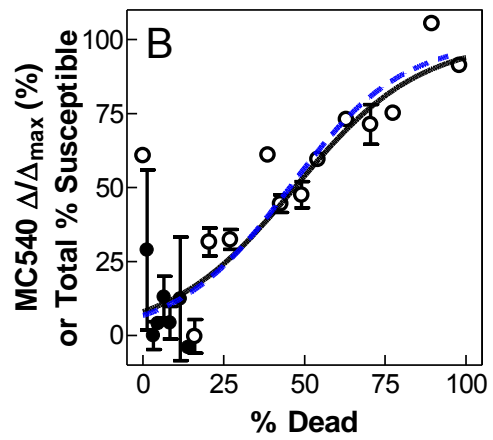
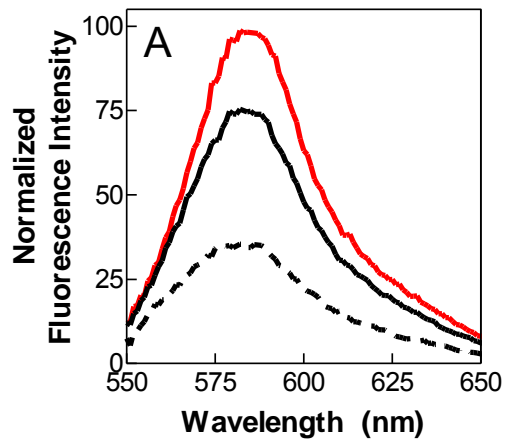


FIGURE 16

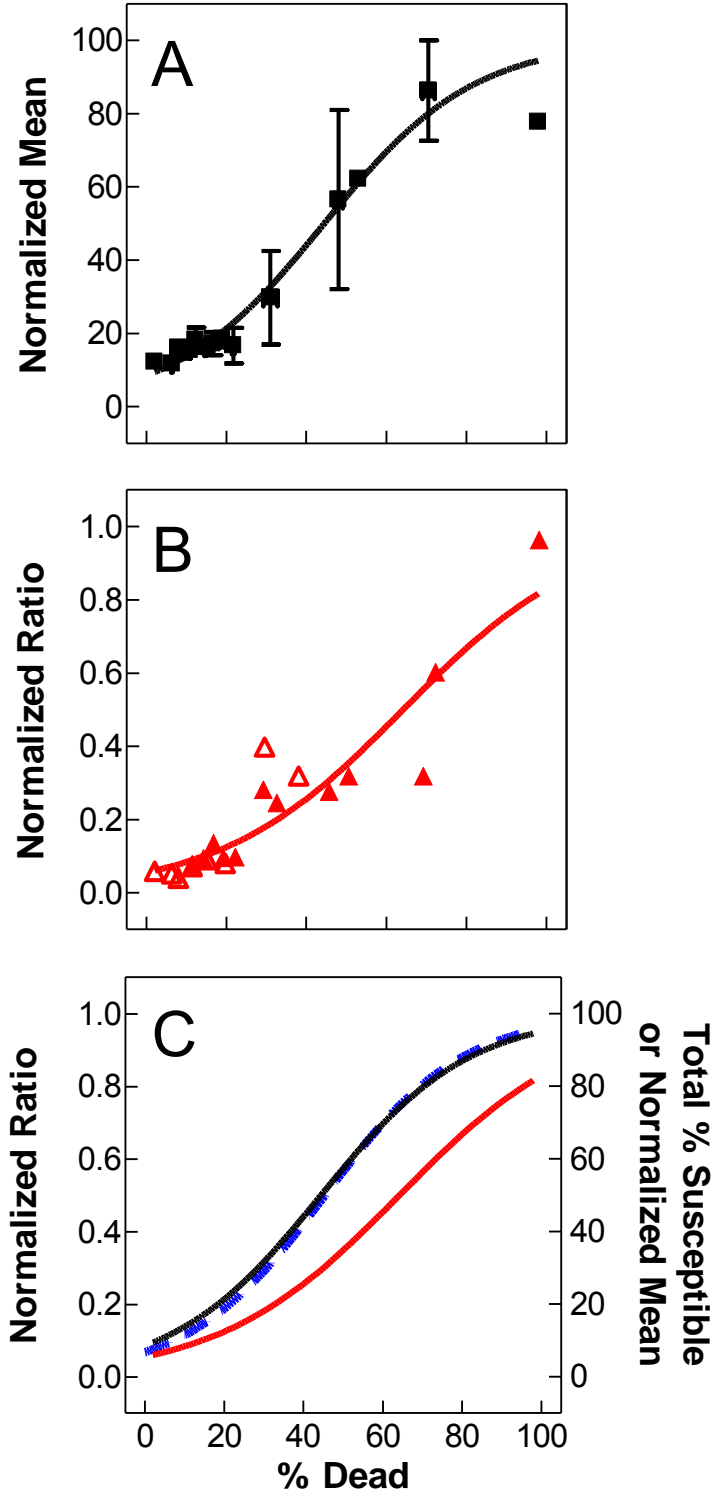


FIGURE 17

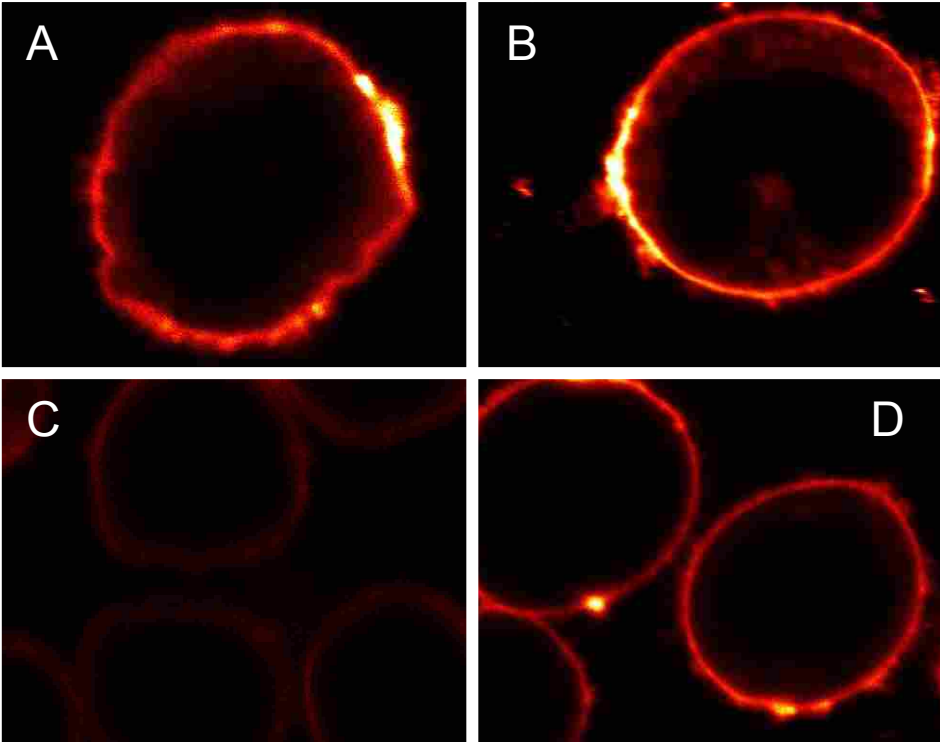


FIGURE 18

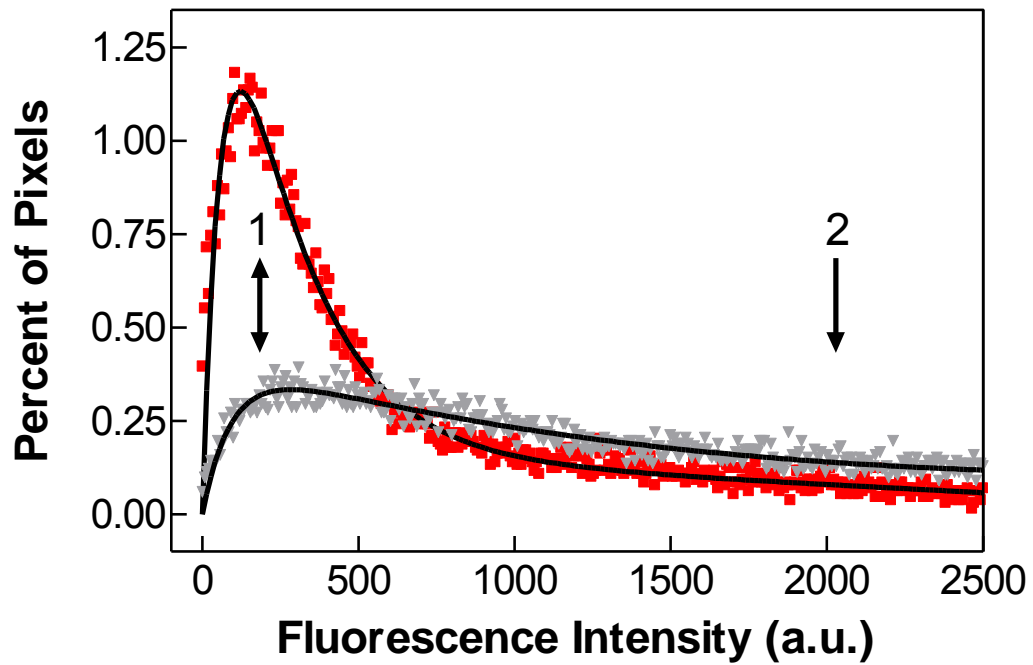


FIGURE 19

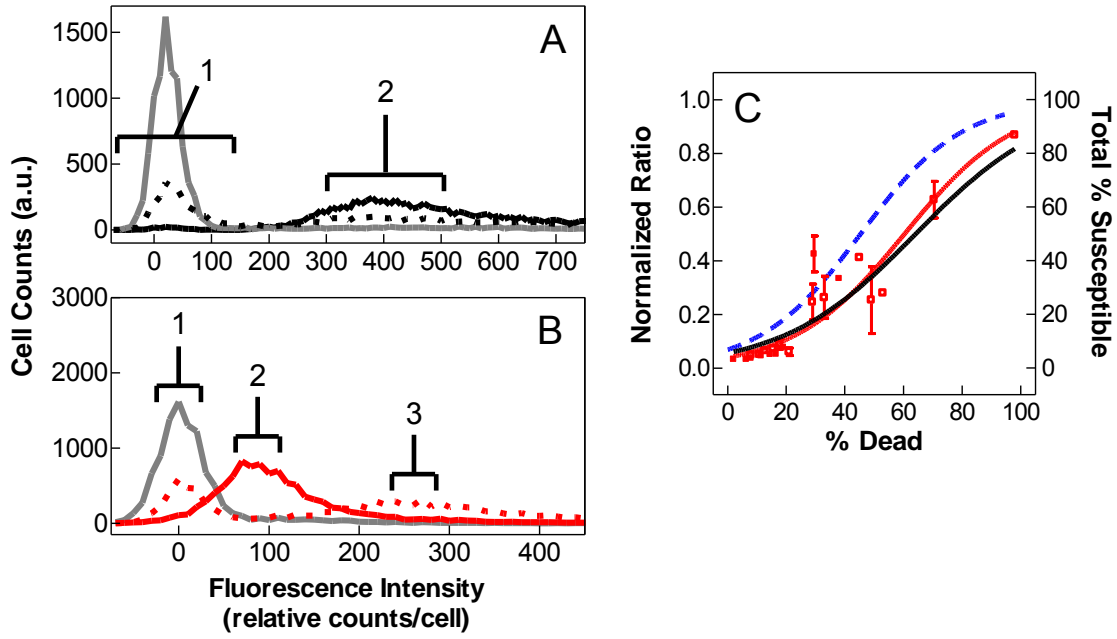




FIGURE 20

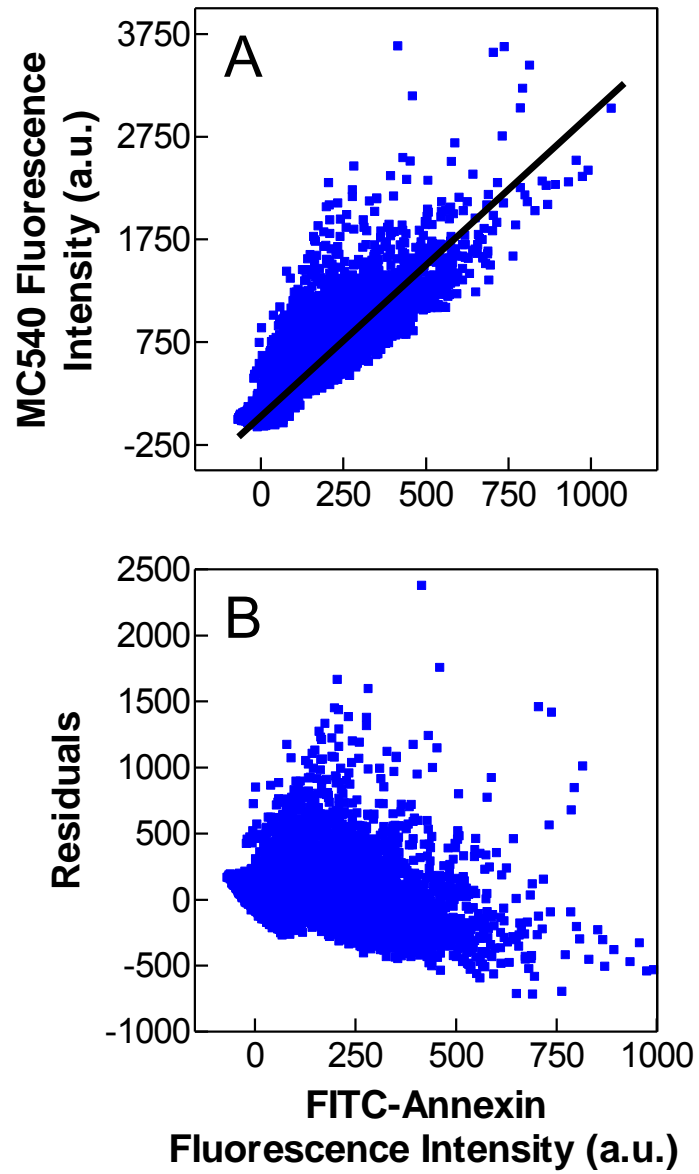


FIGURE 21

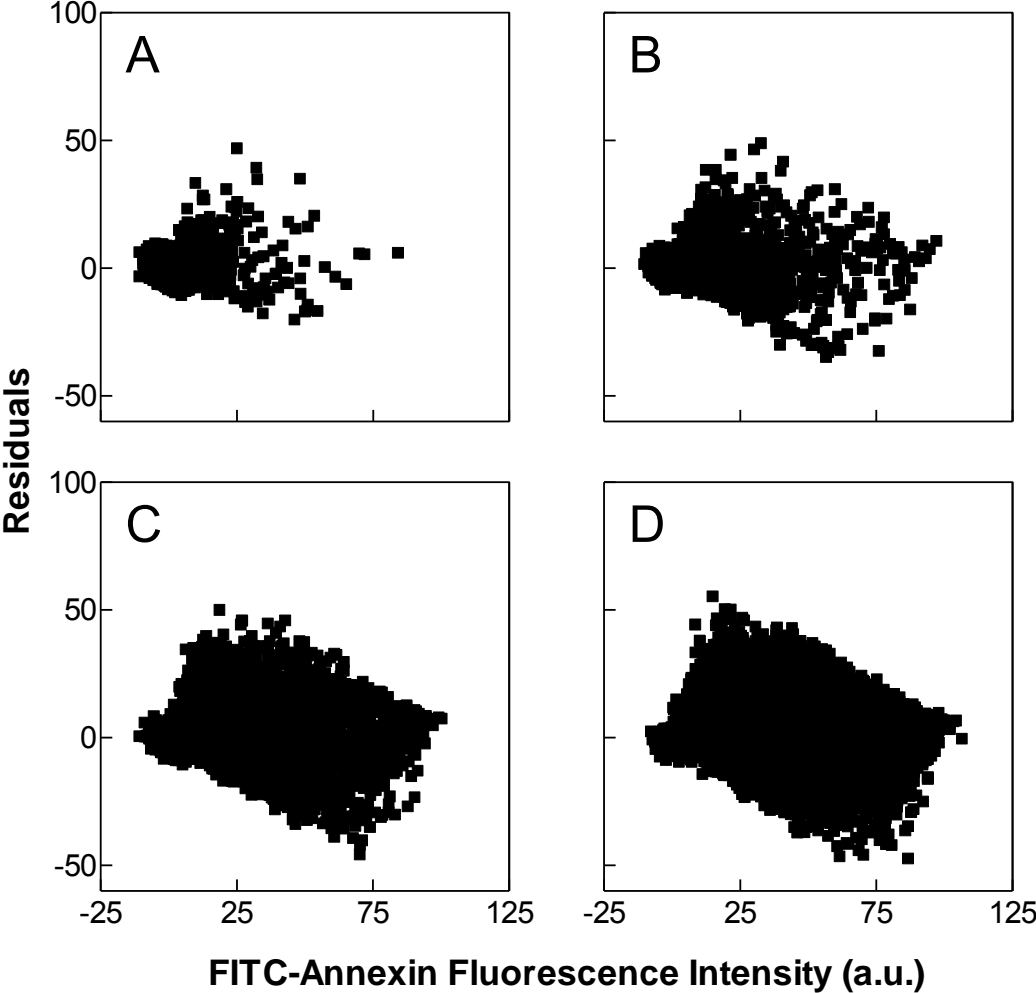


FIGURE 22

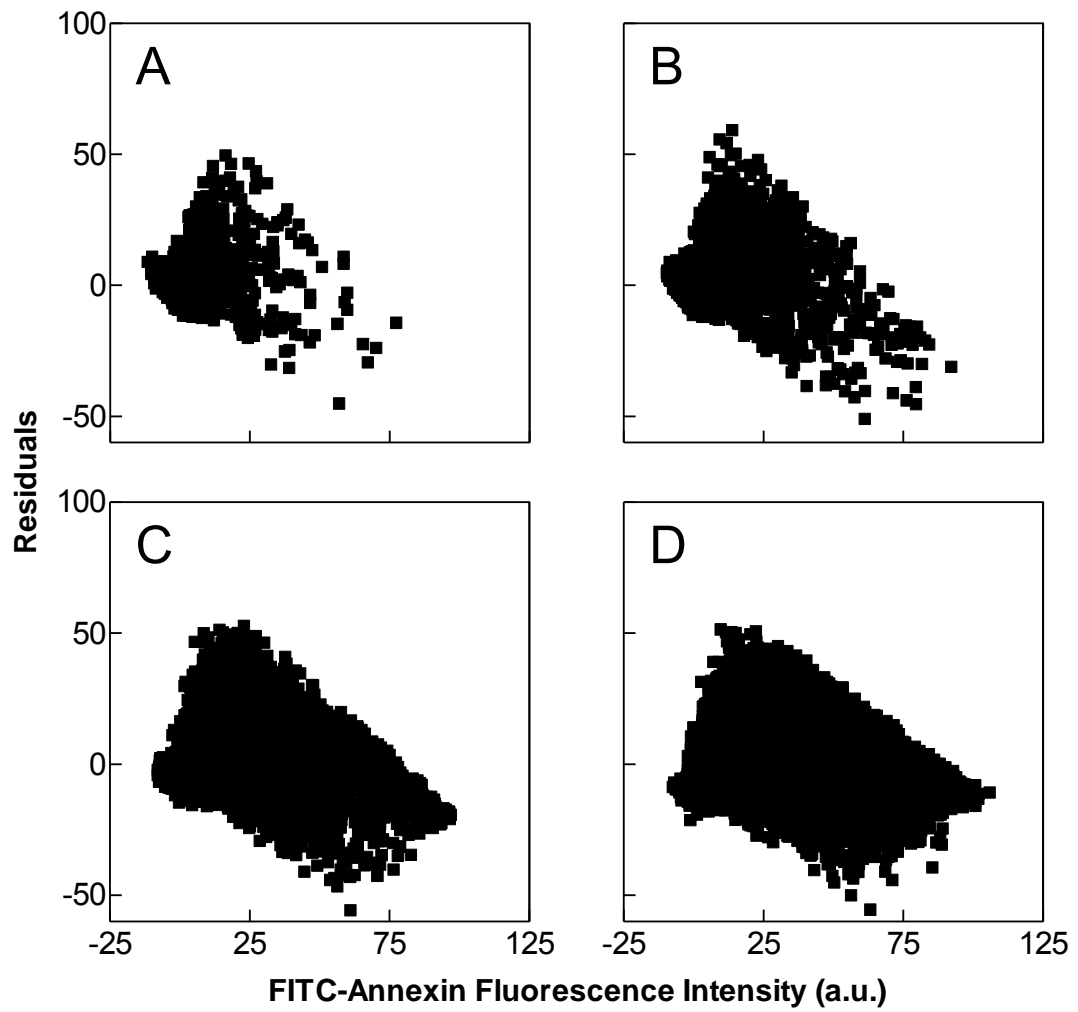
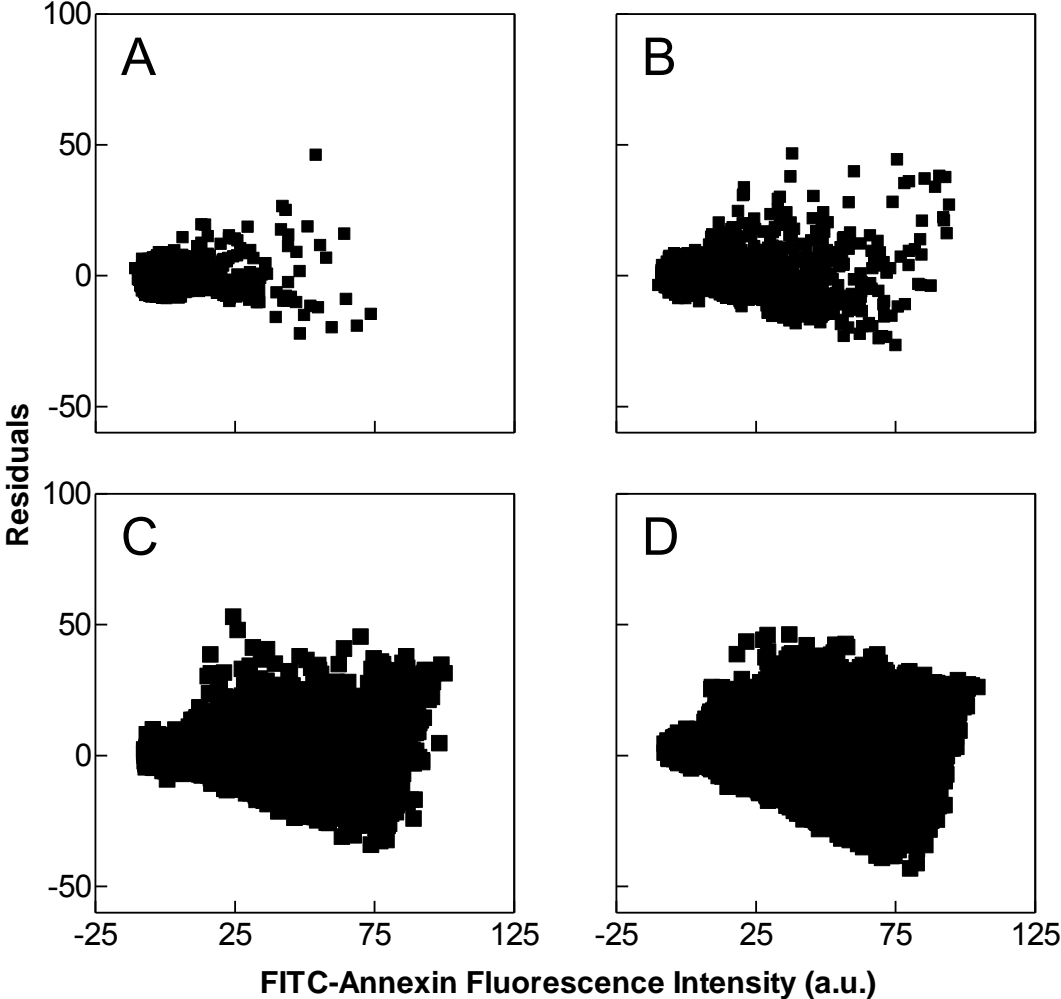


FIGURE 23



**FIGURE 24**

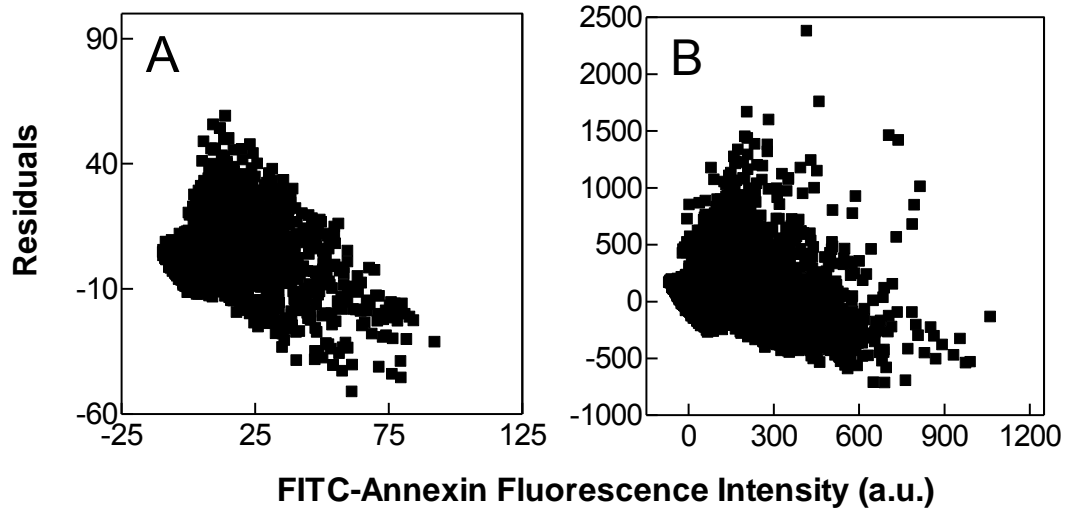
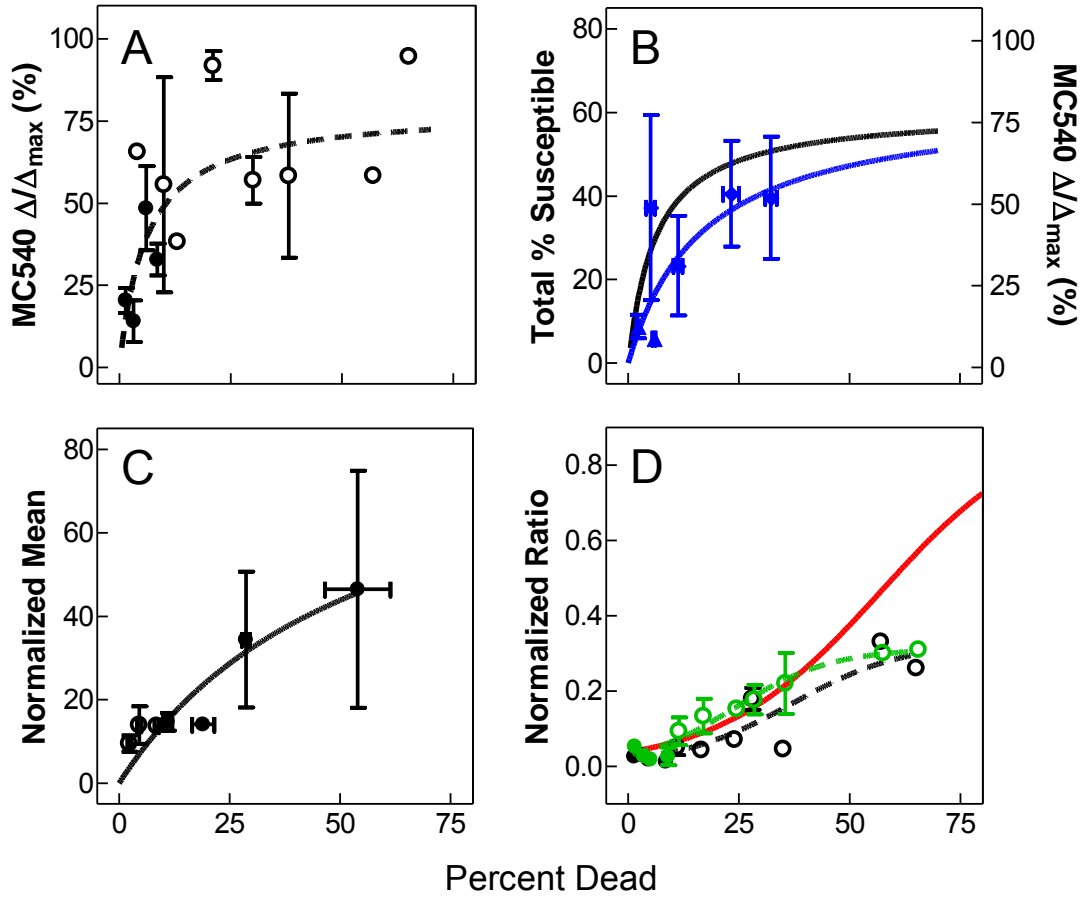


FIGURE 25



**Rachel Williams Bailey**

442 North 200 East apt 5, Provo, UT 84606  
(801) 602-9607  
rwbailey22@hotmail.com

Date of Birth: June 12, 1984  
Place of Birth: Indianapolis, Indiana  
Married to: G. Christopher Bailey

---

**EDUCATION**

---

*Brigham Young University, College of Life Sciences*

**M.S. in Physiology & Developmental Biology** **2006-2008**

Thesis: "Mechanisms by which apoptotic membranes become susceptible to secretory phospholipase A2." Thesis defended on March 7, 2008.

*Brigham Young University, College of Life Sciences*

**B.S. in Biology, Magna Cum Laude** **2002-2006**

Areas of Concentration: Human Physiology, Biophysics.

---

**WORK & TEACHING EXPERIENCE**

---

*Brigham Young University, Graduate Studies*

**President** – Graduate Student Society **2007-2008**

Organizes monthly events attended by 200-1000; participates in four university committees comprised of faculty and students; orchestrates the distribution of research presentation funds to graduate students.

Advocates for graduate student concerns including health insurance, parking, and funding locally and nationally; chairs the 30-member Graduate Student Council; works directly with the deans of Graduate Studies.

*Brigham Young University, Department of Physiology*

**Research Assistant** – Bell Lab **2004-2008**

Designs and conducts spectroscopy and microscopy experiments; performs statistical analyses of data, maintains cancer cell cultures; presents research at weekly lab meetings; trains one new assistant per semester; coordinates schedule of laboratory resources.

**Teaching Assistant** – for Dr. David Busath, "Advanced Physiology" **2006**

Administered weekly online quizzes and written assignments for 40 students; taught monthly two-hour exam reviews; met individually with students 2-4 hours weekly.

*Brigham Young University, Department of Chemistry & Biochemistry*

**Teaching Assistant** – for Dr. John Cannon, "General College Chemistry" **2004-2005**

Taught two weekly recitation sections to 20 students; graded 100 exams and lab write-ups biweekly; met individually with students 5-8 hours weekly; taught monthly three-hour exam reviews; wrote detailed lecture notes for student reference.

Brigham Young University, On-campus Housing

**Resident Assistant** – Helaman Halls

**2003-2004**

Mentored 40 female college freshmen; organized monthly activities and educational programs attended by 20-100; mediated roommate conflicts; assisted residents with emotional, family, and academic challenges.

---

#### FELLOWSHIPS, GRANTS, & SCHOLARSHIPS

---

- *Alterations in Membrane Physical Properties and Their Effect on Susceptibility to Secretary Phospholipase A2 During Apoptosis*. Research under the direction of Dr. John Bell. Funded through the Graduate Student Summer Fellowship, BYU Cancer Research Center, and the Graduate Research Fellowship, BYU Graduate Studies. April/August 2007. Funded for \$11,000.
- \$1,000 Undergraduate Scholarship, AKA Educational Advancement Foundation. April 2006.
- Gordon B. Hinckley Presidential 150% Tuition Undergraduate Scholarship, Brigham Young University. 2002-2006.
- *Determining Secretary Phospholipase A2 Binding Properties Through the Fluorescent Probe Nystatin*. Undergraduate research under the direction of Dr. John Bell. Funded through the BYU Office of Research & Creative Activities. April 2005. Funded for \$1,500.

---

#### PEER-REVIEWED ARTICLES

---

##### *Published*

- Bailey RW, Olson ED; Vu MP; Brueseke TJ; Robertson L; Christensen RE; Parker KH; Judd AM; Bell JD. Relationship between membrane physical properties and secretary phospholipase A2 hydrolysis kinetics in S49 cells during ionophore-induced apoptosis. *Biophysical Journal*. 2007 Oct 1; Vol. 93 (7), pp. 2350-62.

##### *In Progress*

- Bailey RW, Olson ED; Gibbons L; Nguyen T; Robertson L; Judd AM; Bell JD. *Determinants of App D49 secretary phospholipase A2 activity in S49 cells during glucocorticoid-induced apoptosis*.
- Gonzalez L; Heiner A; Bailey RW; Nguyen T; Fairborne J; Brueseke TJ; Bell JD. *Requirements for microvesicle release in human erythrocytes*.
- Novilla MLB, Hanson CL, Barnes MD, Sugiyama L, Bailey R, Reichman P. *Value of family health history on reducing the risk of chronic diseases: Differences in outlook, contemplated action, and actual behavior among respondents from high- and middle-income countries*.

---

#### ORAL PRESENTATIONS & RESEARCH ABSTRACTS

---

- Bailey RW, Hansen RE, Homer G, Reeves LH. *Utilizing graduate students needs and desires to create successful campus-wide events*. National Association of Graduate-Professional Students, Western Regional Meeting. **March 14, 2008**.



- Bailey RW, Gibbons E, Robertson L, Nguyen T, Nelson J, Judd AM, Bell JD. *Biophysical Changes in the Plasma Membrane during Glucocorticoid-stimulated Apoptosis Promote Hydrolysis by Secretory Phospholipase A2*. Biophysical Society 52<sup>nd</sup> Annual Meeting & 16<sup>th</sup> International Biophysics Congress. **February 6, 2008**.
- Olson EO, Nguyen T, Bailey RW, Gibbons E, Judd AM, Bell JD. *A Kinetic Analysis of Isoforms of Secretory Phospholipase A2*. Biophysical Society 52<sup>nd</sup> Annual Meeting & 16<sup>th</sup> International Biophysics Congress. **February 6, 2008**.
- Bailey RW, Hansen RE, Homer G, Reeves LH. *Brigham Young University Graduate Student Society: Get Connected*. University Conference, Brigham Young University. **August 27, 2007**.
- Bailey RW. *Alterations in Membrane Physical Properties and Their Effect on Susceptibility to Secretory Phospholipase A2 During Apoptosis*. Cancer Research Center Fellow Presentations, Summer Cancer Workshop. **August 15, 2007**.
- Bailey RW, Olson ED; Vu MP; Brueseke TJ; Robertson L; Parker KH; Judd AM; Bell JD.. *Application of Membrane Biophysics to Cell Physiology: Mechanisms by which Apoptotic Membranes Become Susceptible to Secretory Phospholipase A2*. Biophysical Society 51<sup>st</sup> Annual Meeting & 15<sup>th</sup> International Biophysics Congress. **March 7, 2007**.
- Bailey RW. *Lipid Ensembles and sPLA2 Activity in Apoptotic Membranes*. Department Seminar, Department of Physiology & Developmental Biology, Brigham Young University. **April 5, 2007**.
- Bailey RW. *Defense of Prospectus of Research for Master's Thesis*. Presented to Thesis Committee: Drs. John Bell, William Bradshaw, & Allan Judd. **October 18, 2006**.

---

#### PROFESSIONAL MEMBERSHIPS

---

- Biophysical Society **2006-2008**
- 

#### HONORS & AWARDS

---

- \$400 Research Presentation Award, BYU Graduate Studies **2007**
  - Lee Undergraduate Teaching Award, BYU Department of Chemistry & Biochemistry **2005**
  - Inducted into Phi Kappa Phi and Golden Key Honor Societies **2005 & 2003**
- 

#### COMMUNITY SERVICE & LEADERSHIP

---

*Healing Hands for Haiti, International*

**Volunteer** – Port-au-Prince, Haiti

**Sep 2007**

Taught classes to 25 caregivers on topics such as rehabilitation techniques, hygiene, and first aid; gained multicultural skills that allowed me to interact effectively with the people while overcoming cultural and linguistical barriers in discussing sensitive health issues in relation to HIV/AIDS.

*Science Power*

**President** – Brigham Young University Chapter **2006-2007**

Promoted science education and career paths among female junior high students through monthly activities attended by 30 participants; taught dissection techniques; coordinated program logistics, publicity, and registration.

*Project MEDD/Charity Anywhere*

**Intern/Translator** – Galapagos Islands, Ecuador **May 2006**

Translated English-Spanish for Dr. Nikole Clark, an American family practice physician, in a medical outreach clinic in Santa Cruz; admitted patients to clinic and assisted with medical records; taught one-on-one dental hygiene lessons to children under 12.

*Brigham Young University, Center for Service & Learning*

**Volunteer Tutor** – Organic Chemistry, Human Anatomy **2005-2006**

Conducted biweekly tutoring sessions with 1-2 undergraduates per semester; taught organization, reading, note-taking, and study skills.

*Benson Institute*

**Public Health Intern** – La Paz, Bolivia Office **Apr-Jun 2004**

Taught nutrition classes in Spanish to 15 mothers as well as hygiene classes to 30 elementary students in rural schools; conducted a breastfeeding workshop for mothers in a nearby village; collaborated with other American interns and University students from La Paz.

Assisted in conducting a 6-month follow-up survey of 3 villages following the installation of water pumps by a local NGO; helped install and maintain small greenhouses at local schools to improve child nutrition through increased intake of fresh vegetables.

*Church of Jesus Christ of Latter-day Saints*

**Volunteer** – Provo Area **2002-2008**

Holds/held various ecclesiastical callings in local congregation including counselor in presidency of the Children's Primary, activities director, and choir director.

---

**SKILLS & CERTIFICATIONS**

---

- Proficiency in spoken and written Spanish.
- College Reading and Learning Association, certified level 1 tutor.
- Proficient in SAS, Excel, Prism GraphPad graphing and statistical software, and QUICK BASIC.